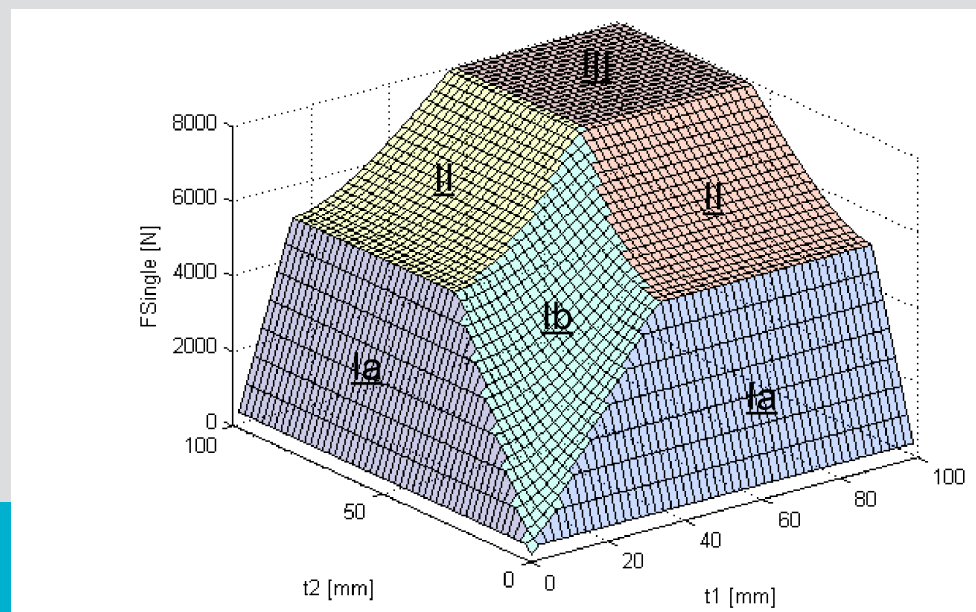


# Group Effect in Timber Joints with Focus on Dowel-Type Fasteners



D-4-08/2014

**Bastian WILDING**

Institut für Holzbau und Holztechnologie  
Technische Universität Graz





Bastian Valentin Wilding, BSc.

# **Group Effect in Timber Joints with Focus on Dowel-Type Fasteners**

## **MASTERARBEIT**

zur Erlangung des akademischen Grades

Diplom-Ingenieur

Masterstudium Bauingenieurwissenschaften - Konstruktiver Ingenieurbau

eingereicht an der

**Technischen Universität Graz**

Betreuer

Univ.-Prof. Dipl.-Ing. Dr.techn. Gerhard Schickhofer

Institut für Holzbau und Holztechnologie

Ass.Prof. Dipl.-Ing.(FH) Dr.techn. Reinhard Brandner  
Institut für Holzbau und Holztechnologie



## **EIDESSTATTLICHE ERKLÄRUNG**

### ***AFFIDAVIT***

Ich erkläre an Eides statt, dass ich die vorliegende Arbeit selbstständig verfasst, andere als die angegebenen Quellen/Hilfsmittel nicht benutzt, und die den benutzten Quellen wörtlich und inhaltlich entnommenen Stellen als solche kenntlich gemacht habe. Das in TUGRAZonline hochgeladene Textdokument ist mit der vorliegenden Masterarbeit identisch.

*I declare that I have authored this thesis independently, that I have not used other than the declared sources/resources, and that I have explicitly indicated all material which has been quoted either literally or by content from the sources used. The text document uploaded to TUGRAZonline is identical to the present master's thesis.*

---

Datum / Date

---

Unterschrift / Signature



## DANKSAGUNG AN...

Meinen Betreuer, Ass.Prof. Dipl.-Ing. (FH) Dr.techn. Reinhard Brandner

Für die interessanten sowie unterhaltsamen Gespräche und Denkanstöße (besonders was die sinnvolle Investition begrenzter Ressourcen angeht). Dass er meine Arbeit mit solcher Sorgfalt und Genauigkeit korrigiert und dadurch seine optische Form eindeutig zum Positiven beeinflusst hat.

Univ.-Prof. Dipl.-Ing. Dr.techn. Gerhard Schickhofer

Für seine unbürokratische Art und dass er jederzeit ein offenes Ohr für Studenten hat.

Simona Hermus

Dafür, dass sie dem Englisch dieser Arbeit, durch einen beeindruckenden Kampf gegen „short forms“ und zeilenlange Sätze, den letzten Schliff gegeben hat.

## KURZFASSUNG

Gängige Bemessungspraxis von Verbindungen mit mehreren Verbindungsmitteln im Holzbau ist es, die Widerstandsfähigkeit des Einzelverbindungsmittels zu berechnen und diese dann mit einem gewissen „*n-effektiv*“ zu multiplizieren, das kleiner (oder gleich) der tatsächlichen Anzahl von eingesetzten Verbindungsmitteln ist. Diese verminderte theoretisch einsetzbare Festigkeit pro Verbindungsmittel ist in einer Spannungsakkumulation in der Verbindung, sowie Imperfektionen des Materials Holz und etwaigen Herstellungsungenauigkeiten begründet.

Im Zuge der Arbeit werden Parameter, die den Widerstand einer Verbindung mit Einzelverbindungsmittel auf Abscheren bestimmen, vorgestellt, sowie die gängige Theorie (Johansens Fließmodell) zur Berechnung der Tragfähigkeit dieser Verbindung untersucht und kritisch betrachtet.

Bisherige (meist) empirische und auf limitierten Versuchsdaten basierende Ansätze zur Ermittlung von „*n-effektiv*“ werden verglichen und die Spannungsakkumulation in der Verbindung wird mit analytisch-mechanischen Mitteln untersucht. Auf diesen basierend, wird ein Versagensmodell hergeleitet und mit Versuchsergebnissen verglichen.

Weiters wird Blockscheren bei Schraubenverbindungen, die orthogonal zur Faser auf Herausziehen belastet werden, untersucht und ein Modell zur Ermittlung der Widerstandsfähigkeit der Verbindung auf Blockscheren erdacht, welches mit Versuchsergebnissen validiert wird.

Abschließend werden bionische Prinzipien auf Verbindungen im Holzbau umgelegt und die Form eines Zugstoßes sowie eines Verbindungsmittels für einen gewissen Lastfall optimiert.

## ABSTRACT

Design practice in timber connections with multiple fasteners is to determine the load carrying capacity of the single fastener connection and in order to obtain the resistance of the multiple fastener joint, it is multiplied with a certain "*n-effective*", which is smaller than (or the same as) the actual number of connectors used. This reduction of the theoretically usable load carrying capacity per fastener originates in an accumulation of stresses within the connection as well as imperfections of the material timber and possible manufacturing imprecisions.

In this thesis parameters determining the resistance of a single fastener connection loaded in shear are presented and the theory (Johansen's Yield Model) employed to actually calculate its load carrying capacity is discussed critically.

Existing (mostly empirical) approaches based on limited test data to obtain "*n-effective*" are compared and stress accumulation within the multiple fastener joint loaded in shear is examined. Based on this, an analytical failure model is derived and validated with test results.

Furthermore group block shear perpendicular to the grain in connections with screws loaded axially in pull-out is presented and a failure model is devised and checked for its accuracy by comparing it to test data.

Concluding principles of biomimicry are presented and applied on connections in timber engineering by optimising the shape of a connection with multiple dowel-type fasteners as well as that of a fastener for a certain load case.



# TABLE OF CONTENT

<b>1</b>	<b>INTRODUCTION</b> .....	<b>4</b>
<b>2</b>	<b>CONNECTIONS WITH FASTENERS LOADED IN SHEAR</b> .....	<b>5</b>
<b>2.1</b>	<b>SINGLE FASTENER CONNECTIONS</b> .....	<b>5</b>
2.1.1	General.....	5
2.1.2	Stress – Strain Behaviour .....	6
2.1.3	Embedment Strength.....	8
2.1.4	Yield Moment of the Fastener .....	11
2.1.5	Johansen’s Yield Model .....	13
<b>2.2</b>	<b>MULTIPLE FASTENER SHEAR CONNECTION</b> .....	<b>30</b>
2.2.1	General.....	30
2.2.2	Minimum Spacings and Distances .....	31
2.2.3	Design with Normal- and Shear Force .....	32
2.2.4	Design with Normal-, Shear Force and Moment .....	39
<b>3</b>	<b>LOAD PATHS</b> .....	<b>40</b>
<b>3.1</b>	<b>LOAD PATHS IN X-Y PLANE</b> .....	<b>40</b>
3.1.1	Way of the Load in a Connection.....	40
3.1.2	The Theoretical Influence of End Fixities .....	43
<b>3.2</b>	<b>LOAD PATHS IN X-Z PLANE</b> .....	<b>47</b>
3.2.1	Load Path in a Connection .....	47
3.2.2	Paths of the Tensile Main Stresses .....	48
<b>4</b>	<b>FURTHER STRESS ANALYSIS</b> .....	<b>50</b>
<b>4.1</b>	<b>EXAMINATION OF STRESSES AT THE FASTENER HOLE</b> .....	<b>50</b>
4.1.1	General.....	50
4.1.2	Fastener Loaded Parallel to the Grain .....	50
4.1.3	Fastener Loaded Perpendicular to the Grain.....	58
4.1.4	Tensile or Compressive Loading of the Timber Member .....	60
<b>4.2</b>	<b>BRIEF DISCUSSION OF FRACTURE MECHANICS</b> .....	<b>60</b>
4.2.1	General.....	60
4.2.2	The Critical Fracture Mechanical Energy .....	61
<b>4.3</b>	<b>DISTRIBUTION OF STRESSES IN A CONNECTION</b> .....	<b>63</b>
4.3.1	The Virtual Crack Width $y_a$ .....	64
4.3.2	Stresses Perpendicular to the Grain .....	66
4.3.3	Shear Stresses in a Connection .....	86
4.3.4	Determination of the Critical Fracture Energy .....	94

<b>5</b>	<b>ANALYTICAL FAILURE MODEL</b> .....	<b>95</b>
<b>5.1</b>	<b>LOAD SITUATION PARALLEL TO THE GRAIN</b> .....	<b>96</b>
5.1.1	Stresses Perpendicular to the Grain.....	96
5.1.2	Shear Stresses .....	98
<b>5.2</b>	<b>LOAD SITUATION UNDER A CERTAIN LOAD ANGLE <math>\alpha</math></b> .....	<b>98</b>
5.2.1	Splitting of the Wedging Force under a Load Angle $\alpha$ .....	100
5.2.2	Calculation of the Critical Fracture Energy $G_c$ under a Load Angle $\alpha$ .....	101
<b>5.3</b>	<b>MULTIPLE ROWS OF FASTENERS PERPENDICULAR TO THE GRAIN</b> .....	<b>101</b>
5.3.1	General.....	101
5.3.2	Load Parallel to the Grain.....	102
5.3.3	Load Perpendicular to the Grain .....	103
5.3.4	Load between $0^\circ < \alpha < \zeta$ .....	104
5.3.5	Load between $\zeta < \alpha < 90^\circ$ .....	106
<b>5.4</b>	<b>RELATION BETWEEN <math>f_v</math> AND <math>f_t</math>, <math>90^\circ</math></b> .....	<b>107</b>
<b>5.5</b>	<b>SIMPLIFICATIONS</b> .....	<b>108</b>
5.5.1	Determination of the Fictitious Shear Strain Layer $h_3$ .....	108
5.5.2	Determination of the Fictitious Length of the Crack Process Region $L_{reg}$ .....	109
<b>5.6</b>	<b>CALCULATION PROCESS</b> .....	<b>109</b>
<b>5.7</b>	<b>VALIDATION</b> .....	<b>110</b>
5.7.1	General.....	110
5.7.2	Loading Parallel to the Grain.....	110
5.7.3	Loading Perpendicular to the Grain .....	112
<b>6</b>	<b>SUMMARY</b> .....	<b>114</b>
<b>7</b>	<b>CONNECTIONS WITH AXIALLY LOADED FASTENERS</b> .....	<b>116</b>
<b>7.1</b>	<b>STRESS-STRAIN BEHAVIOUR</b> .....	<b>116</b>
<b>7.2</b>	<b>STRENGTH INFLUENCING PARAMETERS</b> .....	<b>117</b>
7.2.1	Withdrawal Strength.....	117
7.2.2	Resistance of the Fastener Head against Pull-through .....	117
7.2.3	Tensile Strength of the Fastener .....	117
<b>7.3</b>	<b>MINIMUM DISTANCES</b> .....	<b>118</b>
<b>7.4</b>	<b>N-EFFECTIVE</b> .....	<b>118</b>
<b>7.5</b>	<b>BLOCK SHEAR</b> .....	<b>119</b>
7.5.1	General.....	119
7.5.2	Failure Model .....	119
7.5.3	Validation .....	121
<b>7.6</b>	<b>SUMMARY</b> .....	<b>122</b>
<b>8</b>	<b>BIOMIMICRY IN CONNECTIONS</b> .....	<b>123</b>

<b>8.1</b>	<b>LOAD TRANSFER AND PEAK STRESSES .....</b>	<b>123</b>
<b>8.2</b>	<b>SHAPE OPTIMISATION .....</b>	<b>126</b>
8.2.1	Computer Aided Optimisation .....	126
8.2.2	Analytical Model .....	126
8.2.3	Tension Triangles .....	127
<b>8.3</b>	<b>APPLICATION IN CONNECTIONS.....</b>	<b>129</b>
8.3.1	Shape Optimisation of a Connection with Dowel Type Fasteners .....	130
8.3.2	Shape Optimisation of the Fastener Cross Section .....	135
<b>8.4</b>	<b>EXAMPLE OF A BIONIC CONNECTION.....</b>	<b>138</b>
<b>8.5</b>	<b>SUMMARY .....</b>	<b>139</b>
<b>9</b>	<b>REFERENCES.....</b>	<b>140</b>
<b>9.1</b>	<b>PART I – CONNECTIONS WITH FASTENERS LOADED IN SHEAR .....</b>	<b>140</b>
<b>9.2</b>	<b>PART II – CONNECTIONS WITH FASTENERS LOADED AXIALLY.....</b>	<b>142</b>
<b>9.3</b>	<b>PART III – BIOMIMICRY IN CONNECTIONS.....</b>	<b>142</b>
<b>10</b>	<b>APPENDIX.....</b>	<b>144</b>
<b>10.1</b>	<b>DETERMINATION OF CONSTANTS – BEAM ON ELASTIC FOUNDATION.....</b>	<b>144</b>
<b>10.2</b>	<b>DERIVATION OF THE RELATION <math>w(x) = Vbf_1(x) + Ff_2(x)</math>.....</b>	<b>148</b>
<b>10.3</b>	<b>DERIVATION OF THE RELATION <math>w(x) = Vbf_1(x) + Ff_2(x) = Vbf(x)</math>.....</b>	<b>150</b>
<b>10.4</b>	<b>COMPARISON TEST RESULTS – PARALLEL TO THE GRAIN TO MODEL .....</b>	<b>151</b>
<b>10.5</b>	<b>COMPARISON TEST RESULTS – PERPENDICULAR TO THE GRAIN TO MODEL.....</b>	<b>153</b>
<b>10.6</b>	<b>COMPARISON TEST RESULTS – BLOCK SHEAR SCREWS TO MODEL .....</b>	<b>153</b>

# 1 INTRODUCTION

In general there are two different groups of mechanical connections used in timber constructions considering the way of load support. Firstly, there are connections with fasteners loaded in shear. In these connections mainly dowels and bolts are used to transfer the load. Secondly, there are connections where the fasteners support the load axially. The most commonly used type of fasteners in this kind of connections is screws.

Design practice for both types is to calculate the strength of one fastener and, in order to obtain the resistance of the whole connection, to multiply this value with an effective number of common active fasteners ( $n_{ef}$ ), which is smaller than (or equal to) the actual number of fasteners of the connection. The reduction of the theoretically usable resistance per fastener in a connection with multiple connectors compared to the calculated strength of the single fastener originates in an accumulation of stresses, manufacturing imprecisions and imperfections of the timber [1], [2].

$$F_{\text{Connection}} = F_{\text{Single}} n_{ef} \quad 1.1$$

This way of dimensioning prevailed due to simplicity and the possibility to be quickly calculated by hand. Another reason is that there are so many parameters influencing the strength of a multiple fastener connection, that it seems meaningless to derive general approaches that are valid for all types of certain groups of multiple fastener connections.

To obtain  $n_{ef}$  for quantification of the group effect several approaches, which differ considerably have been developed and used all over the world; some of those equations consider more, some less parameters.

The approaches to obtain  $n_{ef}$  for shear- and axially loaded connections used in Eurocode [3] (and others used in different countries) are based on purely empirical models derived from results of a limited number of tests of certain kinds of connections. This model is, however, interpolated to and used as if it were valid for all possible unlimited configurations of connections. This might lead to an over- as well as an under estimation of the actual carrying capacity of the connection and thus either to the use of too much material by over-dimensioning the connection or in the worst case to failure due to a wrong assessment of the load carrying capacity.

Within this thesis the design practice of multiple fastener connections according to Eurocode [3] and some approaches to obtain  $n_{ef}$  are presented and discussed.

As far as connections with fasteners loaded in shear are concerned, design practice according to Eurocode [3] is discussed in chapter 2. The load paths within a connection are analysed, the most sensitive parts are presented and the influence of end fixities is shown in chapter 3. Furthermore in chapter 4 a way to analytically determine the stresses along a connection is depicted. Based on that, an analytical failure model accounting for the mechanics responsible for the group effect is derived and validated in chapter 5.

Connections with axially loaded fasteners are briefly presented and a model to consider block shear is derived and verified (chapter 7).

To conclude this thesis, an insight into biomimicry in timber engineering with a focus on connections is given in chapter 8 as well as certain ways to reduce peak stresses by shape optimisation are presented.

## **2 CONNECTIONS WITH FASTENERS LOADED IN SHEAR**

In the following chapter the design process according to Eurocode [3] is outlined and discussed. Firstly, the parameters governing the strength of a single fastener connection are presented, as well as Johansen's Yield Theory, the theory used in Eurocode [3] to determine the actual resistance of a single fastener connection, is shown, analysed and discussed critically. Secondly, some of the different approaches to calculate the overall strength of the multiple fastener connection are exhibited, compared and discussed.

### **2.1 Single Fastener Connections**

#### **2.1.1 General**

The strength of a single fastener connection loaded in shear is governed by the embedment strength of the timber, the yield bending capacity of the fastener, the withdrawal resistance of the fastener and the resistance of the timber against splitting [4].

However, the mechanical model used in Eurocode [3] uses mainly the embedment strength of the timber, the yield bending capacity of the fastener and geometrical parameters to determine the strength of a single fastener shear connection ( $F_{\text{Single}}$ ) as well as to predict the way of failure. Therefore, it can be argued that it implicitly also predicts the load – slip behaviour to a certain extent. The withdrawal resistance is also considered even though rather vaguely (as shown in chapter 2.1.5).

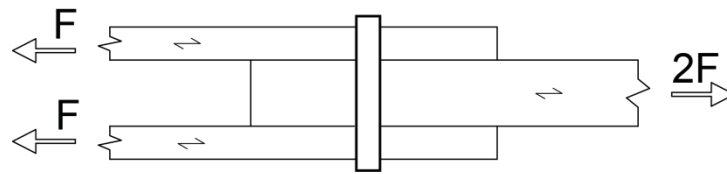


Figure 1: Symmetrical timber double shear single fastener connection

Shear connections can be characterised according to their stress-strain and failure behaviour by using the slenderness, thickness of a timber member divided by the fastener diameter, as the governing parameter. The higher the slenderness of a connection the more ductile is the load - slip behaviour and the failure mode [1], [5].

$$\lambda = \frac{t_i}{d} = C \sqrt{\frac{f_y}{f_h}} \quad 2.1$$

- $\lambda$  slenderness [-]
- $t_i$  thickness of a timber member [mm]
- $d$  (outer or nominal) diameter of the fastener [mm]
- $C$  constant [-]
- $f_y$  yield strength of the fastener [N/mm<sup>2</sup>]
- $f_h$  embedment strength of the timber [N/mm<sup>2</sup>]

### 2.1.2 Stress – Strain Behaviour

Regarding the slenderness of the connection it can be distinguished between stiff, intermediate and slender connections.

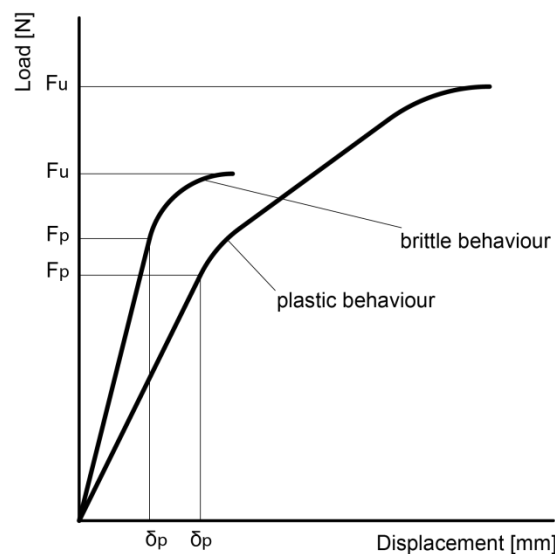


Figure 2: Different load-slip behaviours [1]

Stiff connections have a nearly linear elastic stress strain curve. Their so called proportional limit (stress limit until which the linear elasticity is valid) lies higher than that of slender connections, which however show remarkably more deformation at failure. This, a high bearing capacity and stiffness are features that are strongly demanded and required in contemporary constructions [1].

An example for an approach to mathematically depict the load-slip behaviour is the equation derived empirically by Foschi and Bonac (1977) [1] [11]. The relation (Eq. 2.2) is governed by the initial stiffness  $k_1$  (e. g. chapter 2.2.3), which depicts the slope of the first linear elastic branch of the graph as shown in Figure 3,  $k_2$ , which is responsible for the load level at which the plastic branch starts with a slope according to the stiffness  $k_3$ .

$$\sigma_h = (k_2 + k_3\delta) \left[ 1 - e^{-\frac{k_1\delta}{k_2}} \right] \quad 2.2$$

- $\sigma_h$                     embedment stress                    [N/mm<sup>2</sup>]
- $\delta$                             displacement                            [mm]

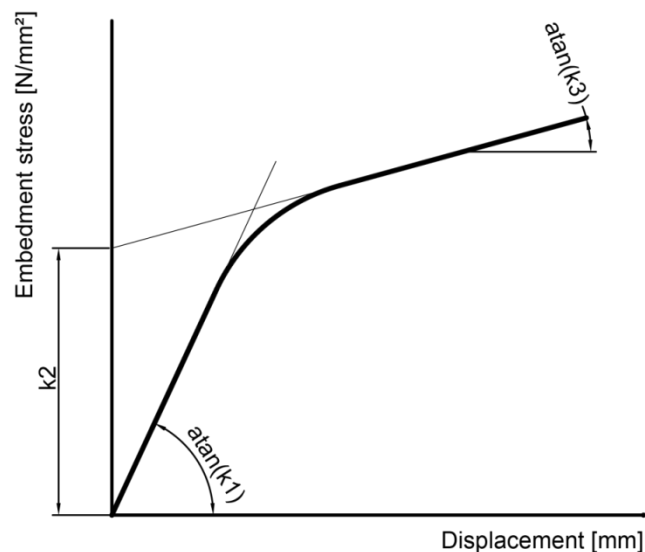


Figure 3: Load-slip relation by Foschi and Bonac (1977) [11]

The different possible load-slip behaviours result in different failure modes. In the following the different failure modes which occur and are covered in Eurocode [3] are described.

### 2.1.2.1 Brittle Failure

In a rigid connection the fastener is not deformed and in symmetrical connections the fastener hole is more or less equally stressed along the whole timber thickness. This type shows a nearly linear elastic stress – strain curve. There are rela-

tively small deformations at failure. In Eurocode [3] brittle failure is only determined by the embedment strength of the timber (and theoretically by the shear strength of the steel fastener as well which is in fact practically never governing). Tests have shown that premature failure might occur before the embedment strength is reached due to timber splitting [1]. This is considered in Eurocode [3] by minimum spacings among the fasteners and minimum distances towards the edges of the connection (introduced in chapter 2.2.2).

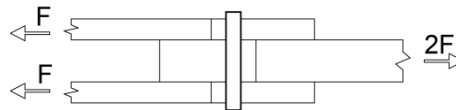


Figure 4: Brittle failure behaviour

### 2.1.2.2 Intermediate Failure

The intermediate behaviour at failure is more ductile than the rigid one. Bigger plastic deformations occur, the fastener is deformed and one plastic hinge in the connector per shear plane arises. So failure also depends (beside the embedment strength) on the bending capacity of the fastener (the yield moment). Even in symmetrical connections the embedment stress is not equally distributed along the fastener hole anymore [1], [2].

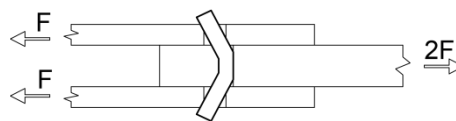


Figure 5: Intermediate failure behaviour

### 2.1.2.3 Ductile Failure

Connections with a high slenderness have the properties that are demanded in state-of-the-art structures. They show rather high plastic deformations at failure and the failure mode is characterised through the emergence of at least two plastic hinges per shear plane [1], [2].

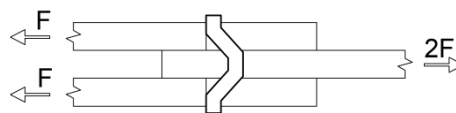


Figure 6: Ductile failure behaviour

## 2.1.3 Embedment Strength

The embedment strength is not a real material property, but rather a property that describes the resistance of the timber against a fastener loaded in shear [2].

According to Eurocode [3] the characteristic (5%-quantile) embedment strength of the timber (Norway spruce) loaded parallel to the grain with dowels and bolts can be determined with:

$$f_{h,0,k} = 0.082(1 - 0.01d)\rho_k \quad 2.3$$

- $\rho_k$  characteristic density of the timber at a moisture content of 12% [kg/m<sup>3</sup>]

Eq. 2.3 is (as visible) not an analytically derived equation, but it is based on regression calculations of test results where a dependency on the density and fastener diameter was found. The embedment strength increases with increasing density and decreases with increasing fastener diameter. The first relationship seems apparent and the second can be explained by stating that there is more wood compressed than just beneath the fastener and an increasing diameter does not mean that the amount of wood that is stressed beside the fastener increases. So, with increasing diameter the ratio between L (wood compressed beside the fastener) and d (diameter of the connector) goes down and therefore the embedment strength decreases [1].

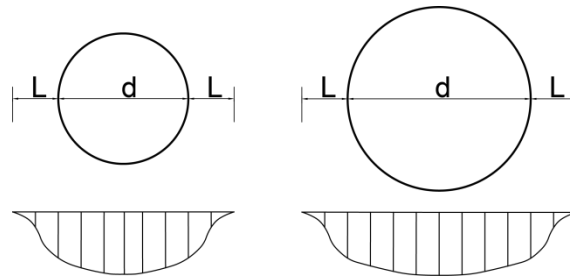


Figure 7: Changing fastener diameter (d) while the size of the wood compressed beside the fastener (L) remains the same

The characteristic embedment strength for another load angle can be obtained by:

$$f_{h,\alpha,k} = \frac{f_{h,0,k}}{k_{90} \sin^2 \alpha + \cos^2 \alpha} \quad 2.4$$

With:

$$k_{90} = \frac{f_{h,0}}{f_{h,90}} \quad 2.5$$

According to Eurocode [3], the ratio  $k_{90}$  can be determined as follows:

For softwoods:

$$k_{90} = 1.35 + 0.015d \quad 2.6$$

For hardwoods:

$$k_{90} = 0.95 + 0.015d \quad 2.7$$

- $f_{h,90}$       embedment strength perpendicular to the grain      [N/mm<sup>2</sup>]
- $\alpha$           angle between direction of the loading and the grain      [°]

Equations 2.6 and 2.7 show, that the diameter of the fastener also has an effect on the ratio between  $f_{h,0}$  and  $f_{h,90}$  ( $k_{90}$ ). In other words, the bigger the diameter the smaller the embedment strength in grain direction (Eq. 2.4) and the even smaller becomes the embedment strength perpendicular to the grain (Eq. 2.5, 2.6 and 2.7).

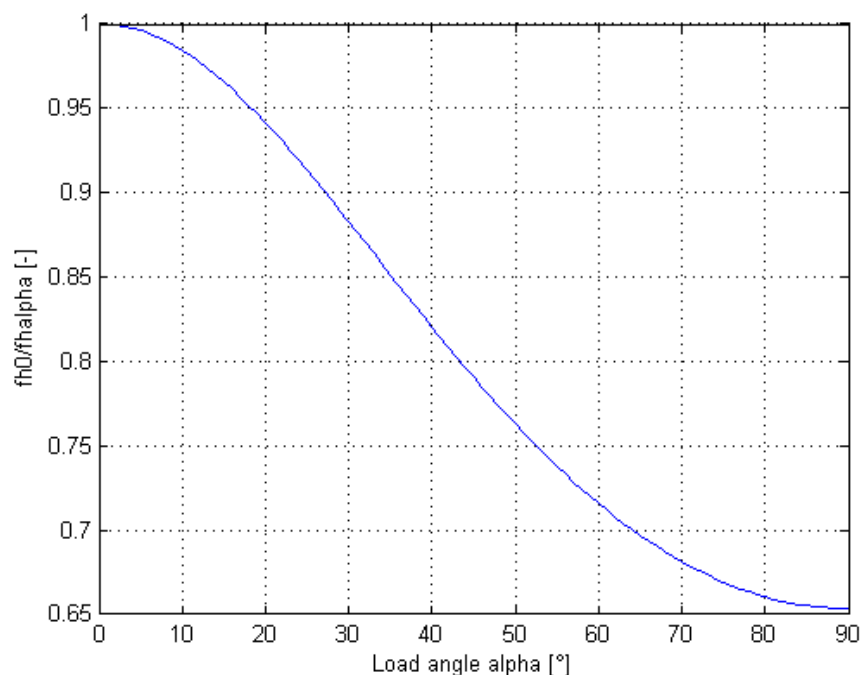


Figure 8: Reduction of embedment strength with increasing load angle ( $d = 12\text{mm}$ )

The embedment stress distribution used for calculation is idealised and distinguishes from the real one. Therefore, equation 2.8 is used to link the applied force to the occurring embedment stresses [1].

$$F_{\text{Fastener}} = \sigma_h t d \quad 2.8$$

- $\sigma_h$  embedment stress [N/mm<sup>2</sup>]

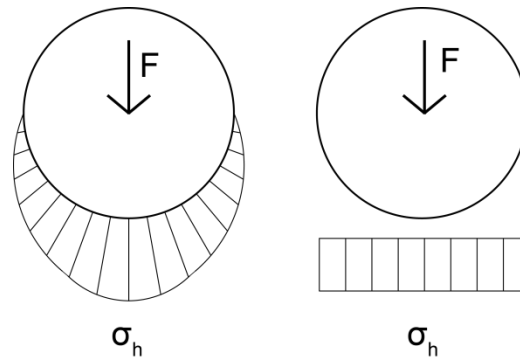


Figure 9: Comparison between the real embedment stress distribution and the stress distribution used in usual calculations

### 2.1.4 Yield Moment of the Fastener

The plastic moment of a fastener can theoretically be derived with:

$$M_y = 2 f_y z A = 2 f_y \frac{2d}{3\pi} \frac{d^2\pi}{4} = \frac{f_y d^3}{6} \quad 2.9$$

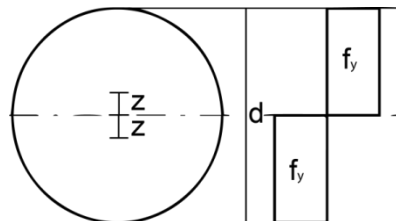


Figure 10: Stresses in a fastener subjected to plastic moment [2]

According to EN 409 [17], the yield capacity in bending can be determined by carrying out a four-point bending test. It is assumed that the maximum load carrying capacity in bending is reached at a bending angle of 45° (or at the angle failure occurs if it is less than 45°). A second possibility of obtaining the plastic bending moment is provided by EN 26891 [18]. Here a whole connection can be tested [1], [2].

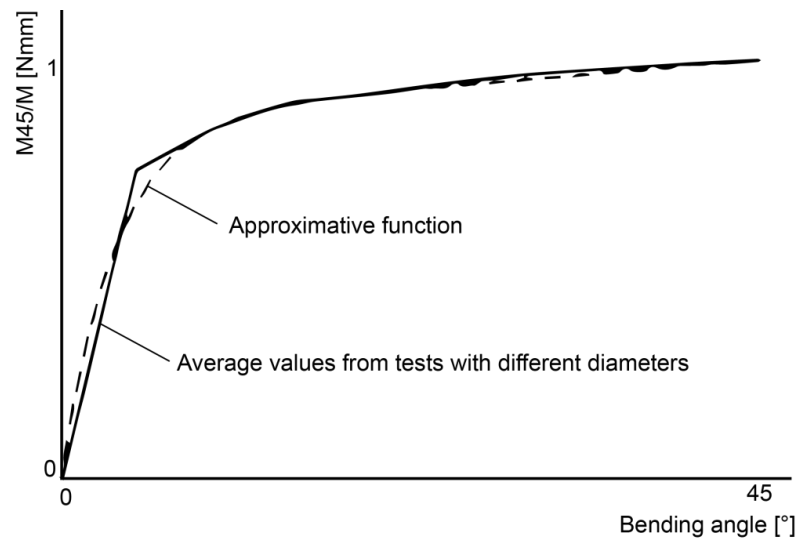


Figure 11: Relation between bending angle and bending moment [2]

However, tests with connections have shown that the bending angle at connection failure never reaches 45°. In cases of slender fasteners' failure it occurred between 8° and 15°, decreasing with increasing diameter (fastener diameters between 8 mm and 16 mm). For this reason, the theoretical bending moment might never be attained at failure [1], [2].

As provided in Eurocode [3], the yield moment of a fastener can be calculated with:

$$M_y = 0.3 f_{u,k} d^{2.6} \quad 2.10$$

- $f_{u,k}$  characteristic (5%-quantile) tensile strength of the fastener in bending [N/mm<sup>2</sup>]

Apparently the equation provided in Eurocode [3] (Eq. 2.10) differs from the theoretically derived one (Eq. 2.9). Eq. 2.10 employs the tensile strength ( $f_{u,k}$ ) of the fastener instead of the yield strength ( $f_{y,k}$ ), which for pure tension is generally about 0.6 times smaller, while in bending the yield strength is higher due to strain hardening in the steel [1]. Furthermore, the powers of the fastener diameters are different too. If the fact that a bending angle of 45° is practically never attained is also taken into consideration Eq. 2.10 might lead to more accurate results [2]. Both functions are compared in Figure 12 with the following parameters used.

- $f_{u,k} = 360 \text{ N/mm}^2$                        $f_{y,k} = 0.7 f_{u,k}$

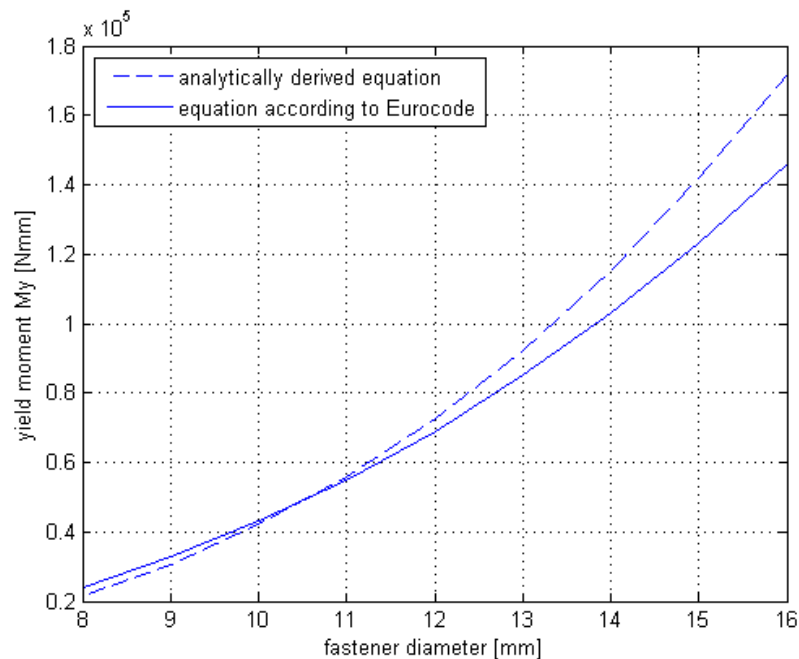


Figure 12: Comparison of the different functions to determine the yield moment of a fastener

Apparently the two functions do not considerably differ until the fastener diameters become rather high. Here, the equation in Eurocode [3] provides more conservative results.

### 2.1.5 Johansen's Yield Model

Johansen (1949) [19] derived a model that was later extended by Meyer (1957) [20] for the strength of a single fastener connection per shear plane which takes all the before presented failure modes into account. Failure is reached as soon as either the embedment strength is exceeded and/or the fastener yields [1], [2].

Which mode arises is dependent on the geometry of the connection, the plastic yielding moment of the fastener and the embedment strength of the timber members. The equations are derived by examining equilibrium in the connection at failure and by assuming an ideal plastic behaviour of the fasteners and the timber [2].

The following shear connection types are described in Johansen's model:

#### 2.1.5.1 Single Shear Timber Connection

The equations determining the force  $F$  for the different failure modes that can occur according to Johansen's Yield Theory are derived for a single shear timber – timber connection in the following:

It shall be:

$$\beta = \frac{f_{h2}}{f_{h1}} \quad 2.11$$

Failure Mode Ia - brittle:

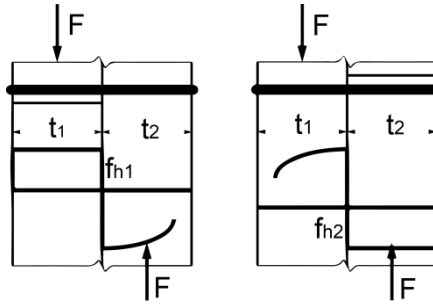


Figure 13: Failure mode Ia - brittle

Vertical forces equilibrium per timber member yields:

$$F = f_{h1} t_1 d \quad 2.12$$

$$F = f_{h2} t_2 d = \beta f_{h1} t_2 d \quad 2.13$$

Failure Mode Ib – brittle:

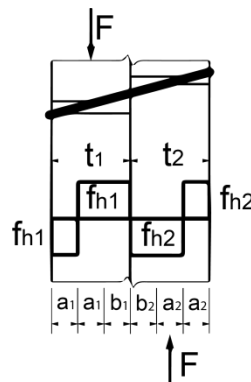


Figure 14: Failure mode Ib - brittle

Vertical forces equilibrium per timber member:

$$F = f_{h1} b_1 d = f_{h2} b_2 d = \beta f_{h1} b_2 d \quad 2.14$$

Following:

$$b_1 = \beta b_2 \quad 2.15$$

A moment equilibrium of the internal forces around the shear gap results in:

$$f_{h1}d \left[ -a_1 \left( \frac{3a_1}{2} + b_1 \right) + \frac{(a_1 + b_1)^2}{2} \right] - f_{h2}d \left[ a_2 \left( \frac{3a_2}{2} + b_2 \right) - \frac{(a_2 + b_2)^2}{2} \right] = 0 \quad 2.16$$

$$f_{h1}d \left( -a_1^2 + \frac{b_1^2}{2} \right) - \beta f_{h1}d \left( a_2^2 - \frac{b_2^2}{2} \right) = 0 \quad 2.17$$

$$-a_1^2 + \frac{b_1^2}{2} - \beta a_2^2 + \frac{\beta b_2^2}{2} = 0 \quad 2.18$$

Include Eq. 2.15:

$$-a_1^2 + \frac{b_1^2}{2} - \beta a_2^2 + \frac{b_1^2}{2\beta} = 0 \quad 2.19$$

With  $a_1 = \frac{t_1 - b_1}{2}$  and  $a_2 = \frac{t_2 - b_2}{2}$ :

$$-\frac{(t_1 - b_1)^2}{4} + \frac{b_1^2}{2} - \frac{\beta \left( t_2 - \frac{b_1}{\beta} \right)^2}{4} + \frac{b_1^2}{2\beta} = 0 \quad 2.20$$

$$-\frac{t_1^2}{4} + \frac{t_1 b_1}{2} - \frac{b_1^2}{4} + \frac{b_1^2}{2} - \frac{\beta t_2^2}{4} + \frac{t_2 b_1}{2} - \frac{b_1^2}{4\beta} + \frac{b_1^2}{2\beta} = 0 \quad 2.21$$

$$b_1^2 \left( -\frac{1}{4} + \frac{1}{2} - \frac{1}{4\beta} + \frac{1}{2\beta} \right) + b_1 \left( \frac{t_1}{2} + \frac{t_2}{2} \right) - \frac{t_1^2}{4} - \frac{\beta t_2^2}{4} = 0 \quad 2.22$$

$$\frac{b_1^2}{4} \left( \frac{\beta + 1}{\beta} \right) + \frac{b_1}{2} (t_1 + t_2) - \frac{1}{4} (t_1^2 + \beta t_2^2) = 0 \quad 2.23$$

Solving Eq. 2.23 equation for  $b_1$  leads to:

$$b_1 = \frac{t_1}{1 + \beta} \left[ \sqrt{\beta + 2\beta^2 \left[ 1 + \frac{t_2}{t_1} + \left( \frac{t_2}{t_1} \right)^2 \right] + \beta^3 \left( \frac{t_2}{t_1} \right)^2} - \beta \left( 1 + \frac{t_2}{t_1} \right) \right] \quad 2.24$$

The carrying capacity for this failure mode can be obtained by inserting Eq. 2.24 into Eq. 2.12:

$$F = \frac{f_{h1} t_1 d}{1 + \beta} \left[ \sqrt{\beta + 2\beta^2 \left[ 1 + \frac{t_2}{t_1} + \left( \frac{t_2}{t_1} \right)^2 \right] + \beta^3 \left( \frac{t_2}{t_1} \right)^2} - \beta \left( 1 + \frac{t_2}{t_1} \right) \right] \quad 2.25$$

According to Eurocode [3] the equation for this failure mode is:

$$F_d = \frac{f_{h1,d} t_1 d}{1 + \beta} \left[ \sqrt{\beta + 2\beta^2 \left[ 1 + \frac{t_2}{t_1} + \left( \frac{t_2}{t_1} \right)^2 \right] + \beta^3 \left( \frac{t_2}{t_1} \right)^2} - \beta \left( 1 + \frac{t_2}{t_1} \right) \right] + \frac{F_{ax,d}}{4} \quad 2.26$$

As apparent the factor  $\frac{F_{ax,d}}{4}$  is not obtained by the derivation in Eq. 2.25. It was added to incorporate the withdrawal capacity of a fastener with end fixities (washer and nut). In that case, an additional axial force is introduced in the fastener which, in consequence, increases the overall carrying capacity of a single fastener connection. This is the so called “rope effect” and is examined in more detail in chapter 3.1.2.

*Failure Mode II – intermediate*

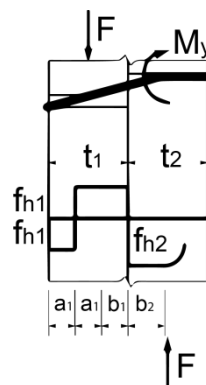


Figure 15: Failure mode II - intermediate

Vertical equilibrium per timber member again shows:

$$F = f_{h1} b_1 d = f_{h2} b_2 d = \beta f_{h1} b_2 d \quad 2.27$$

$$b_1 = \beta b_2 \quad 2.28$$

Moment equilibrium of internal forces and moments around the shear plane yields:

$$f_{h1} d \left[ \frac{(a_1 + b_1)^2}{2} - a_1 \left( \frac{3}{2} a_1 + b_1 \right) \right] + f_{h2} d \frac{b_2^2}{2} - M_y = 0 \quad 2.29$$

$$f_{h1} d \left[ \frac{a_1^2}{2} + a_1 b_1 + \frac{b_1^2}{2} - \frac{3}{2} a_1^2 - a_1 b_1 + \frac{\beta b_2^2}{2} \right] - M_y = 0 \quad 2.30$$

$$f_{h1} d \left[ -a_1^2 + \frac{b_1^2}{2} + \frac{\beta b_2^2}{2} \right] - M_y = 0 \quad 2.31$$

With  $a_1 = \frac{t_1 - b_1}{2}$  and Eq. 2.28:

$$f_{h1} d \left[ -\frac{(t_1 - b_1)^2}{4} + \frac{b_1^2}{2} + \frac{b_1^2}{2\beta} \right] - M_y = 0 \quad 2.32$$

$$-\frac{t_1^2}{4} + \frac{t_1 b_1}{2} - \frac{b_1^2}{4} + \frac{b_1^2}{2} + \frac{b_1^2}{2\beta} - \frac{M_y}{f_{h1} d} = 0 \quad 2.33$$

$$b_1^2 \left( -\frac{1}{4} + \frac{1}{2} + \frac{1}{2\beta} \right) + b_1 \frac{t_1}{2} - \frac{t_1^2}{4} - \frac{M_y}{f_{h1} d} = 0 \quad 2.34$$

$$b_1^2 \left( \frac{\beta + 2}{4\beta} \right) + b_1 \frac{t_1}{2} - \frac{t_1^2}{4} - \frac{M_y}{f_{h1} d} = 0 \quad 2.35$$

Solving Eq. 2.35 for  $b_1$  gives the following result:

$$b_1 = \frac{t_1}{2 + \beta} \left[ \sqrt{2\beta(1 + \beta) + \frac{4\beta(2 + \beta)M_y}{f_{h1} d t_1^2}} - \beta \right] \quad 2.36$$

Inserting this into Eq. 2.27 yields:

$$F = \frac{f_{h1} t_1 d}{2 + \beta} \left[ \sqrt{2\beta(1 + \beta) + \frac{4\beta(2 + \beta)M_y}{f_{h1} d t_1^2}} - \beta \right] \quad 2.37$$

According to Eurocode [3] the equation for this failure mode is:

$$F_d = 1.05 \frac{f_{h1,d} t_1 d}{2 + \beta} \left[ \sqrt{2\beta(1 + \beta) + \frac{4\beta(2 + \beta)M_{y,d}}{f_{h1,d} d t_1^2}} - \beta \right] + \frac{F_{ax,d}}{4} \quad 2.38$$

Again it is noticeable that the withdrawal resistance for connectors with end fixities has been included in Eurocode [3]. Moreover, there is an additional empirical factor 1.05 increasing the strength of the connection. This is because according to Eurocode [3] the strength of a single fastener connection is to be calculated with characteristic values and is brought to design level later on. To account for the different partial safety factors of timber (1.30 for sawn timber and 1.25 for glulam) and steel (1.10 for steel parts subjected to bending) the above mentioned value has been introduced.

A very similar derivation can be conducted for a plastic hinge in the other timber member which is why it is not presented here. The failure mode would exhibit this image:

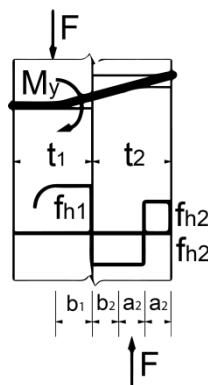


Figure 16: Failure mode II - intermediate

The load carrying capacity according to Eurocode [3] is:

$$F_d = 1.05 \frac{f_{h1,d} t_2 d}{1 + 2\beta} \left[ \sqrt{2\beta^2(1 + \beta) + \frac{4\beta(1 + 2\beta)M_{y,d}}{f_{h1,d} d t_2^2}} - \beta \right] + \frac{F_{ax,d}}{4} \quad 2.39$$

*Failure Mode III – ductile*

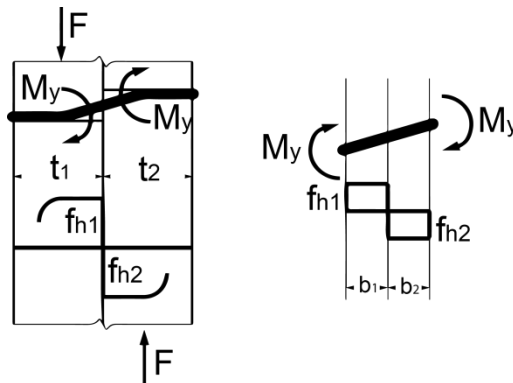


Figure 17: Failure mode III - ductile

Vertical equilibrium per shear plane gives:

$$F = f_{h1} d b_1 = f_{h2} d b_2 = \beta f_{h1} d b_2 \quad 2.40$$

$$b_1 = \beta b_2 \quad 2.41$$

Moment equilibrium around the shear plane results in:

$$f_{h1} d \frac{b_1^2}{2} + f_{h2} d \frac{b_2^2}{2} - 2M_y = 0 \quad 2.42$$

With Eq. 2.41:

$$f_{h1} d b_1^2 \left( \frac{\beta + 1}{2\beta} \right) - 2M_y = 0 \quad 2.43$$

$$b_1 = \sqrt{\frac{2M_y}{f_{h1} d} \left( \frac{2\beta}{1 + \beta} \right)} \quad 2.44$$

Inserted in Eq. 2.40:

$$F = \sqrt{2M_y f_{h1} d \left( \frac{2\beta}{1 + \beta} \right)} \quad 2.45$$

According to Eurocode [3] the resistance is calculated with:

$$F = 1.15 \sqrt{\frac{2\beta}{1 + \beta}} \sqrt{2M_{y,d} f_{h1,d} d + \frac{F_{ax,d}}{4}} \quad 2.46$$

Figure 18 graphically depicts the different failure modes that can emerge over the member thicknesses  $t_1$  and  $t_2$ . The values have been calculated with characteristic values according to Johansen [19], [20]. This is also the case for the following figures in this section. The following parameters were used to create the figure:

- $d = 12 \text{ mm}$        $\rho_1 = 400 \text{ kg/m}^3$        $\rho_2 = 400 \text{ kg/m}^3$        $f_u = 360 \text{ N/mm}^2$

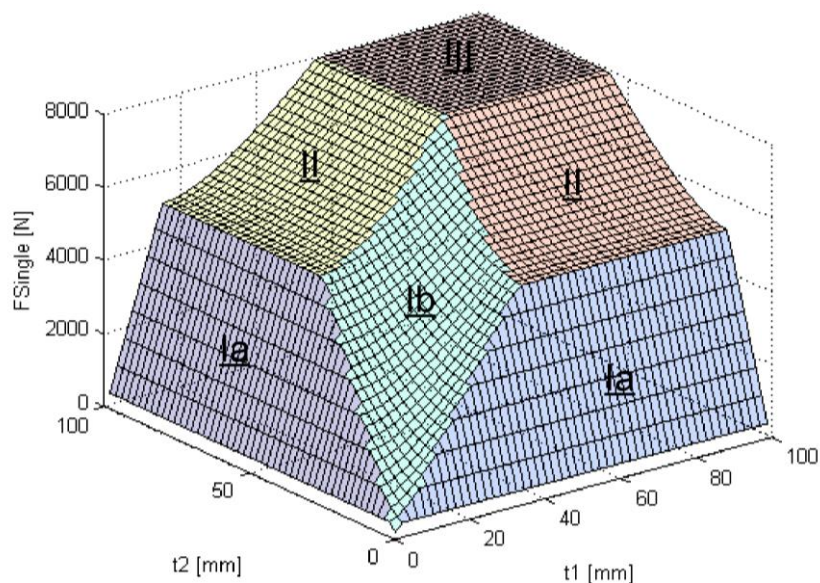


Figure 18: Failure surface of a single shear timber connection

The different failure modes are easily distinguishable by the different shapes and colours of the surface. The failure load of the single fastener connection, dependent on  $t_1$  and  $t_2$  lies on the presented surface.

### 2.1.5.2 Double Shear Timber Connection

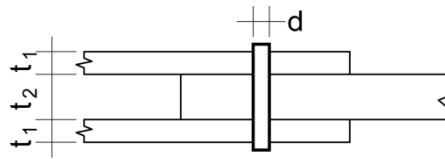


Figure 19: Single fastener double shear timber connection

The derivation of the ultimate bearing load of the connection in the different failure modes works equally to the above presented. Therefore, it is not further conducted for the shown equations. However these are the equations to be found in Eurocode [3] governing the strength of a symmetrical double shear timber connection per shear gap. In the following equations the design values ( $f_{h,d}$ ,  $M_{y,d}$ ,  $F_{ax,d}$ ,  $F_d$ ) are used according to Eurocode [3]:

*Failure mode I – brittle*

$$F = f_{h1}t_1d \quad 2.47$$

$$F = 0.5f_{h2}t_2d \quad 2.48$$

The failure mode Ib cannot emerge since the symmetry of the connection prevents it.

*Failure mode II – intermediate*

$$F = 1.05 \frac{f_{h1}t_1d}{2 + \beta} \left[ \sqrt{2\beta(1 + \beta) + \frac{4\beta(2 + \beta)M_y}{f_{h1}dt_1^2}} - \beta \right] + \frac{F_{ax}}{4} \quad 2.49$$

*Failure mode III – ductile*

$$F = 1.15 \sqrt{\frac{2\beta}{1 + \beta}} \sqrt{2M_y f_{h1}d + \frac{F_{ax}}{4}} \quad 2.50$$

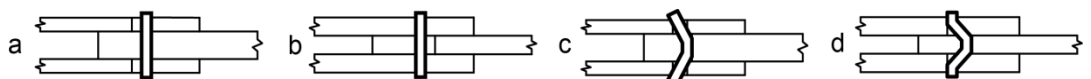


Figure 20: Johansen failure modes for a single fastener double shear timber connection (a: mode I - outer members, b: mode I - inner members, c: mode II, d: mode III)

The different failure modes that can emerge are depicted graphically over the member thicknesses  $t_1$  and  $t_2$  in Figure 19 by using the following parameters.

- $d = 12 \text{ mm}$        $\rho_1 = 400 \text{ kg/m}^3$        $\rho_2 = 400 \text{ kg/m}^3$        $f_u = 360 \text{ N/mm}^2$

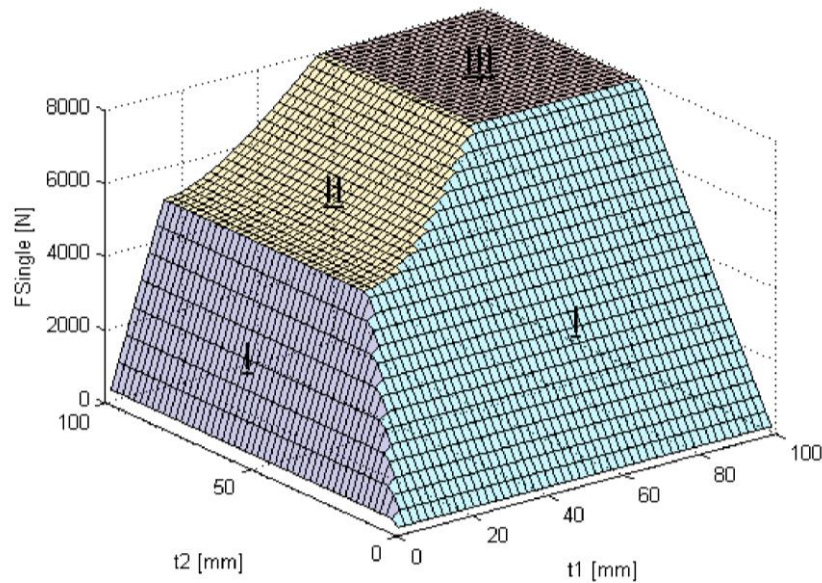


Figure 21: Failure surface per shear plane of a double shear timber connection

The actual resistance  $F_{\text{Single}}$  of the single fastener connection can be calculated with:

$$F_{\text{Single}} = \min[F_i] \cdot s \quad 2.51$$

- $s$       number of shear planes      [-]

### 2.1.5.3 Single Shear Timber – Steel Connection with Outer Thin Steel Plate

Thin steel plate:  $t \leq 0.5d$

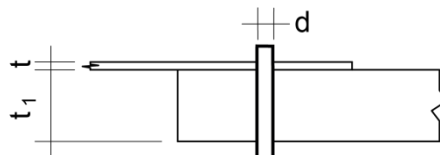


Figure 22: Single fastener single shear timber steel connection (thin steel plate)

Failure mode I – brittle:

$$F = 0.4f_{h2}t_2d \quad 2.52$$

Failure mode II cannot occur due to the geometry of the connection.

*Failure mode III – ductile:*

$$F = 1.15 \sqrt{2M_y f_{h2} d} + \frac{F_{ax}}{4} \quad 2.53$$

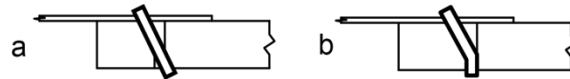


Figure 23: Single fastener single shear timber steel connection (thin steel plate) failure modes (a: mode I, b: mode III)

#### 2.1.5.4 Single Shear Timber – Steel Connection with Outer Thick Steel Plate

Thick steel plate:  $t \geq d$

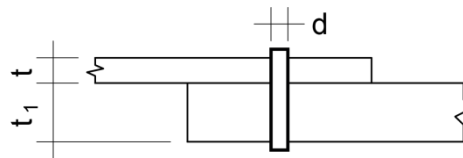


Figure 24: Single fastener single shear timber steel connection (thick steel plate)

*Failure mode I – brittle:*

$$F = f_{h2} t_2 d \quad 2.54$$

*Failure mode II – intermediate:*

$$F = f_{h2} t_2 d \left[ \sqrt{2 + \frac{4M_y}{f_{h2} d t_2^2}} - 1 \right] + \frac{F_{ax}}{4} \quad 2.55$$

*Failure mode III – ductile:*

$$F = 2.3 \sqrt{M_y f_{h2} d} + \frac{F_{ax}}{4} \quad 2.56$$



Figure 25: Single fastener single shear timber steel connection (thick steel plate) failure modes (a: mode I, b: mode II, c: mode III)

For an intermediate  $\frac{t}{d}$  ratio a linear interpolation between the load carrying capacities is required.

The different failure modes that can emerge depicted graphically over the timber member thickness  $t_2$  and the steel plate thickness to fastener diameter ratio are shown in Figure 26 with the following parameters used.

- $d = 12 \text{ mm}$        $\rho_2 = 400 \text{ kg/m}^3$        $f_u = 360 \text{ N/mm}^2$

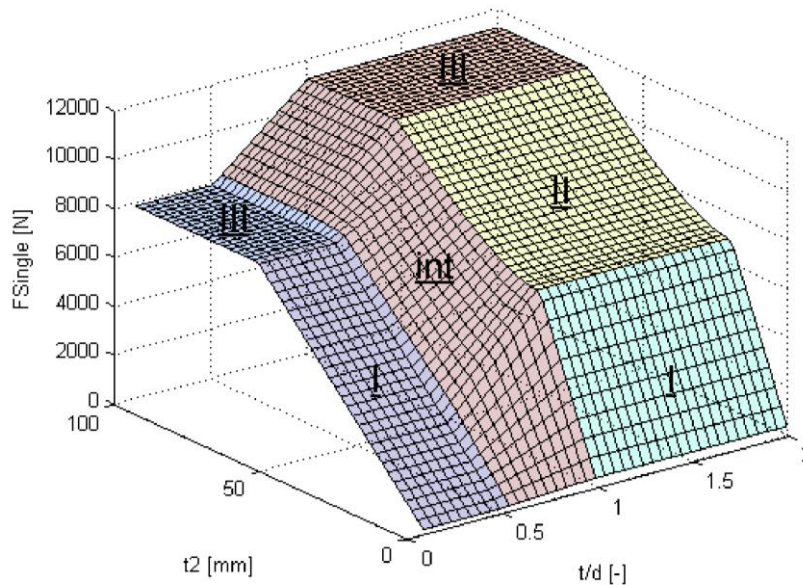


Figure 26: Failure surface of a single shear steel-timber-connection

### 2.1.5.5 Double Shear Timber – Steel Connection with Inner Steel Plate

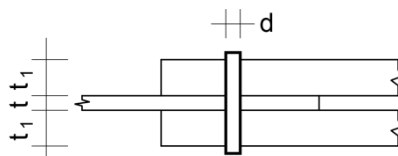


Figure 27: Single fastener double shear timber steel connection with inner steel plate

*Failure mode I – brittle:*

$$F = f_{h1} t_1 d \quad 2.57$$

*Failure mode II – intermediate:*

$$F = f_{h1}t_1d \left[ \sqrt{2 + \frac{4M_y}{f_{h1}dt_1^2} - 1} \right] + \frac{F_{ax}}{4} \quad 2.58$$

*Failure mode III – ductile:*

$$F = 2.3 \sqrt{M_y f_{h1} d + \frac{F_{ax}}{4}} \quad 2.59$$



Figure 28: Single fastener double shear timber steel connection with inner steel plate failure modes (a: mode I, b: mode II, c: mode III)

Figure 29 shows the different failure modes that can emerge over the timber member thickness  $t_1$ , with these parameters used to create it:

- $d = 12 \text{ mm}$        $\rho_1 = 400 \text{ kg/m}^3$        $f_u = 360 \text{ N/mm}^2$

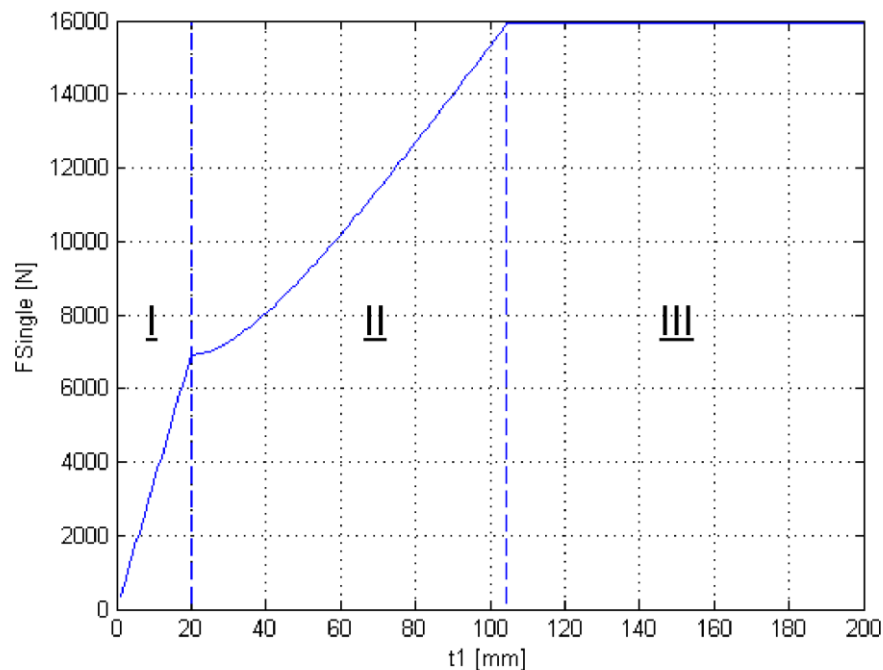


Figure 29: Failure Line of a T-S-T-Connection per shear plane

The actual resistance  $F_{Single}$  of the single fastener connection can be calculated with:

$$F_{\text{Single}} = \min[F_i] \cdot s \quad 2.60$$

### 2.1.5.6 Double Shear Steel – Timber Connection with Outer Thin Steel Plates

Thin steel plate:  $t \leq 0.5d$

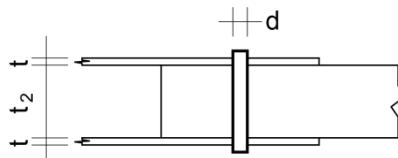


Figure 30: Double shear single fastener timber steel connection with outer (thin) steel plates

*Failure mode I – brittle:*

$$F = 0.5f_{h2}t_2d \quad 2.61$$

Failure mode II cannot emerge as the steel plates prevent the fastener from deforming like that.

*Failure mode III – ductile:*

$$F = 1.15 \sqrt{2M_y f_{h2} d} + \frac{F_{ax}}{4} \quad 2.62$$



Figure 31: Double shear single fastener timber steel connection with outer (thin) steel plates, failure modes (a: mode I, b: mode III)

### 2.1.5.7 Double Shear Steel – Timber Connection with Outer Thick Steel Plates

Thick steel plate:  $t \geq d$

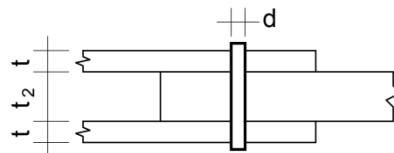


Figure 32: Double shear single fastener timber steel connection with outer (thick) steel plates

*Failure mode I – brittle:*

$$F = 0.5f_{h2}t_2d \quad 2.63$$

Failure mode II again cannot emerge because the steel plates prevent the fastener from deforming like that.

*Failure mode III – ductile:*

$$F = 2.3 \sqrt{M_y f_{h2} d + \frac{F_{ax}}{4}} \quad 2.64$$



Figure 33: Double shear single fastener timber steel connection with outer (thick) steel plates, failure modes (a: mode I, b: mode III)

For an intermediate  $\frac{t}{d}$  ratio a linear interpolation between the failure strengths is required.

The different failure modes that can emerge are depicted graphically in Figure 34 over the timber member thickness  $t_2$  and the steel plate thickness to fastener diameter ratio with the following parameters used:

- $d = 12 \text{ mm}$        $\rho_2 = 400 \text{ kg/m}^3$        $f_u = 360 \text{ N/mm}^2$

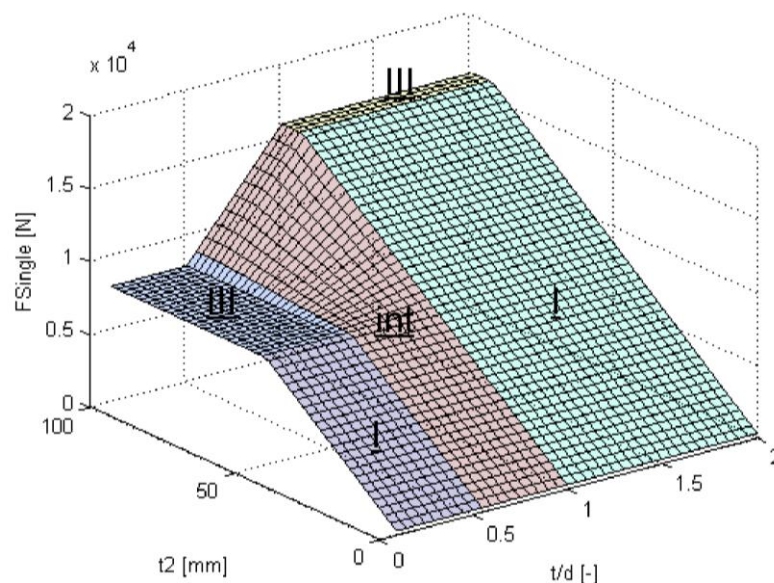


Figure 34: Failure surface of a double shear S-T-S-Connection per shear plane

The actual resistance  $F_{\text{Single}}$  of the single fastener connection can be calculated with:

$$F_{\text{Single}} = \min[F_i] \cdot s \quad 2.65$$

### 2.1.5.8 Multiple Shear Connections

Extending the presented types to multiple shear connections simply requires a combination according to the connection that has to be dimensioned.

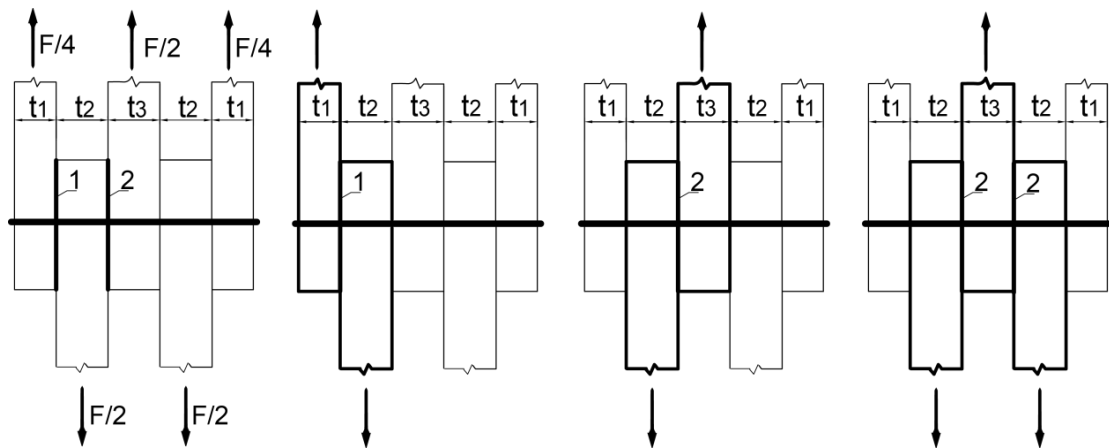


Figure 35: Calculation process for multiple shear connections; here two geometrically different shear planes have to be considered and all the possible Johansen type connections that can possibly cover these shear planes have to be accounted for individually.

The connection is virtually split into types covered by the Johansen equations. For every shear plane the load carrying capacity is determined by using every Johansen type the connection members bordering the plane can possibly create. Afterwards the smallest carrying capacity per shear plane is summed up to the actual carrying capacity of the multiple fastener connection [2].

It has to be remarked that some of the failure modes that might occur in a real Johansen-Type connection are not able to emerge in the virtually cut out one, as geometrical and material restraints keep them from arising. In other words, the bending line of the fastener has to be able to emerge in reality. So, only the failure modes that actually can occur due to the geometry and due to the materials used in the multiple fastener connection have to be taken into consideration [2].

### 2.1.5.9 Benefits and Limitations of Johansen's Yield Theory

Generally, it has to be stated that the Johansen equations constitute a mechanical model based on a limited data set which can also be extrapolated to other combinations of parameters that have not yet been tested. Even though this might seem appealing at first sight since the number of combinations of the pa-

parameters representing a single fastener connection is infinite, there is a huge uncertainty if this model can depict the real behaviour of all the possible cases appropriately [4].

One limitation of the model is that it does not consider that timber splitting can occur in rigid connections prematurely to the predicted carrying capacity of mode I [1]. Although minimum distances have been introduced to avoid this, it is not entirely clear if this measure is sufficient to get rid of premature timber splitting completely as minimum distances are (again) just based on a limited number of test results of limited connection configurations. An analytical model that accounts for it would be preferable.

Furthermore, friction that might emerge between the timber members as well as the timber and the fastener introducing a force that acts against load direction and thereby increases the resistance of the connection is not taken into account [2].

Possible end fixities of connectors cause additional tensile axial forces in the fasteners that are responsible for force components acting against the load direction and components that increase friction between the members, which, as a consequence, heightens the connection strength (i.e. “rope-effect”). This effect is also not considered in Johansen’s model and only rather roughly in Eurocode [2], [3]. However, it is questionable if such fixities shall be taken into consideration at all as the actual transferable axial force depends on several factors like shape and area of the fixity, if a pre-stressing is applied, the difference in humidity of the timber during construction and later on (shrinkage if the timber dries out which has a loss of a potential pre-stressing as consequence) as well as possible imprecisions in the manufacturing process [7].

It has been shown that the humidity influences the behaviour of the timber in terms of ductility. The drier the wood the higher is the tendency to fail brittle caused by cracking and vice versa [7]. This influencing parameter however isn’t accounted for either.

As it will be discussed in chapter 4.1.4, there is a difference in the stress situation in a timber member if the connection is loaded in tension or compression. In a member loaded in tension, the stresses have to take a “detour” around the fasteners which leads to higher stresses perpendicular to the grain and thus a higher likelihood of failure at lower loads. Jorissen (1998), however, just found a slight difference in failure loads concerning the kind of loading in tests but this just applies to a limited set of tests of a limited number of configurations of symmetrical double shear timber-timber connections loaded in grain direction [1]. In other connection types and configurations this might have a stronger and more serious effect on the load carrying capacity. The potential influence of this difference in loading is not accounted for in the contemporary design process in Eurocode [3].

To derive the Yield Model, Johansen assumed an ideal plastic behaviour of the timber and the steel as soon as failure is attained and the described failure modes develop. This simplification renders calculations remarkably easier and has little impact on the result. Johansen conducted tests to validate the results of the Yield Model. The set-up was a row of multiple fasteners in grain direction with a spacing among the connectors of 10 times the fastener diameter and a loaded edge distance in grain direction of 7 times the diameter. It was assumed that edge distance and spacing were chosen large enough to guarantee that no negative interaction (stress accumulation) between the fasteners would be taking place, so the results would also hold valid for a single fastener connection. The tests showed a good agreement with the predicted loads as long as the influence of the rope-effect was negligibly small [2]. It is questionable if there is really no stress accumulation at this loaded edge distance and spacing among the fasteners. The current version of Eurocode [3] assumes little interaction even at a spacing that is 13 times the fastener diameter among the connectors in grain direction (see chapter 2.2.3.1). If there is still interaction between fasteners at a spacing of  $10d$  it could be that Johansen's equations provide little conservative results for the single fastener connection.

However, if the influence of these effects remains small, the Johansen theory will serve as a good approximation of reality [1]. Furthermore, it is a mechanical model and therefore superior to purely empirical models. As it describes the mechanical behaviour, it is not as sensitive to a variation of parameters as empirical models tend to be [4].

Due to its simplicity and a consensus among the engineers in using it, this model has prevailed until now and is used in the Eurocode [3] as well as many other codes around the world to determine the strength of a connection with one single fastener.

---

## 2.2 Multiple Fastener Shear Connection

### 2.2.1 General

The same influences governing the strength of a single fastener connection determine the resistance of a multiple fastener connection too. Nevertheless there are some more effects a multiple fastener connection is especially sensitive to such as material imperfections, fabrication tolerances, manufacturing imprecisions and therefore uneven load distribution and different load slip-behaviours among the connectors as well as the arrangement of the fasteners [5].

Overall, the distribution of stresses among the connection, the deformation of the single fasteners as well as the connection as such is harder to predict and there-

fore more complicated to calculate and design. There is a variety of failure images, some of which are presented in Figure 36:

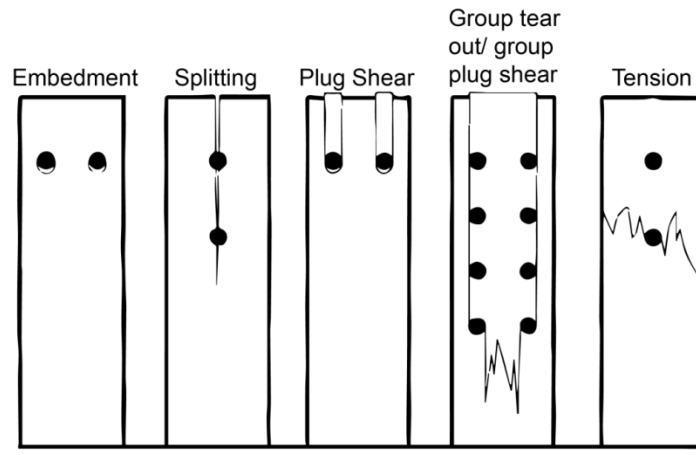


Figure 36: Some of the different failure types [1]

### 2.2.2 Minimum Spacings and Distances

Minimum distances and spacings for the fasteners have been introduced to avert stress accumulation of tensile stresses perpendicular to the grain and shear stresses, which are responsible for premature cracking of the timber as those stresses are not considered explicitly in calculation and to grant a proper load transfer throughout the connection [2].

Another failure phenomenon that shall be avoided by demanding engineers to comply with the minimum distances is plug shear of a group of fasteners. It can occur if dowel type fasteners with large diameter are used or the connectors are situated within great proximity. Failure does not occur through exceeding the embedment strength of a timber member, the yield carrying capacity of the fastener or tensile stresses perpendicular to the grain but through shear stresses along the line of connectors in direction of the grain. If there are at least two lines of fasteners in grain direction the result is that the whole wood bordered by the fasteners shears out [2].

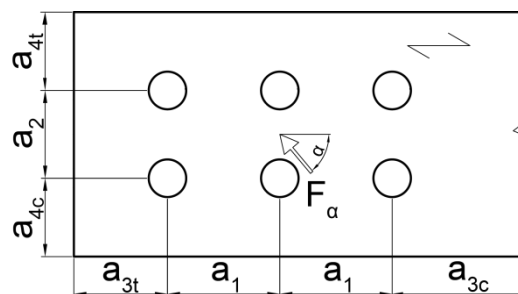


Figure 37: Minimum distances and spacings

- $a_1$  spacing between the fasteners parallel to the grain [mm]
- $a_2$  spacing between the fasteners perpendicular to the grain [mm]
- $a_{3t}$  distance at loaded end grain [mm]
- $a_{3c}$  distance at unloaded end grain [mm]
- $a_{4t}$  loaded edge distance [mm]
- $a_{4c}$  unloaded edge distance [mm]

The minimum distances according to Eurocode [3] are presented in Table 1.

Table 1: Minimum distances for multiple fastener connections loaded in shear [3]

spacing and distance	dowels	bolts
$a_1$	$(3 + 2 \cos\alpha )d$	$(4 +  \cos\alpha )d$
$a_2$	$3d$	$4d$
$a_{3t}$	$\max[7d; 80\text{mm}]$	$\max[7d; 80\text{mm}]$
$a_{3c}$	$\max[a_{3t} \sin\alpha ; 3d]$	$\max[(1 + 6\sin\alpha)d; 4d]$
$a_{4t}$	$\max[(2 + 2\sin\alpha)d; 3d]$	$\max[(2 + 2\sin\alpha)d; 3d]$
$a_{4c}$	$3d$	$3d$

### 2.2.3 Design with Normal- and Shear Force

If there are only normal and shear forces acting on the centre of gravity of a connection, the established practice is to multiply the strength of a single fastener, obtained through employing the Johansen equations with a certain  $n_{ef}$ , which is equal or smaller than the actual number of connectors used.

The actual force a connection with multiple fasteners can transfer is smaller than the force a single connector is able to withstand times the number of connectors used. This might be the case due to a stress accumulation of shear stresses and tensile stresses perpendicular to the grain, imperfections in the timber specimen as well as imprecisions in the manufacturing process of the connection [1], [2].

However many ways to determine “n-effective” have been developed, some of them are presented in the following paragraphs.

### 2.2.3.1 $n_{ef}$ according to Eurocode 1995-1-1

The equation for  $n_{ef}$  presented by Eurocode 1995-1-1 [3] is purely empirical and considers the spacing between the fasteners in grain direction, the connector diameter and the load angle to the grain.

$$n_{ef} = n^{0.9} \sqrt[4]{\frac{a_1}{13d}} \frac{90 - \alpha}{90} + n \frac{\alpha}{90} \leq n \quad 2.66$$

For a load angle of  $0^\circ$  (load parallel to the grain) Eq. 2.66 simplifies to:

$$n_{ef} = n^{0.9} \sqrt[4]{\frac{a_1}{13d}} = 0.5266 n^{0.9} \left(\frac{a_1}{d}\right)^{0.25} \leq n \quad 2.67$$

For a load angle of  $90^\circ$  (load perpendicular to the grain) however Eq. 2.66 is reduced to:

$$n_{ef} = n \quad 2.68$$

Thus no reduction has to be taken into consideration.

### 2.2.3.2 Equations of Jorissen

The first design rule proposed by Jorissen (1998) [1] takes the spacing between the fasteners in grain direction, as well as the slenderness calculated with the middle timber member (and thus limited to symmetrical double shear timber connections) into account. Eq. 2.69 was obtained empirically by examining a vast number of results of conducted symmetrical double shear timber connection tests and comparing them to values determined with the Johansen equations [1].

$$n_{ef} = 0.37 n^{0.9} \left(\frac{a_1}{d}\right)^{0.3} \left(\frac{t_m}{d}\right)^{0.2} \leq n \quad 2.69$$

- $t_m$  thickness of the middle timber member [mm]

The second simplified design rule (Eq. 2.70) does not consider the slenderness anymore because regression calculations by Jorissen (1998) [1] have shown that it has the least influence of the used parameters on the load carrying capacity. It represents the basis for the present equation used in Eurocode [3]. Interestingly it has been derived based on tests of one kind of connection (symmetrical double

shear timber connection) and is used in a slightly modified form in Eurocode [3] to calculate  $n_{ef}$  for all of Johansen-Type connections.

$$n_{ef} = 0.9 \cdot 0.56 \cdot n^{0.9} \left(\frac{a_1}{d}\right)^{0.25} = 0.504 \cdot n^{0.9} \left(\frac{a_1}{d}\right)^{0.25} \leq n \quad 2.70$$

### 2.2.3.3 Theory of van der Put

Van der Put (1976) [14] developed an equation for  $n_{ef}$  based on an analytical linear elastic approach. The fasteners of the shear connection are replaced by a layer between the timber members (like a glued connection) with stiffness  $c$ , which results in an equal linear load slip curve for every fastener. Furthermore equal stresses across the cross section of the timber and equal spacing between the fasteners are assumed [1]. The derivation is partly exercised in chapter 3.1.1.

$$n_{ef} = \frac{\sqrt{E_s A_s E_m A_m (E_s A_s + E_m A_m)} \sinh(\omega L)}{L(E_s A_s + E_m A_m \cosh(\omega L)) \sqrt{c}} * n$$

$$\leq \frac{\sqrt{E_s A_s E_m A_m (E_s A_s + E_m A_m)} \sinh(\omega L)}{L(E_m A_m + E_s A_s \cosh(\omega L)) \sqrt{c}} * n \quad 2.71$$

With:

$$L = (n - 1) a_1 \quad 2.72$$

$$\omega = \sqrt{\frac{c(E_s A_s + E_m A_m)}{E_s A_s E_m A_m}} \quad 2.73$$

$$c \approx \frac{k_1}{a_1} \quad 2.74$$

- $E_s$  modulus of elasticity timber side member [N/mm<sup>2</sup>]
- $A_s$  cross sectional area timber side member [mm<sup>2</sup>]
- $E_m$  modulus of elasticity timber middle member [N/mm<sup>2</sup>]
- $A_m$  cross sectional area timber middle member [mm<sup>2</sup>]
- $k_1$  initial stiffness in load slip curve [N/mm]  
(chapter 2.1.2) (e.g. ~25000N/mm)

One disadvantage of this approach is that with an increasing  $a_1$  the  $n_{ef}$  decreases which does not agree with reality at all.

#### 2.2.3.4 Theory of Lantos

Lantos (1969) [15] presented an analytical solution for a symmetrical double shear timber connection. He assumed linear load slip behaviour and derived equations for fastener 1 and  $n$ . The maximum force emerges either in the first or the  $n^{\text{th}}$  fastener (except  $E_s A_s = \frac{E_m A_m}{2}$ , then both fasteners have to bear the highest load) [1].

$$n_{ef} = \frac{1}{C_1} \leq \frac{1}{C_2} \quad 2.75$$

With:

$$C_1 = 1 - \beta_1(1 + \mu) + \mu + (\beta_1 - \beta_2) \frac{\beta_1^n(1 + \mu) - \mu}{\beta_1^n - \beta_2^n} \quad 2.76$$

$$C_2 = -\mu + \beta_1^{n-1}(1 + \mu) - (\beta_1^{n-1} - \beta_2^{n-1}) \frac{\beta_1^n(1 + \mu) - \mu}{\beta_1^n - \beta_2^n} \quad 2.77$$

$$\mu = -\frac{1}{1 + \frac{E_m A_m}{E_s A_s}} \quad 2.78$$

$$\beta_1 = \frac{\omega + \sqrt{\omega^2 - 4}}{2} \quad 2.79$$

$$\beta_2 = \frac{\omega - \sqrt{\omega^2 - 4}}{2} \quad 2.80$$

$$\omega = 2 + k_1 a_1 \left( \frac{1}{E_m A_m} + \frac{1}{E_s A_s} \right) \quad 2.81$$

This model was used in Canada and the USA. As shown in chapter 2.2.3.7, this theory provides rather high values of  $n_{ef}$  compared to the other approaches.

### 2.2.3.5 $n_{ef}$ according to the Canadian Code

Eq. 2.82 for  $n_{ef}$  is an empirical approach and resembles the one used in Eurocode [3]; it just considers the slenderness of the middle member in addition. As the exponents are smaller, this theory is the most conservative for brittle connections (small  $t_m$ ) known by the author. For slender connections, however, it might be way less conservative than the European approach as the exponent for  $\frac{t_m}{d}$  is rather high.

$$n_{ef} = 0.33 n^{0.7} \left(\frac{a_1}{d}\right)^{0.2} \left(\frac{t_m}{d}\right)^{0.5} \quad 2.82$$

### 2.2.3.6 $n_{ef}$ according to the Australian Code

In Australian design practice this issue is approached in a different way. Instead of providing a function dependent on certain parameters, a table with values for  $n_{ef}$  is given. Additionally, it is distinguished between seasoned and unseasoned timber.

Table 2: Australian values for  $k_{17}$  [6]

Type of joint	Values of $k_{17}$				
	$n_a \leq 4^{***}$	$n_a = 5$	$n_a = 10$	$n_a = 15$	$n_a \geq 16$
Seasoned timber	1	1	1	1	1
Unseasoned timber (no transverse restraint <sup>**</sup> )	1	0.95	0.8	0.55	0.5
Unseasoned timber (transverse restraint <sup>**</sup> )	0.5	0.5	0.5	0.5	0.5

$n_a$ : total number of rows of fasteners per interface.

<sup>\*\*</sup>: the term transverse restraint refers to the possibility of restraint to timber shrinkage due to the joint detail.

<sup>\*\*\*</sup>: where a connection consists of a single fastener,  $k_{17}$  is taken as 1 for all timbers.

$k_{17}$  is the Australian factor for the effects of multiple fasteners decreasing the load carrying capacity per connector, it is multiplied by  $n$ . Eq. 2.83 shows how to determine the design capacity ( $\Phi N_j$ ) of the multiple fastener joint.

$$(\Phi N_j) = \Phi k_1 k_{16} k_{17} n Q_{sk} \quad 2.83$$

- $\Phi$  capacity factor [-]
- $k_1$  factor for duration of the load [-]
- $k_{16}$  factor considering the influence of possible metal side plates of adequate strength [-]
- $n$  number of fasteners resisting design action in shear [-]
- $Q_{sk}$  characteristic capacities [N]

This regulation does not differentiate regarding fastener arrangement or slenderness. Furthermore a reduction has not to be taken into consideration for seasoned timber – a circumstance which is at least questionable.

### 2.2.3.7 Comparison and Discussion of the different Approaches

Different comparisons of the approaches of calculating  $n_{ef}$  are shown in the following by using examples of symmetrical double shear timber-timber connections.

The first comparison is for a brittle connection with the following parameters:

- $d = 12 \text{ mm}$      $a_1 = 7d$      $t_1 = 14 \text{ mm}$      $t_2 = 28 \text{ mm}$
- $h_1 = 72 \text{ mm}$      $h_2 = 72 \text{ mm}$      $E_i = 12000 \text{ N/mm}^2$      $k_1 = 25000 \text{ N/mm}$

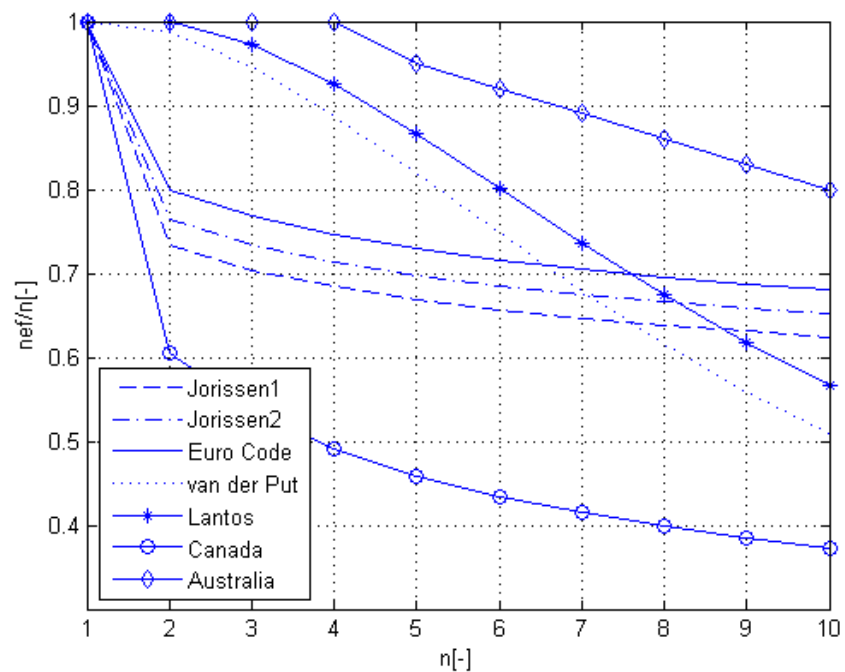


Figure 38: Comparison  $n_{ef}/n$  vs.  $n$  – brittle connection

The second comparison is for an intermediate connection according to Johansen's equations with the following parameters changed:

- $t_1 = 40 \text{ mm}$      $t_2 = 80 \text{ mm}$

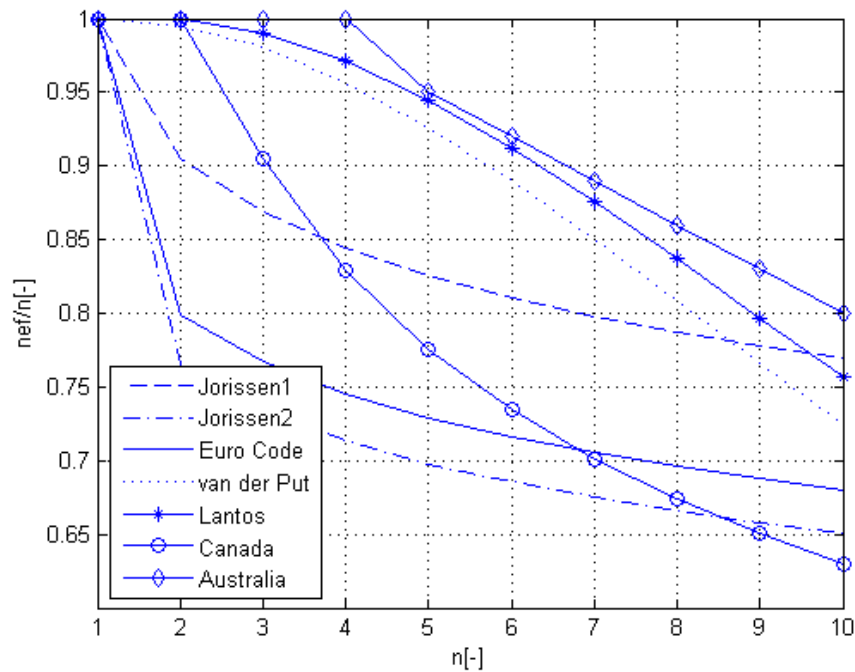


Figure 39: Comparison  $n_{ef}/n$  vs.  $n$  – intermediate connection

Thirdly the different approaches will be examined by looking at a slender connection with the following parameters changed:

- $t_1 = 60 \text{ mm}$     $t_2 = 120 \text{ mm}$

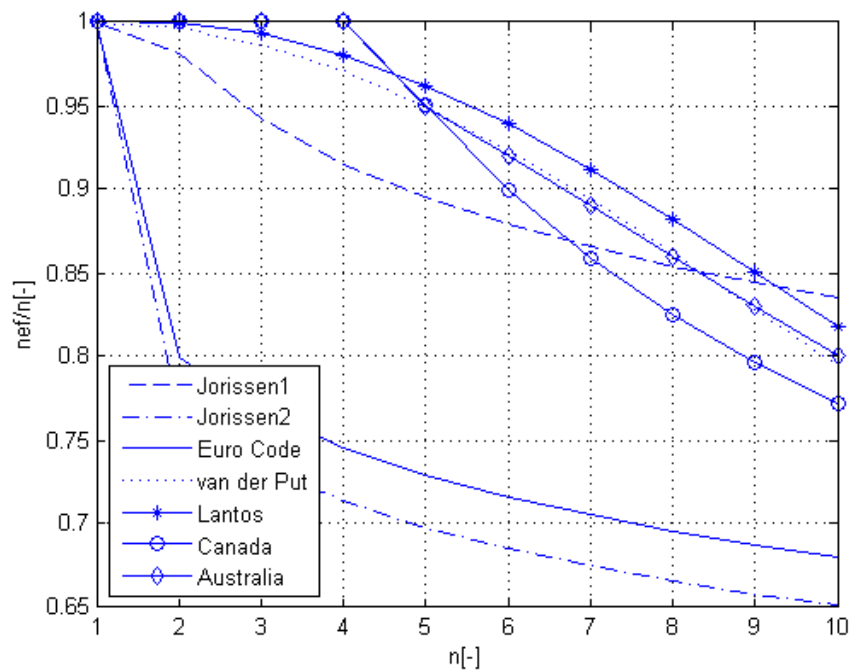


Figure 40: Comparison  $n_{ef}/n$  vs.  $n$  – ductile connection

It is apparent that the equation for  $n_{ef}$  used in Eurocode [3] was derived from Jorissen's simplified design suggestion [1]. Regarding the example of slender

failure, Eurocode might give rather conservative results compared to the first proposal of Jorissen, as it does not take the slenderness into account while the suggestion does.

However, it is interesting to observe that the Australian Code (unseasoned timber no transverse restraint) does not take any reduction of  $n$  into account until five fasteners in a row. That totally contradicts test results, which show that the amount of load reduction per fastener is biggest for the first fasteners and decreases the more fasteners are arranged in a row [1].

Lantos' and van der Puts' approaches show qualitatively the same shape which again depicts the load reduction per connector behaviour of multiple fastener connections in contradiction to test results.

In conclusion, it can be said that the approach used in Eurocode [3] and based on Jorissen's suggestions [1] seems to predict the group effect rather well (at least according to Jorissen's test results, listed in chapter 10.4) compared to the other approaches presented, although slenderness is not considered. Nevertheless, it is still, as already mentioned, just an empirical approximation of test results. It was derived based on a limited data set of symmetrical double shear timber connection tests but is used for shear connections with all parameter combinations possible. It is questionable if an empirical model can really depict the load reduction effect of multiple fasteners accurately enough for all the infinite cases.

#### **2.2.4 Design with Normal-, Shear Force and Moment**

In the case of an additional moment acting on the centre of gravity of a shear connection the situation is rather different concerning the stress situation per fastener. Not all the fasteners are equally loaded at failure anymore but the outermost connectors have to bear the highest loads as they are used primarily to transfer the moment due to their larger leverage. Thus, the load per fastener decreases towards the centre of the connection. As a result, stress accumulation might not have this high influence anymore.

In terms of dimensioning, this situation is taken into account by calculating only the force acting on the outermost connectors resulting of moment, shear- and normal force and comparing this one with the strength of one single fastener obtained through the Johansen equations.

However, as examination of load cases including moments are not within the scope of this thesis, no further comments are made.

### 3 LOAD PATHS

A qualitative presentation of the paths of forces acting in a shear connection with dowel type fasteners is conducted and the effect of end fixities applied on the fastener is examined. Additionally, the generally most sensitive part of the timber member is determined. Furthermore, the stress paths of the major main stresses in a timber member are shown based on Wyss (1923) [13] and some general construction advises are given accounting for them.

#### 3.1 Load Paths in x-y Plane

##### 3.1.1 Way of the Load in a Connection

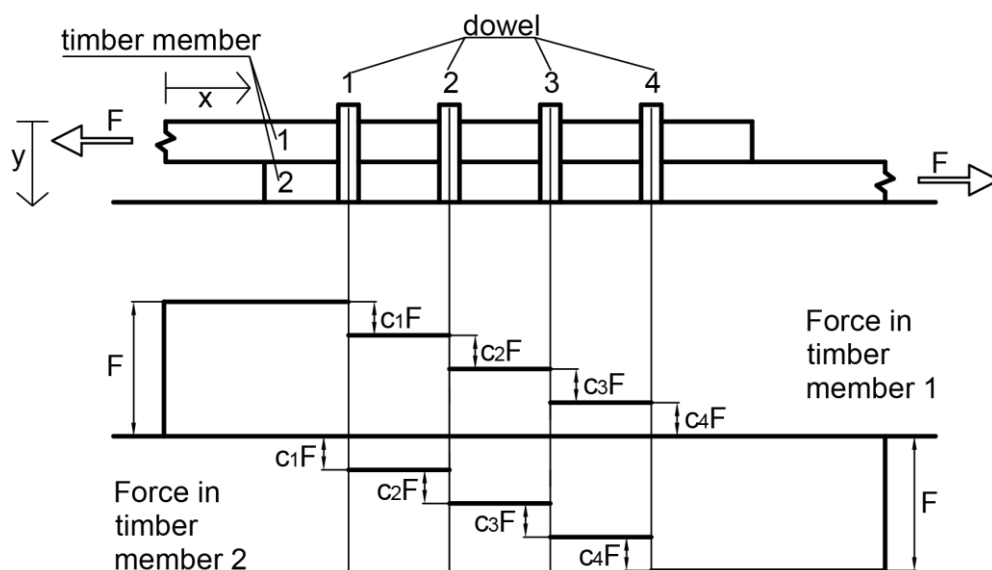


Figure 41: Load situation in x-y plane ( $n=4$ )

Firstly, the way of the load  $F$  is shown from timber member 1 to timber member 2. As presented in Figure 41 the load in member one is reduced with a certain factor  $c_i$  times  $F$  per fastener. This factor will be somewhere around  $1/n$  if a uniform load distribution among the fasteners is assumed. This is however theoretically only the case for entirely stiff members.

If the elasticity of the members is taken into consideration, an uneven load distribution among the fasteners during linear-elastic loading is the consequence. Manufacturing imprecisions and imperfections in the material further contribute to this inequality. This leads to different local load-slip curves and therefore a different load level among the fasteners at one global displacement of the connection. Some authors (e.g. Lantos) assume an uneven load distribution in deriving their equations for  $n_{ef}$  as exhibited in chapter 2.2.3.

To illustrate the effect of elasticity of the timber members, a linear elastic analysis is conducted in the following [1]. The flow of the load in a connection where the

connectors are replaced by a continuous layer with a certain stiffness  $c$  between the members, like in a glued shear connection (see Figure 42), is examined.

The following derivation is also used by van der Put (1976) [14] to obtain an approach for  $n_{ef}$  as shown in chapter 2.2.3.3.



Figure 42: Shear connection with an elastic layer between the members

Figure 42 shows the considered system. The derivative of the normal force distribution in member one ( $N_1(x)$ ) can be depicted as the difference of the displacements ( $u_1, u_2$ ) of the members times the stiffness of the elastic layer.

$$\frac{dN_1}{dx} = c(u_1 - u_2) \quad 3.1$$

Building the second derivative yields:

$$\frac{d^2N_1}{dx^2} = c \left( \frac{du_1}{dx} - \frac{du_2}{dx} \right) \quad 3.2$$

The derivative of the displacement can be seen as the strain ( $\epsilon$ ), thus:

$$\frac{du}{dx} = \epsilon = \frac{N}{EA} \quad 3.3$$

Therefore:

$$\frac{d^2N_1}{dx^2} = c \left( \frac{N_1}{E_1A_1} - \frac{N_2}{E_2A_2} \right) \quad 3.4$$

By stating that the sum of the normal forces in both members always has to equal the applied force:

$$F = N_1 + N_2 \quad 3.5$$

This relation can be established:

$$\frac{d^2 N_1}{dx^2} = c \left( \frac{N_1}{E_1 A_1} - \frac{F - N_1}{E_2 A_2} \right) \quad 3.6$$

$$\frac{d^2 N_1}{dx^2} - N_1 c \frac{E_1 A_1 + E_2 A_2}{E_1 A_1 E_2 A_2} + F c \frac{1}{E_2 A_2} = 0 \quad 3.7$$

These factors are introduced:

$$\omega = \sqrt{c \frac{E_1 A_1 + E_2 A_2}{E_1 A_1 E_2 A_2}} \quad 3.8$$

$$C = \frac{c}{E_2 A_2} \quad 3.9$$

A solution to the second order inhomogeneous differential equation (Eq. 3.7) for  $N_1(x)$  can be given:

$$N_1(x) = C_1 \sinh(\omega x) + C_2 \cosh(\omega x) + \frac{C}{\omega^2} F \quad 3.10$$

The constants  $C_1$  and  $C_2$  can be obtained with the following boundary conditions:

- $x = 0$ :

$$N_1(x = 0) = F \quad 3.11$$

$$C_2 = F \left( 1 - \frac{C}{\omega^2} \right) \quad 3.12$$

- $x = L$ :

$$N_1(x = L) = 0 \quad 3.13$$

$$C_1 = \frac{-C_2 \cosh(\omega L) - \frac{C}{\omega^2} F}{\sinh(\omega L)} \quad 3.14$$

- $A_1$  cross sectional area member 1 [mm<sup>2</sup>]
- $E_1$  modulus of elasticity member 1 [N/mm<sup>2</sup>]
- $A_2$  cross sectional area member 2 [mm<sup>2</sup>]
- $E_2$  modulus of elasticity member 2 [N/mm<sup>2</sup>]
- $c$  stiffness of the elastic layer [N/mm<sup>2</sup>]

The graphical presentation of the equations for  $N_1(x)$  and  $N_2(x)$  is given in Figure 43.

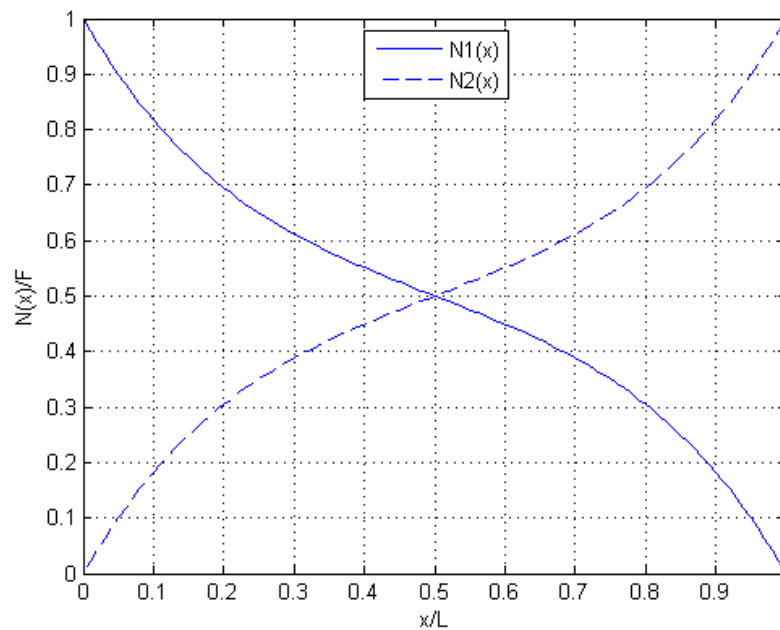


Figure 43: Force distribution in the two members of a glued shear connection according to linear elastic analysis

Apparently the distribution of the load is not linear but shows peaks at the edges. This is one reason for an uneven load distribution among the fasteners in the linear elastic branch of the loading- and unloading process.

### 3.1.2 The Theoretical Influence of End Fixities

If end fixities are used, an axial tensile force can be already introduced in the fastener by pre-stressing in the manufacturing process and occurs anyway as soon

as the fastener forms in bending. This axial force ( $F_{ax}$ ) is also responsible for the emergence of (increased) friction between the timber members ( $q_f$ ). The axial force however is hard to assess and to determine as several factors influencing it cannot be predicted beforehand (shrinkage due to humidity change, real pre-stressing on the construction site) as already discussed. As  $F_{ax}$  acts favourably on the carrying capacity, it is safer and more conservative to neglect it.

The “rope-effect” can also be described as introduction of a moment into the connection. The horizontal components of  $F_{ax}$  are applied on the timber members with a certain leverage in between. The leverage per shear plane is formed by the distance between the plastic hinge and the end fixity (mode II) or the two plastic hinges of the fastener (mode III). In a symmetric connection (e.g. double shear timber-timber connection) two moments are introduced (one per shear plane) and their vertical (eccentric) effect is neutralised while in single shear connections the introduced moment decreases the moment that has already been introduced by the loading ( $F$ ) due to the eccentricity of the load flow throughout the connection and helps to stabilise it.

The mechanical reason for the force ( $F_{ax}$ ) however can roughly be derived if the assumption is made that no shrinkage occurs (short-time loading) and pre-stressing is unaccounted for as well as that the fixity sits tightly on the timber.

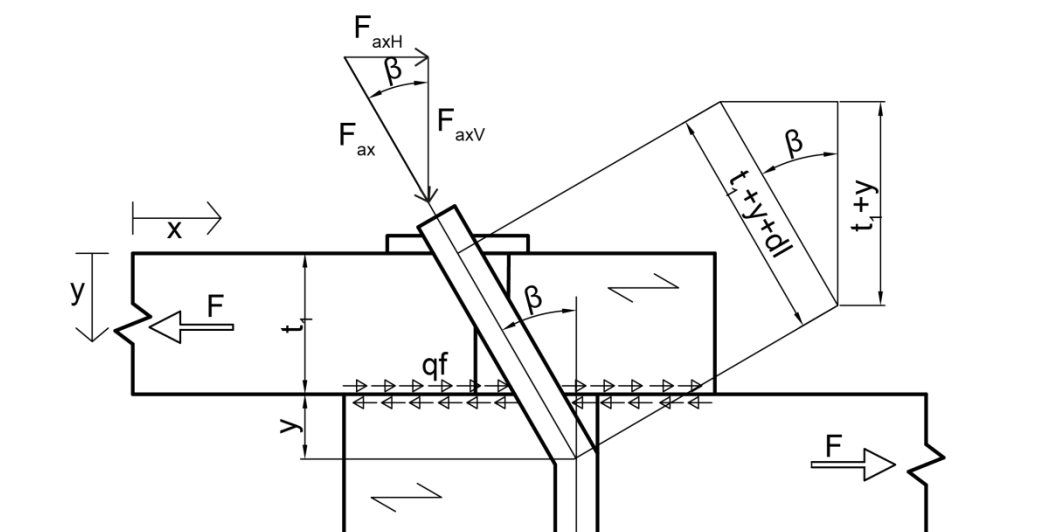


Figure 44: Single fastener connection (failure mode II) with deformed fastener and axial force due to end fixity

As shown in Figure 44, in order to still agree with geometry, the deformed fastener would have to be longer than the non-deformed. Certainly, the fastener elongates to some amount but most of the additional length ( $dI$ ) is achieved by deformation of the timber since the moduli of elasticity differ strongly (timber:  $E_{90} \sim 400 \text{ N/mm}^2$  steel:  $E_s \sim 210000 \text{ N/mm}^2$ ). Thus, it can be written:

$$dl = \frac{\varepsilon_t t_1}{\cos(\beta)} + \varepsilon_f l_f = \frac{F_{ax} v t_1}{AE_{90} \cos(\beta)} + \frac{F_{ax} l_f}{A_f E_s} = F_{ax} \left( \frac{t_1}{AE_{90}} + \frac{t_1 + \frac{t_2}{2}}{A_f E_s} \right) \quad 3.15$$

With:

- $\varepsilon_1$  strain of timber member 1 [-]
- $\varepsilon_t$  strain of the fastener [-]
- $l_f$  length fastener [mm]
- $\beta$  bending angle of the fastener [°]
- $d$  diameter of the fastener [mm]
- $t_2$  thickness of timber member 2 [mm]
- $A$  area of the fixity that is attached to the timber [mm<sup>2</sup>]
- $A_f$  cross section area of the fastener [mm<sup>2</sup>]

This approach is based on linear elasticity but in case of a fastener that already bends, a plastic hinge develops and the connector (partly) yields. To account for this, a reduced modulus of elasticity for the steel ( $E_s$ ) could be used as the fastener will elongate with less resistance than if it still were entirely in the linear elastic field.

The length  $dl$ , however, can also be calculated with:

$$dl = (t_1 + y) \left( \frac{1}{\cos(\beta)} - 1 \right) \quad 3.16$$

Combining yields:

$$F_{ax} = \frac{(t_1 + y) \left( \frac{1}{\cos(\beta)} - 1 \right)}{\frac{t_1}{AE_{90}} + \frac{t_1 + \frac{t_2}{2}}{A_f E_s}} \quad 3.17$$

The length  $y$  can be determined by assuming that this is the length that has to bear the embedment strength  $f_{h2}$  uniformly in the derivation of Johansen failure mode II and thus, it can be calculated with:

$$y = \frac{F_{\text{Johansen}}}{df_{h2}} \quad 3.18$$

Inserting Eq. 3.18 into Eq. 3.17 yields:

$$F_{\text{ax}} = \frac{\left(t_1 + \frac{F_{\text{Johansen}}}{df_{h2}}\right) \left(\frac{1}{\cos(\beta)} - 1\right)}{\frac{t_1}{AE_{90}} + \frac{t_1 + \frac{t_2}{2}}{A_f E_s}} \quad 3.19$$

- $F_{\text{Johansen}}$  Carrying capacity according to Johansen [N]  
Mode II without “ $F_{\text{ax,d}}$  term”
- $f_{h2}$  embedment strength timber member 2 [N/mm<sup>2</sup>]

To sum up, it can be said that the emergence of the axial force  $F_{\text{ax}}$  is forced by a prevented possibility for the fastener to move in axial direction and therefore, when the fastener bends,  $F_{\text{ax}}$  is introduced. Its horizontal part increases the load carrying capacity of the connection. The size of the force, however, is mainly governed by the presented parameters.

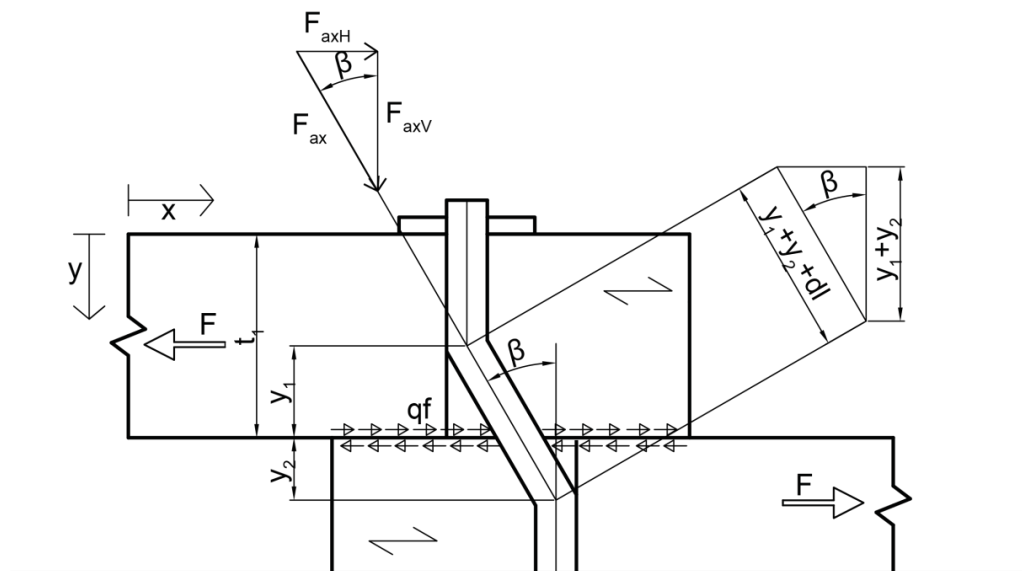


Figure 45: Single fastener connection (failure mode III) with deformed fastener and axial force due to end fixity

The same is valid for failure mode III but the geometrical boundary conditions are somehow different as shown in Figure 45. In this case the leverage of the moment caused by the application of  $F_{\text{ax,H}}$  on the timber members is made up by the distance between the plastic hinges, which is why it might be smaller (dependent on the thicknesses of the timber members of course that form the failure modes)

and why the stabilising effect on the moment caused by the loading in unsymmetrical connections decreases. It is not clear if the additional length  $dl$  (which is responsible for the emergence of  $F_{ax}$ ) gets smaller, because even if the leverage decreases, the bending angle  $\beta$  is larger in mode III (see chapter 4.3.1).

## 3.2 Load Paths in x-z Plane

### 3.2.1 Load Path in a Connection

The load situation is shown in the x-z plane in Figure 46. For more than one row of fasteners in grain direction ( $m > 1$ ) the load is divided between the rows. The factor  $c_{ij}$  tends to be somewhat around  $1/nm$ , but as before the uniformity of the load distribution along the rows of fasteners in grain direction can differ.

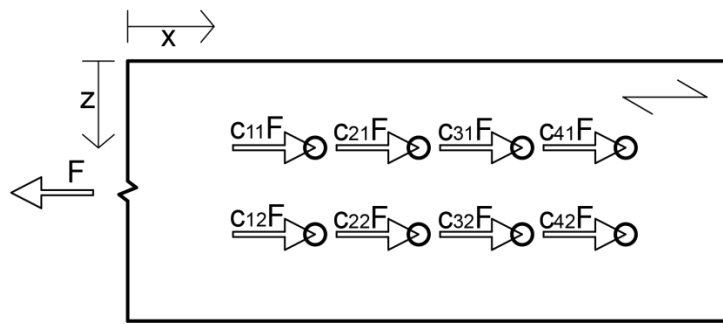


Figure 46: Loaded timber member in x-z plane ( $n = 4$ ,  $m = 2$ )

The forces acting on the holes in the timber member introduce also a force acting perpendicular to their direction. This is because of deformation effects at the fastener hole and the real distribution of the embedment stresses which distinguishes from the idealised one that is used for usual calculation purposes. This is further explained and examined in chapter 4.1.

If the timber member is split into virtual beams along its rows of fasteners in grain direction the forces acting in every virtual plane and thus on each beam can be depicted (Figure 47, Figure 48).

External loading provokes a stress situation in the plane between the virtual beams where shear stresses and tensile stresses perpendicular to the grain interact. As the strength of timber against tensile stresses perpendicular to the grain and shear is rather limited ( $f_{t,90,mean} \sim 3 \text{ N/mm}^2$ ,  $f_{v,mean} \sim 4.5 \text{ N/mm}^2$ , while  $f_{t,0,mean}$  and  $f_{c,0,mean} \sim 30 \text{ N/mm}^2$ ) these virtual planes among the rows of fasteners in grain direction can be regarded as the weak point of the connection. In other words under normal (geometrical) conditions failure of the timber member occurs due to interaction of shear and tensile stresses perpendicular to the grain.

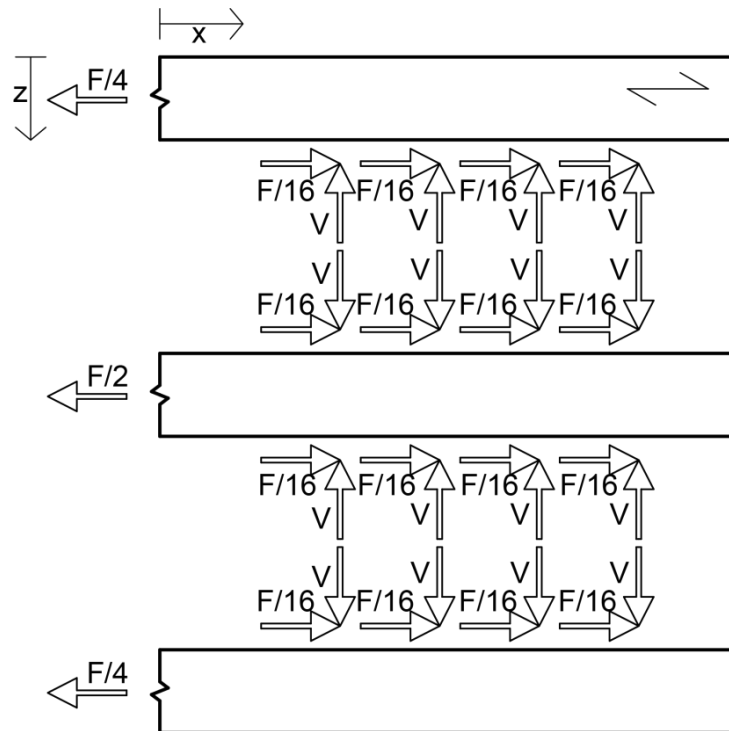


Figure 47: Load situation in x-z plane - timber member split into virtual beams ( $c_{ij} = 1/\text{nm}$ )

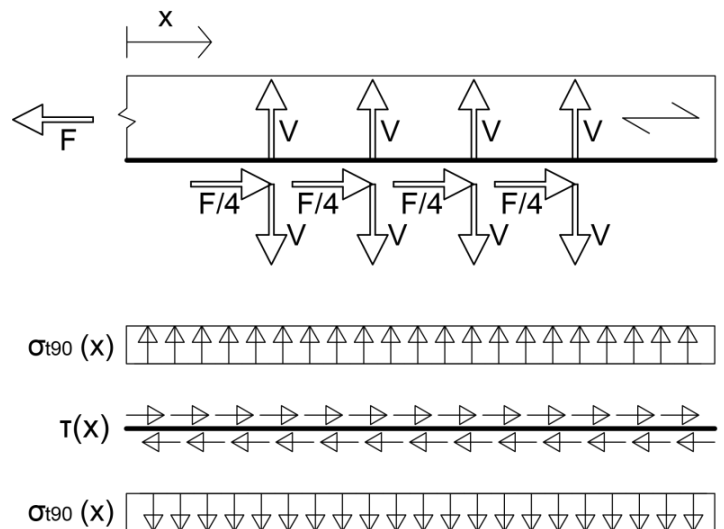


Figure 48: Forces and resulting shear stresses and tensile stresses perpendicular to the grain in the virtual plane (1)

### 3.2.2 Paths of the Tensile Main Stresses

By taking the flow of the tensile main stresses in the loaded timber member into account, some general observations can be made. In the following figure the stress paths are depicted based on Wyss (1923) [13] who derived the paths analytically from strain measurements in isotropic steel plates while the material examined here is the orthotropic wood. However the main idea is coherent.

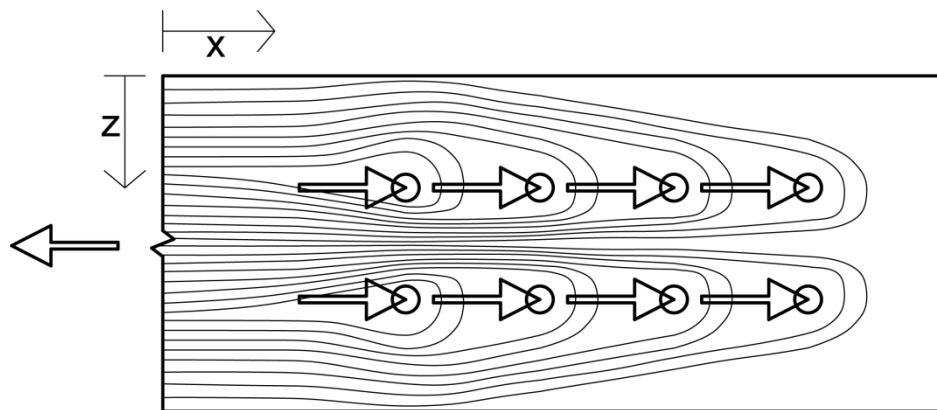


Figure 49: Qualitative paths of the tensile main stresses, according to [13]

Firstly, it is apparent that the stresses always tend to “hold back” every fastener hole and secondly, that they use to go the most direct way possible. This means that between the two rows of fasteners more tensile stresses and, therefore, a higher force accumulates than in the outer parts which only have to bear roughly half of the force the middle part has to support. Consequently, if  $a_2$  is taken too small a failure of the timber member due to tear out in combination with plug shear of the middle part might be the consequence. This is because the tensile stresses exceed the tensile strength of the timber.

Apparently the arrangement of the fasteners has a high influence on a proper load transfer throughout the connection. Situating fasteners too narrowly leads to an accumulation of stresses in x- as well as z-direction. Also inserting singular fasteners between the two rows (in Figure 49) of connectors to increase the load carrying capability of the connection might have the opposite effect as even more stresses have to be transferred between the rows. A suggestion for a different and probably more efficient arrangement of connectors than the usual (straight rows in grain direction) based on consideration of the load flow is given in chapter 8.3.1

## 4 FURTHER STRESS ANALYSIS

Hitherto the design practice of shear connections according to Eurocode [3] was presented, examined and discussed. Benefits of the approaches used were shown, disadvantages and not considered influences and parameters were demonstrated too.

In chapter 4, a more comprehensive study of the forces and stresses acting at the fastener hole is conducted. Furthermore a brief section introducing fracture mechanics is presented and a way of analytically approximating the stresses interacting in the shear plane along a connection is demonstrated.

### 4.1 Examination of Stresses at the Fastener Hole

#### 4.1.1 General

The situation at the fastener hole exhibits a rather complex condition. First the stress situation at the fastener hole is dependent on the angle between load and grain direction and second the friction angle between timber and the fastener has a huge influence as well, this influence however is not accounted for in Eurocode [3] at all.

#### 4.1.2 Fastener Loaded Parallel to the Grain

##### 4.1.2.1 The Theoretical Situation at the Fastener Hole

Dependent on the angle of friction between the fastener and the timber  $\varphi$ , the circumference of the hole can be divided into three sections. Firstly, it can be distinguished between a contact region, where, as the name already points out, the fastener actually has a somewhat force transferring contact with the timber and a non-contact region. Secondly, the contact region is made up of the section directly in load direction, where the timber fibres are compressed and crushed. In the other part the timber fibres are rather pressed to the side and a force acting perpendicular is introduced which is responsible for the emergence of stresses perpendicular to the grain. The borders between these two parts comprising the contact region represent the lines where the shear planes at failure occur. It is assumed that these crack planes arise dependent on the friction angle  $\varphi$  [1], [5], [7]. Consequently, if no friction is assumed the two crack planes become one.

The friction angle  $\varphi$  varies according to the surface condition of the fastener [7]:

- |                    |                                   |                      |
|--------------------|-----------------------------------|----------------------|
| • Small friction:  | connectors with plastic cover     | $\varphi = 7^\circ$  |
| • Normal friction: | ordinary steel fastener           | $\varphi = 18^\circ$ |
| • High friction:   | connectors with a surface pattern | $\varphi = 30^\circ$ |

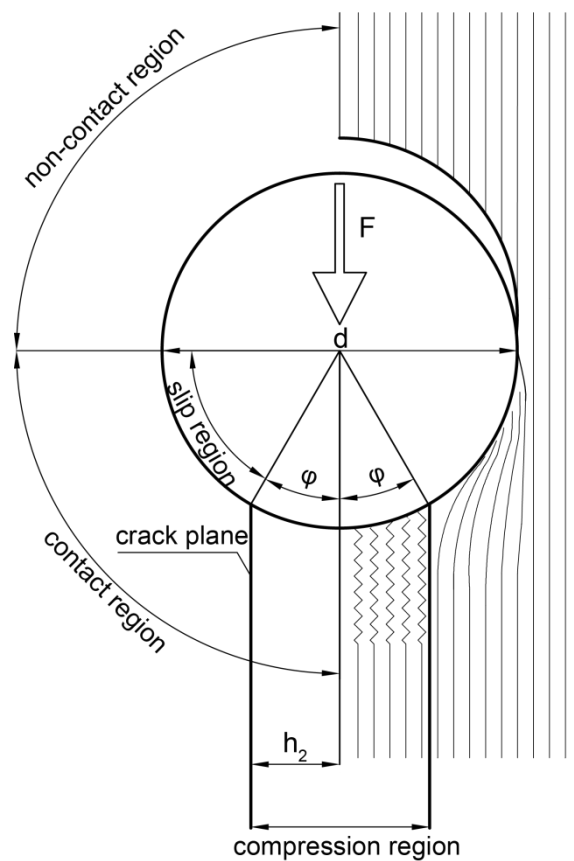


Figure 50: The situation of a fastener loaded parallel to the grain

Figure 51, Figure 52 and Figure 53 of FEM-calculations by Schmid et al. (2002) [10] depict the stress situation at the fastener hole loaded parallel to the grain concerning stresses perpendicular to the grain and shear stresses around a fastener hole.

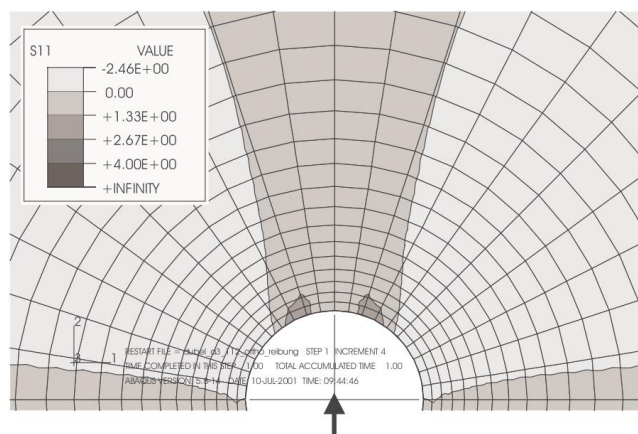


Figure 51: Stresses perpendicular to the grain ( $\varphi=19^\circ$ ) (taken from [10])

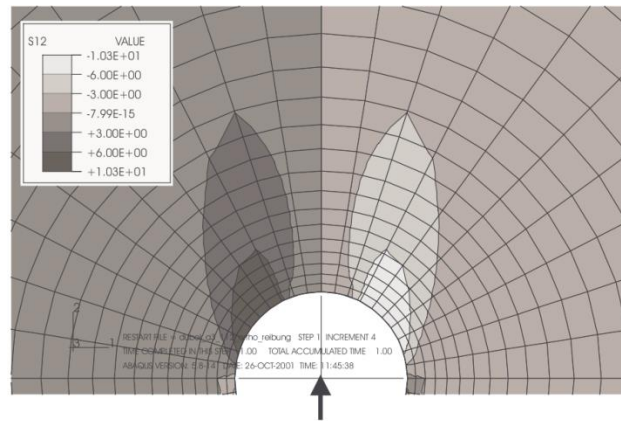


Figure 52: Shear stresses ( $\varphi=19^\circ$ ) (taken from [10])

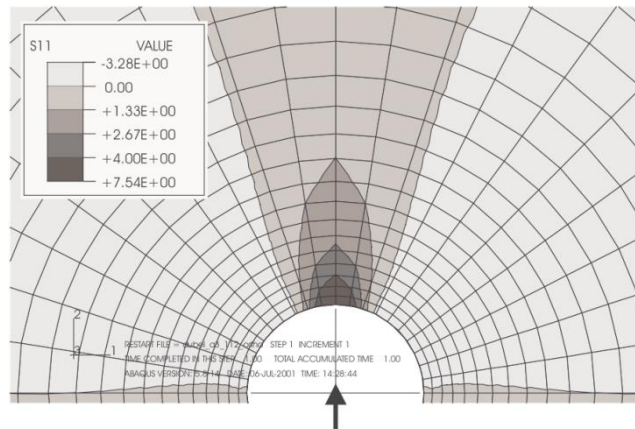


Figure 53: Stresses perpendicular to the grain ( $\varphi=0^\circ$ ) (taken from [10])

As apparent, there is a good agreement with theory concerning the distribution of stresses at the fastener hole and the assumed emergence of the crack plane(s).

#### 4.1.2.2 An Analytical Approach to Determine the Wedging Force and Stresses

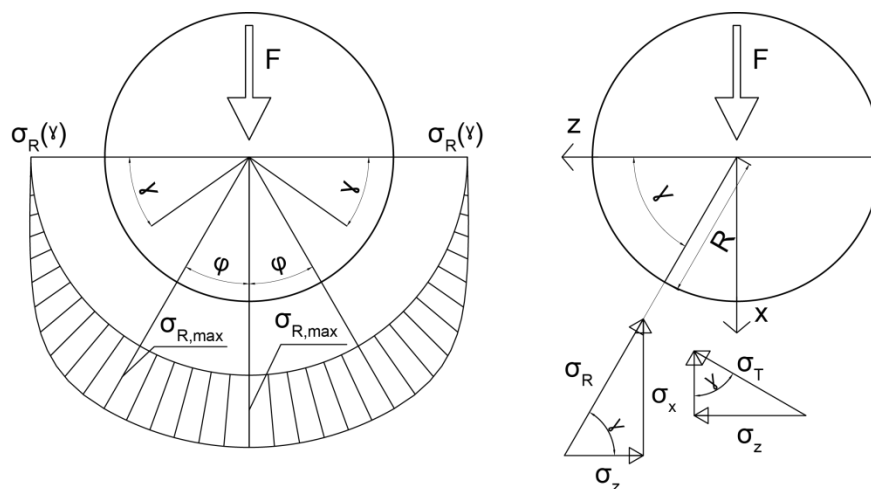


Figure 54: Assumed embedment stress distribution around the fastener hole

The assumed embedment (radial) stress distribution, accounting for the present situation at the fastener hole, can be depicted approximately by Eq. 4.1:

$$\sigma_R(\gamma) = \begin{cases} \text{for } \gamma \leq \frac{\pi}{2} - \varphi: \sigma_{R,\max} \sin^2\left(\frac{\gamma\pi}{\pi - 2\varphi}\right) \\ \text{for } \gamma > \frac{\pi}{2} - \varphi: \sigma_{R,\max} \end{cases} \quad 4.1$$

The tangential stresses occur due to friction and are therefore:

$$\sigma_T(\gamma) = \sigma_R(\gamma) \tan(\varphi) \quad 4.2$$

Having determined that, the stresses in direction of the grain  $\sigma_x(\gamma)$  can be obtained with:

$$\sigma_x(\gamma) = \sigma_R(\gamma) \sin(\gamma) + \sigma_T(\gamma) \cos(\gamma) = \sigma_R(\gamma) (\sin(\gamma) + \cos(\gamma) \tan(\varphi)) \quad 4.3$$

An expression for the stresses perpendicular to the grain can also be given:

$$\sigma_z(\gamma) = \sigma_R(\gamma) \cos(\gamma) - \sigma_T(\gamma) \sin(\gamma) = \sigma_R(\gamma) (\cos(\gamma) - \sin(\gamma) \tan(\varphi)) \quad 4.4$$

The (yet unknown) maximum embedment stresses  $\sigma_{R,\max}$  can be obtained by using the condition that the integral of the stresses in grain direction  $\sigma_x$  has to equal the force F. Thus:

$$\frac{F}{2} = \int_{\gamma=0}^{\gamma=\frac{\pi}{2}} \sigma_x(\gamma) t R d\gamma = t R \int_{\gamma=0}^{\gamma=\frac{\pi}{2}} \sigma_R(\gamma) (\sin(\gamma) + \cos(\gamma) \tan(\varphi)) d\gamma \quad 4.5$$

t                      thickness of the timber member                      [mm]

All discrete values of  $\sigma_R(\gamma)$  will represent a certain value multiplied by  $\sigma_{R,\max}$ . Therefore,  $\sigma_R(\gamma)$  can be written as:

$$\sigma_R(\gamma) = \sigma_{R,\max} f_P(\gamma) \quad 4.6$$

By inserting Eq. 4.6 in Eq. 4.5, the following can be obtained:

$$\begin{aligned} \frac{F}{2} &= t d \int_{\gamma=0}^{\gamma=\frac{\pi}{2}} \sigma_{R,\max} f_P(\gamma) (\sin(\gamma) + \cos(\gamma) \tan(\varphi)) d\gamma \\ &= t R \sigma_{R,\max} \int_{\gamma=0}^{\gamma=\frac{\pi}{2}} f(\gamma) d\gamma \end{aligned} \quad 4.7$$

Thus:

$$\sigma_{R,\max} = \frac{F}{2t R \int_{\gamma=0}^{\gamma=\frac{\pi}{2}} f(\gamma) d\gamma} \quad 4.8$$

The calculated stresses around the fastener hole for a force  $F$  determined according to Johansen's Yield Theory (mode I) in Eq. 4.9 are shown in Figure 55 for different friction angles. Thus, the stress distributions around the fastener hole at failure are approximated and depicted in Figure 55 with the following parameters:

- $t = 24 \text{ mm}$      $d = 12 \text{ mm}$      $\rho = 400 \text{ kg/m}^3$      $\varphi = 7,18,30^\circ$

$$F = 0.082(1 - 0.01d)\rho dt = 8312.8\text{N} \quad 4.9$$

It can be observed that the stresses perpendicular to the grain are zero at the friction angle  $\varphi$ , explaining the emergence of the crack planes as the sign of the stresses changes, while they decrease with increasing friction angle in the area  $0 \leq \gamma \leq \frac{\pi}{2} - \varphi$  and their total value increases with increasing friction in the compression region.

The stresses in the compression region however are to be considered with care as they in fact neutralise each other due to their opposing acting directions and therefore, they would not lead to failure.

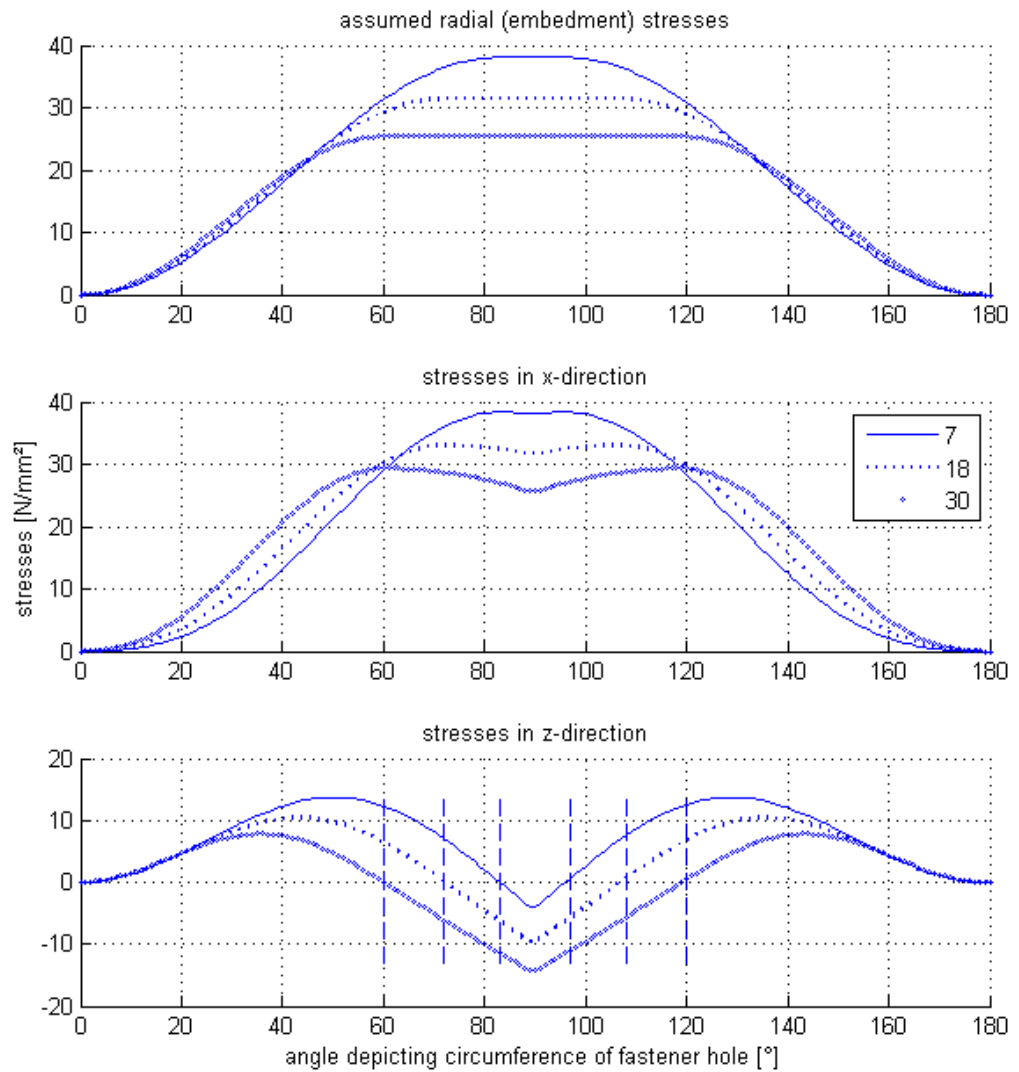


Figure 55: Stress distributions around the fastener hole

Considering the size of stresses perpendicular to the grain in the slip region, it has to be stated that their values are too high. Failure would have occurred much earlier according to this model. This is because it does not take any plastic capability at the fastener hole with diversion of stresses into less stressed parts into account. Also, as already mentioned, the predicted strength of the fastener according to Johansen's Yield Model might be too high because it does not account for timber splitting. Furthermore, the orthotropy of the material wood is just considered implicitly by the approach to approximate the embedment stress distribution (Eq. 4.1).

Timber subjected to tensile stresses behaves brittle. At a small scale, however, it is capable of conducting plastic deformations [7]. This can be accounted for approximately by assuming a uniform distribution of stresses perpendicular to the grain in the area  $0 \leq \gamma \leq \frac{\pi}{2} - \varphi$  due to plastic behaviour of the timber at the fastener hole. Furthermore, it is assumed that stresses are diverted away from the

hole, as well. Hence, it is estimated that twice the area of the uniform stress distribution ( $\sigma_{z,F}$ ) has to equal the area of the above obtained stress distribution of the stresses perpendicular to the grain at the fastener hole at failure. The factor 2 is introduced rather deliberately to account for a certain diversion of the stresses away from the fastener hole. The results in Table 3 show that the factor might be quite accurate if the Johansen equation shall be valid.

$$2\sigma_{z,F} R \left(\frac{\pi}{2} - \varphi\right) t = \int_{\gamma=0}^{\gamma=\frac{\pi}{2}-\varphi} \sigma_z(\gamma) R t d\gamma \quad 4.10$$

Thus:

$$\sigma_{z,F} = \frac{\int_{\gamma=0}^{\gamma=\frac{\pi}{2}-\varphi} \sigma_z(\gamma) d\gamma}{2 \left(\frac{\pi}{2} - \varphi\right)} \quad 4.11$$

However the wedging force  $V$  introduced by the force  $F$  can be calculated by integrating the stresses perpendicular to the grain in the slip region:

$$V = \int_{\gamma=0}^{\gamma=\frac{\pi}{2}-\varphi} \sigma_z(\gamma) R t d\gamma = 2\sigma_{z,F} R \left(\frac{\pi}{2} - \varphi\right) t \quad 4.12$$

Kuipers (1960) [25] devised an analytical approach to calculate the wedging force introduced by a force acting parallel to the grain by assuming the embedment stress distribution based on the shown conditions at the fastener hole too, although with the effect of friction already incorporated. Furthermore he let the location variable angle  $\gamma$  start in the compression region. Thus a definition of the embedment stress used by him can be provided:

$$\sigma_R(\gamma) = \left\{ \begin{array}{l} 0 \leq \gamma \leq \varphi: \sigma_R = \sigma_{Rmax} \\ \varphi < \gamma \leq \frac{\pi}{2}: \sigma_R(\gamma) = \frac{\sigma_{Rmax} \cos(\gamma)}{\cos(\varphi)} \end{array} \right\} \quad 4.13$$

According to his approach the wedging force can be determined with [1]:

$$V = F \left[ \frac{1 - \sin^2(\varphi) \cos(\varphi) - \left( \frac{\pi}{4} - \frac{\varphi}{2} - \frac{\sin(2\varphi)}{4} \right) \sin(\varphi)}{2 \cos(\varphi)} \right] = Ff_V(\varphi) \quad 4.14$$

Kuipers equation is accurate according to Jorissen (1998) [1] who compared results of this equation with computer model calculations by Werner (1993) [7] since they show a quite good agreement. The forces determined with this equation are 10-15% lower than the results obtained by Werner [1]. Figure 56 shall serve as a graphical presentation of the equation.

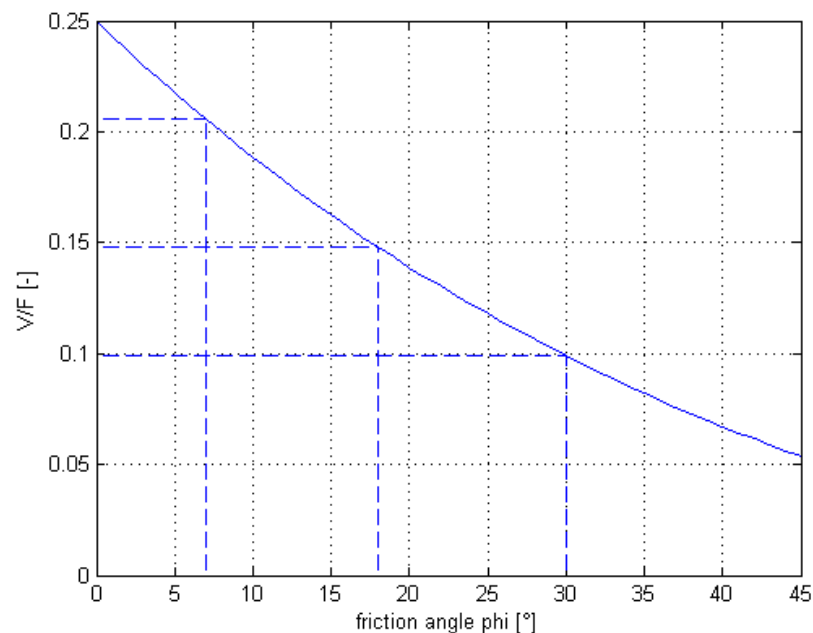


Figure 56: V/F ratio over friction angle  $\varphi$

It is apparent that with an increasing friction angle between timber and the fastener the load acting perpendicular to the grain that is introduced by a force parallel to the grain decreases. Friction introduces a force with a component acting perpendicular to the grain as well but in the opposite direction. The amount of the perpendicular acting force varies between 0.1 times the load parallel to the grain for high friction and about 0.21 times the load for small friction.

By again assuming a uniform distribution of stresses perpendicular to the grain in the slip region with additional diversion due to plasticity,  $\sigma_{zF}$  can be calculated by using Kuipers' approach which requires less calculation- and therefore also less computation effort.

$$V = Ff_V(\varphi) = 2\sigma_{z,F} t R\left(\frac{\pi}{2} - \varphi\right) \quad 4.15$$

Thus:

$$\sigma_{z,F} = \frac{V}{2tR\left(\frac{\pi}{2} - \varphi\right)} = \frac{Ff_V(\varphi)}{2tR\left(\frac{\pi}{2} - \varphi\right)} \quad 4.16$$

The results are compared in Table 3 and they are quite similar:

Table 3: Comparison of the wedging force and maximum stress perpendicular to the grain at the fastener hole

	Derivation	Kuipers	
$\sigma_{zF}(\varphi = 7^\circ)$	3.8	4.1	N/mm <sup>2</sup>
$V(\varphi = 7^\circ)$	1570.99	1708.6	N
$\sigma_{zF}(\varphi = 18^\circ)$	2.9	3.4	N/mm <sup>2</sup>
$V(\varphi = 18^\circ)$	1038.84	1229.7	N
$\sigma_{zF}(\varphi = 30^\circ)$	2.22	2.72	N/mm <sup>2</sup>
$V(\varphi = 30^\circ)$	651.53	821.72	N

It is apparent that the assumed friction angle between the timber member and the steel fastener has a huge influence on the emerging stresses and therefore on the carrying capacity of the connection. Nevertheless, the friction that finally emerges in a real connection is hard to assess beforehand during the design process.

### 4.1.3 Fastener Loaded Perpendicular to the Grain

If a force acts perpendicular to the grain the fibres under the fastener are crushed perpendicular to their direction, the fastener is pressed “into” them and tensile stresses perpendicular to the grain emerge, leading to the possible occurrence of one crack plane in grain direction and its propagation until failure [11].

It is assumed that the fibres fail due to tensile stresses perpendicular to the grain at an angle of  $\frac{\pi}{4} + \varphi$ . This assumption is made due to the fact that, according to

Eurocode [3], openings in beams are calculated by stating that the maximum stresses perpendicular to the grain appear at an angle of  $45^\circ$  and the idea that with increasing friction angle more fibres are “held” and compressed beneath the fastener instead of getting “pushed” to the side [3].

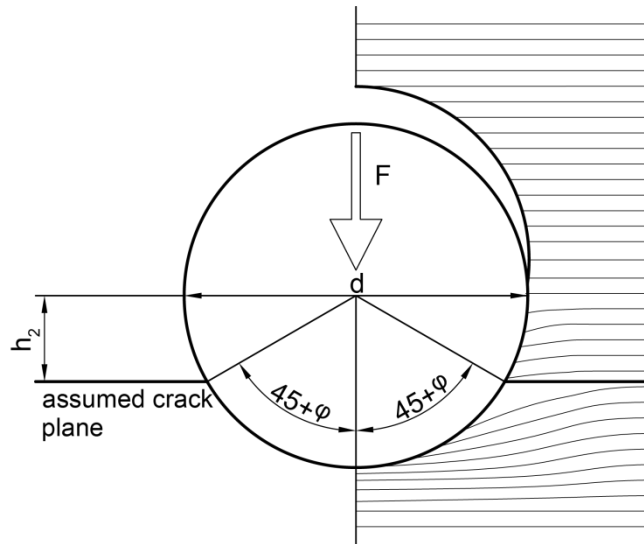


Figure 57: The situation of a fastener loaded perpendicular to the grain

FEM-calculations conducted by Schoenmakers (2010) [11] are presented in Figure 58 and Figure 59 which depict the stress situation of fasteners loaded perpendicular to the grain.

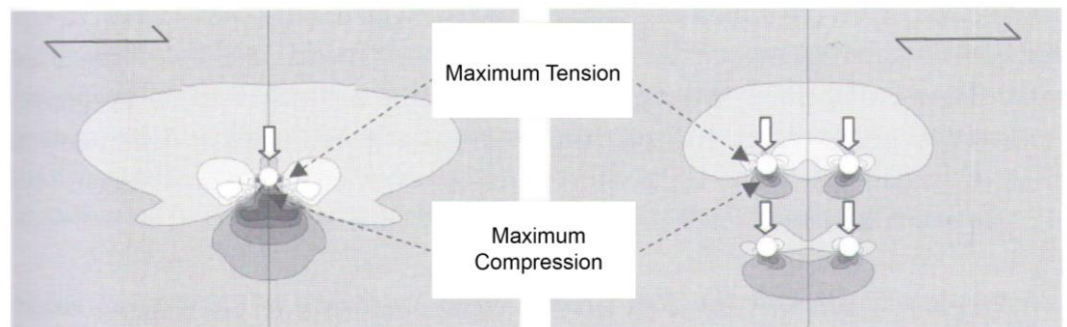


Figure 58: Situation of stresses perpendicular to the grain around fastener holes loaded perpendicular to the grain (taken from [11])

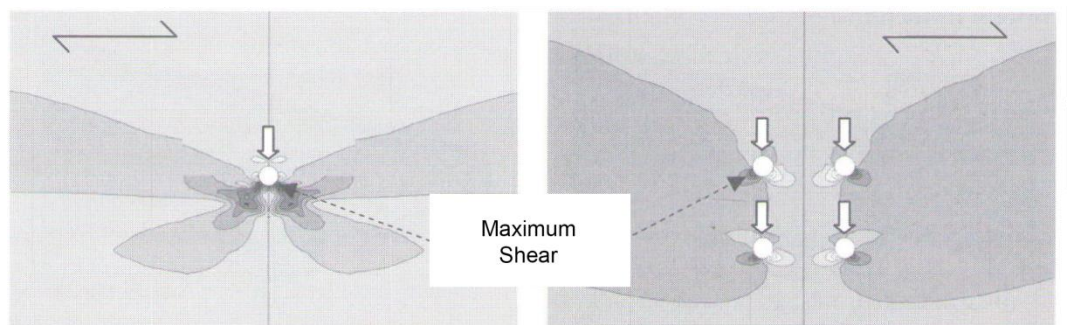


Figure 59: Situation of shear stresses around fastener holes loaded perpendicular to the grain (taken from [11])

#### 4.1.4 Tensile or Compressive Loading of the Timber Member

The stress paths differ if a timber member is loaded in tension or in compression. If loaded in tension, the stresses have to take a “detour” which results in higher tensile stresses perpendicular to the grain as the stresses have to “run around” the fastener hole. Therefore, the premature splitting of timber might be more likely due to higher tensile stresses perpendicular to the grain [1], [5]. In case of compressive loading, the stresses take the “direct” way. This difference in loading, however, is not accounted for in Eurocode [3].

Figure 60 shows the qualitative trajectories (i.e. directions of the bigger main stresses) for both loading situations. For tensile loading the depicted qualitative directions of main stresses represent tensile stresses and for compressional loading the main stresses shown are, of course, compression stresses.

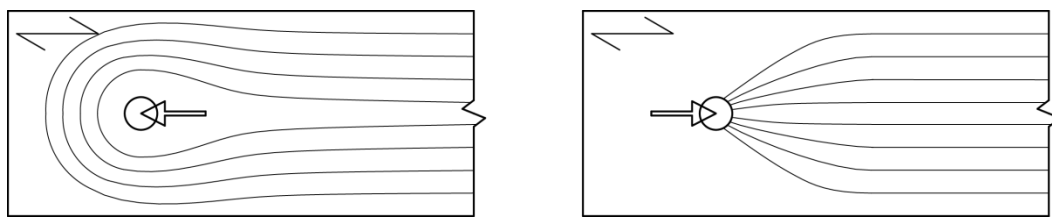


Figure 60: Timber member with hole loaded in tension (left) and compression (right)

## 4.2 Brief Discussion of Fracture Mechanics

### 4.2.1 General

Fracture mechanics theories can provide a more accurate assessment of the load carrying capacity in cases where brittle failure due to stresses perpendicular to the grain and shear occurs. In Eurocode notched beams or beams with holes are designed based on fracture mechanics [1], [3].

As already mentioned rigid connections show a tendency for premature timber splitting, which is not accounted for in the design process as regulated in Eurocode [3].

Generally it can be said that a crack can arise due to three different modes of fracture or a combination of them.

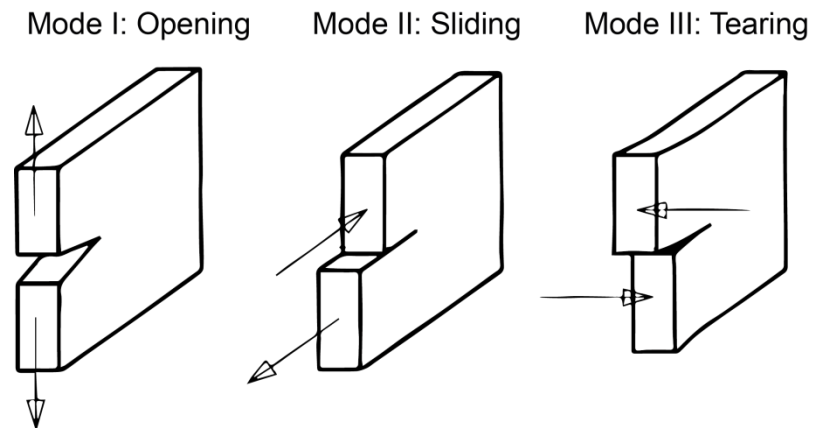


Figure 61: The fracture modes (taken from [1])

In the case of timber, however, a combination of the opening mode (tensile stresses perpendicular to the grain) and the sliding mode (shear stresses) cause the emergence of cracks [1], [7].

The behaviour of timber loaded in tension perpendicular to the grain is brittle. However, it is still able to reduce stress peaks to a certain extent (like those occurring at a fastener hole) by creating small plastic zones. If the tensile strength perpendicular to the grain is exceeded, additional deformations occur only in a very limited zone (the fracture process region). At small deformations the process region is capable of transferring relatively high stresses. The smaller this zone at the tip of the crack is, the more brittle the material behaves [7].

#### 4.2.2 The Critical Fracture Mechanical Energy

In order to have some variable to approach this process mechanically, the fracture mechanical energy  $G_c$  was introduced. This parameter describes the critical fracture mechanical energy that is required for an instable crack propagation to emerge. In other words it can be understood as the force per length unit acting at the front of the crack being responsible for letting the crack grow [1], [7].

A connection between the timber density and the critical energy was found out in tests and an empirical relation was derived. Thus it can be calculated depending on the timber density according to Gustafsson (1992) [1], [7]:

$$G_{Ic} = -162 + 1.07\rho \quad 4.17$$

$$G_{IIc} = 3.5G_{Ic} \quad 4.18$$

Van der Put (2007) determined the critical fracture energy for mode 2 analytically as [11]:

$$G_{IIc} = 4G_{Ic} \quad 4.19$$

- $G_{Ic}$  fracture energy opening mode [Nm/m<sup>2</sup>]
- $G_{IIc}$  fracture energy sliding mode [Nm/m<sup>2</sup>]

An equation for the combination of the both above mentioned modes was derived by Petersson (1995) [16]:

$$G_c = \frac{1}{\kappa_1} \left( 1 + \frac{\kappa_2}{2\kappa_1} \left( 1 - \sqrt{1 + \frac{4\kappa_1}{\kappa_2}} \right) \right) \quad 4.20$$

With:

$$\kappa_1 = \frac{1 - \kappa_3}{G_{IIc}} \quad 4.21$$

$$\kappa_2 = \frac{\kappa_3}{G_{Ic}} \quad 4.22$$

$$\kappa_3 = \frac{\left( \frac{\sigma_{t,90}}{\sigma_v} \right)^2}{\left( \frac{\sigma_{t,90}}{\sigma_v} \right)^2 + \sqrt{\frac{E_{90}}{E_0}}} \quad 4.23$$

- $\sigma_{t,90}$  stress perpendicular to the grain [N/mm<sup>2</sup>]
- $\sigma_v$  shear stress [N/mm<sup>2</sup>]
- $E_{90}$  modulus of elasticity perpendicular to the grain [N/mm<sup>2</sup>]
- $E_0$  modulus of elasticity parallel to the grain [N/mm<sup>2</sup>]

A graphical presentation of the relation is exhibited in Figure 62, with the following parameters used to create it:

- $E_0 = 12000 \text{ N/mm}^2$                        $E_{90} = 400 \text{ N/mm}^2$
- $\rho = 300,400,500,600 \text{ kg/m}^3$                $G_{IIc} = 3.5G_{Ic}$

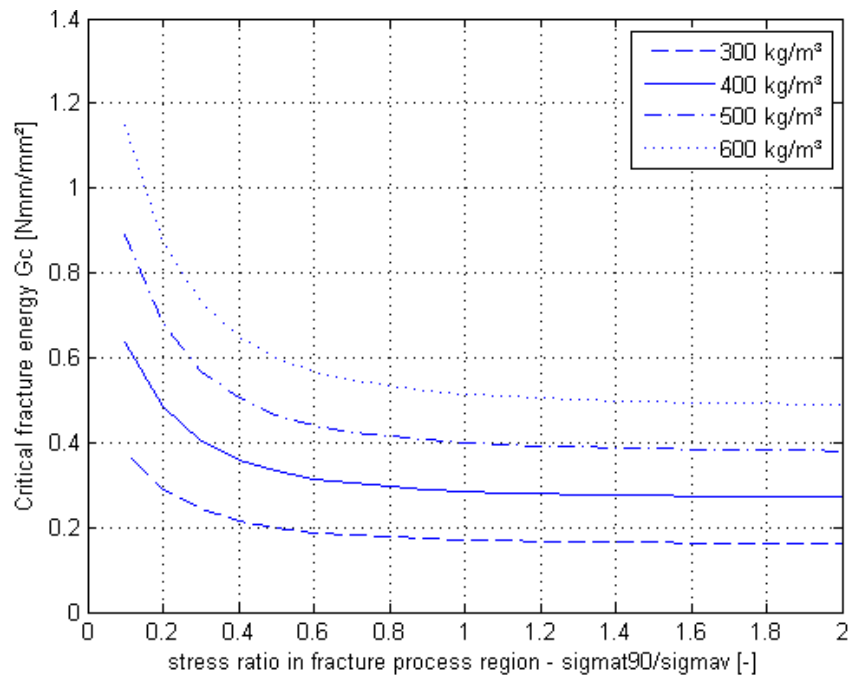


Figure 62: Graph of the critical fracture energy

As apparent the fracture energy is dependent on the ratio of the tensile stresses perpendicular to the grain to the shear stresses acting in the fracture process region of the crack plane. The derivation of this parameter is carried out later. In the further analysis  $G_c$  is treated as a known parameter.

### 4.3 Distribution of Stresses in a Connection

In chapter 4.3 a linear elastic analytical model, which incorporates fracture mechanics and accounts for plasticity to a certain (but limited) extend (see chapter 4.1.2), to determine the distribution of the stresses acting along the connection is shown based on the work of Jorissen (1998) [1].

In general it has been observed that in multiple fastener connections failure due to tensile stresses perpendicular to the grain and shear stresses with crack propagation as a consequence occurs also in non-brittle connections. It is, therefore, of great interest to calculate those stresses and to obtain a more accurate way of predicting the load carrying capacity of multiple fastener connections.

For the following analysis a timber member is considered with one fastener loaded parallel to the grain with a force  $2F$  and consequently also a wedging force  $V$  arising perpendicular to the grain. This results in the emergence of two cracks. It is assumed that the area enclosed by these cracks transfers the whole load which contradicts the assumption made in 4.1.2. This simplification is made because it renders calculations easier and has a negligible effect on the distribution of stresses along the connection.

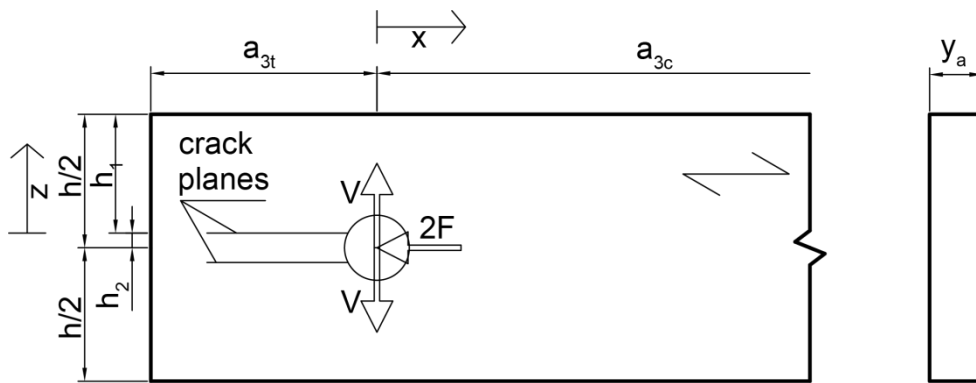


Figure 63: Sketch of the system considered in the analysis; wedging forces introduced by loading of the fastener and resulting crack planes

### 4.3.1 The Virtual Crack Width $y_a$

In a brittle connection the embedment stress is generally uniform over the whole timber member thickness, while in intermediate and slender connections those stresses are (according to Johansen's model) only uniformly distributed over a certain length  $y$ . This length can be determined with:

$$y = \frac{F}{f_h d} \quad 4.24$$

For brittle connections, however,  $y$  equals the member thickness  $t$  while for intermediate and slender connections this length is smaller. Same holds true for the assumed depth of crack propagation in a timber member at failure. As a consequence, Jorissen (1998) [1] introduced the length  $y_a$ , which represents the depth at which crack propagation due to shear stresses and due to tensile stresses perpendicular to the grain occurs. It equals  $t$  for brittle connections and is slightly larger (but always smaller  $t$ ) than the actual  $y$  for non-brittle ones.

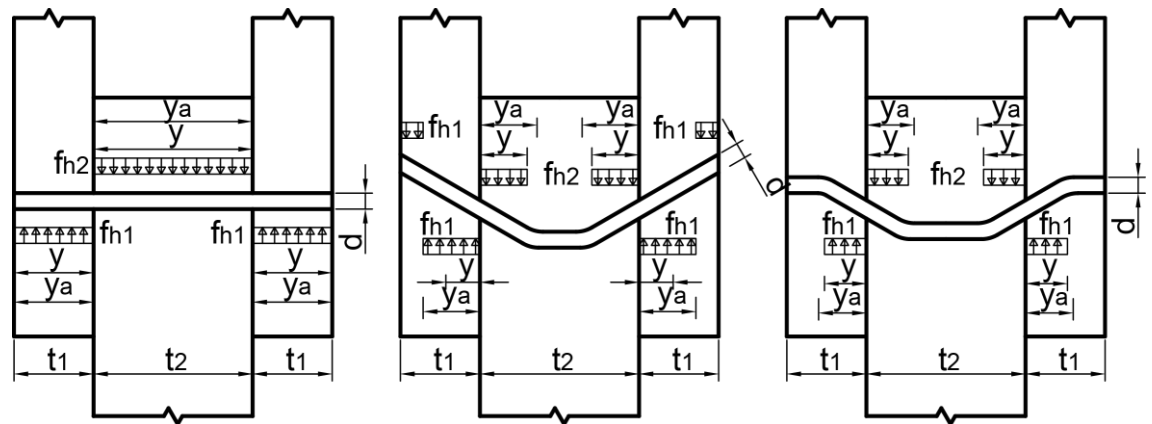


Figure 64:  $y$  and  $y_a$  in Johansen failure mode I (left, both members fail which is not necessarily the case but depicted for showing purposes) and Johansen failure modes II (middle) and III (right)

Jorissen [1] proposed a relationship for  $y_a$ , based on a linear interpolation between  $y$  and  $t$  altered with an empirical factor  $C_y$ , which he obtained by fitting it to test results of symmetrical double shear timber connections loaded parallel to the grain.

$$y_a = \left(1 + C_y \frac{t - y}{t}\right) y \quad 4.25$$

$$C_y = 0.3 \frac{a_1}{7d} \quad 4.26$$

In the following a different approach is shown to determine  $y_a$  by considering the geometry of the deformed fastener at failure.

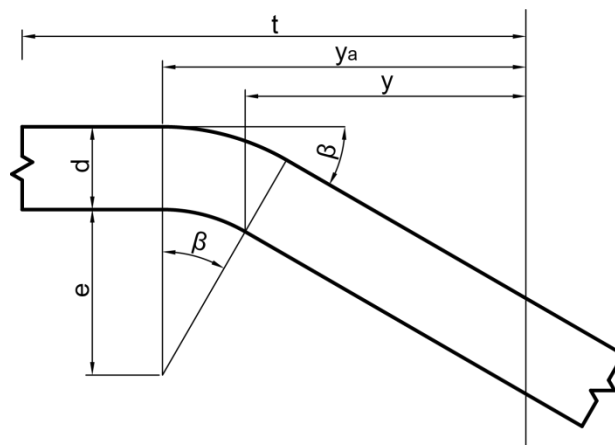


Figure 65: Geometrical conditions at a plastic hinge of the fastener

It is assumed that the length  $y$  is the length covering the deformed fastener until the plastic hinge. Here, however,  $f_h$  is not reached anymore but the crack might

start further away where the plastic hinge commences, in other words, where the fastener (and thus also the timber) starts to be deformed. Adding this length to  $y$  renders  $y_a$ . Furthermore, the bending angle  $\beta$  of the fastener and the bending radius  $e$  is introduced. With these assumptions  $y_a$  can be given as follows:

$$y_{ai} = y_i + e \sin(\beta) \quad 4.27$$

By assuming that  $e$  is approximately  $2d$ :

$$y_{ai} = y_i + 2d \sin(\beta) \quad 4.28$$

As already stated in chapter 2, for slender connections a bending angle of  $\beta = 15^\circ$  is attained. For intermediate connections the bending angle is smaller due to smaller deformations at failure. Therefore  $\beta$  is chosen as  $10^\circ$  for intermediate connections [2]. Thus:

Brittle:

$$y_a = y = \frac{F}{f_h d} \quad 4.29$$

Intermediate:

$$y_a = y + 2d \sin\left(\frac{\pi}{18}\right) \quad 4.30$$

Slender:

$$y_a = y + 2d \sin\left(\frac{\pi}{12}\right) \quad 4.31$$

### 4.3.2 Stresses Perpendicular to the Grain

To obtain the distribution of stresses perpendicular to the grain the model of a beam on an elastic foundation is chosen. The system can be divided into three parts: Two beams on elastic foundation and one ordinary beam, where the fastener hole and the cracks are situated. However the ordinary beam is neglected, as its length is very short compared to the beams on elastic foundation, so it can rather be considered a stiff plate loaded in plane. Thus, the model comprises only two beams on an elastic foundation.

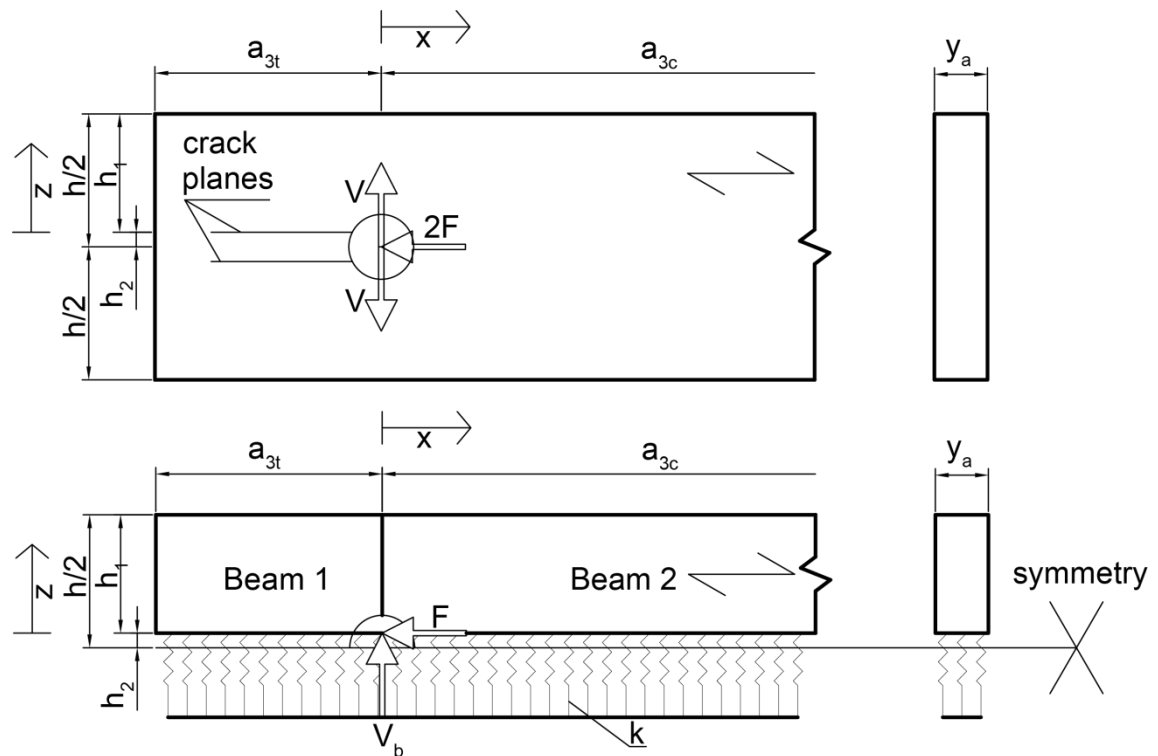


Figure 66: The considered system and virtually cut out elastically supported beams for the determination of the distribution of the stresses acting perpendicular to the grain

This model, however, is not capable of exhibiting peak stresses at the fastener hole, as previously obtained analytically, shown by De Jong (1983) or in FEM-calculations by Werner (1993) and Schmid (2002) [5], [7], [10], [21]. Therefore, another model is incorporated by adding peak stresses obtained by fracture mechanics considerations at the fastener hole.

The wedging force  $V$  is split into one part ( $V_a$ ) being responsible for the peak stresses at the fastener hole and one ( $V_b$ ) acting as load on the elastic beam.

$$V = V_a + V_b \quad 4.32$$

The equation for the stresses perpendicular to the grain for a single fastener connection at the fastener hole can be expressed as follows:

$$\sigma_{t,90}(x = 0) = \sigma_{t,90,a}(x = 0) + \sigma_{t,90,b}(x = 0) \quad 4.33$$

- $\sigma_{t,90,a}(x)$  stresses perpendicular due to peak stresses [N/mm<sup>2</sup>]
- $\sigma_{t,90,b}(x)$  stresses perpendicular due to analytical stress distribution model [N/mm<sup>2</sup>]

### 4.3.2.1 Elastic Beam Model

The stresses perpendicular due to the distribution model can be obtained with:

$$\sigma_{t,90,b}(x) = \frac{w(x)k}{y_a} \quad 4.34$$

- $w(x)$  displacement of the beam on elastic foundation [mm]
- $k$  foundation modulus of the beam [N/mm<sup>2</sup>]

### 4.3.2.2 Displacement Distribution of the Elastic Beam

The displacement distribution along the connection is obtained via the beam on elastic foundation theory as derived by Jorissen [1] based on Hetenyi (1974) [26].

Bending and shear are accounted for as the ratio of the height of the virtual beam and its length is rather small [8]. Consequently, the Timoshenko-beam theory has to be applied. This means that from the original two assumptions of the Euler-Bernoulli beam (which only considers bending); plane sections normal to the axis remain plane and plane sections are always normal to the beam axis, only the first one is still assumed.

An infinitely small beam element (with bending and shear) is considered:

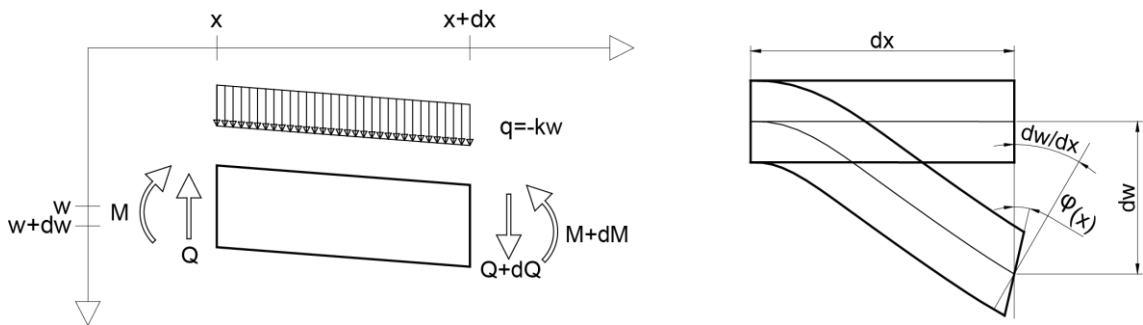


Figure 67: Infinitely small beam element in bending

Vertical equilibrium:

$$dQ = kw dx \quad 4.35$$

Moment equilibrium:

$$Q dx = dM \quad 4.36$$

Constitutive relations:

$$M = -EI \frac{d\varphi}{dx} = -c_1 \phi' \quad 4.37$$

$$Q = \kappa GA \left( -\phi + \frac{dw}{dx} \right) = c_2 w' - c_2 \phi \quad 4.38$$

With:

$$EI = c_1 \quad 4.39$$

$$\kappa GA = c_2 \quad 4.40$$

$$\frac{d\varphi}{dx} = \phi' \quad 4.41$$

$$\frac{dw}{dx} = w' \quad 4.42$$

By combining Eq. 4.35 – Eq. 4.38 two differential equations can be obtained, describing the behaviour of the loaded beam.

$$kw = c_2 w'' - c_2 \phi' \quad 4.43$$

$$c_2 w' - c_2 \phi = -c_1 \phi'' \quad 4.44$$

Which can be further decomposed to:

$$c_1 \phi''' = -kw \quad 4.45$$

$$w' = \phi - \frac{c_1}{c_2} \phi'' \quad 4.46$$

Combining Eq. 4.45 and Eq. 4.46 leads to a fourth-order homogeneous differential equation describing the bending angle.

$$\phi'''' - \frac{k}{c_2} \phi'' + \frac{k}{c_1} \phi = 0 \quad 4.47$$

Equivalently Eq. 4.45 and Eq. 4.46 can be combined to the same differential equation describing the displacement  $w(x)$  as variable, but due to an easier derivation later the bending angle is preferred.

By applying the approach:

$$\phi(x) = Ce^{\alpha x} \quad 4.48$$

The following equation can be obtained:

$$\alpha^4 - \frac{k}{c_2} \alpha^2 + \frac{k}{c_1} = 0 \quad 4.49$$

A solution for  $\alpha^2$  would be:

$$\alpha^2 = \frac{k}{2c_2} \pm \sqrt{\frac{\left(\frac{k}{2c_2}\right)^2 - \frac{k}{c_1}}{\left(\frac{k}{2\kappa GA}\right)^2 - \frac{k}{EI}}} \quad 4.50$$

For  $\frac{k}{EI} > \left(\frac{k}{2\kappa GA}\right)^2$  which should be valid for most practical cases Eq. 4.50 can be rearranged:

$$\alpha^2 = \frac{k}{2c_2} \pm i \sqrt{\frac{k}{c_1} - \left(\frac{k}{2c_2}\right)^2} \quad 4.51$$

With:

$$i = \sqrt{-1} \quad 4.52$$

An approach to obtain  $\alpha$  can be given:

$$\alpha = \beta + i\eta \quad 4.53$$

Thus:

$$\alpha^2 = \beta^2 + 2i\beta\eta - \eta^2 \quad 4.54$$

Where:

$$\beta^2 - \eta^2 = \frac{k}{2c_2} \quad 4.55$$

$$2\beta\eta = \sqrt{\frac{k}{c_1} - \left(\frac{k}{2c_2}\right)^2} \quad 4.56$$

Rearranging yields:

$$\beta\eta = \sqrt{\frac{k}{4c_1} - \left(\frac{k}{4c_2}\right)^2} \quad 4.57$$

The factor  $\lambda^4$  is introduced:

$$\lambda^4 = \frac{k}{4c_1} = \frac{k}{4EI} \quad 4.58$$

This results in:

$$\beta\eta = \sqrt{\left(\lambda^2 + \left(\frac{k}{4c_2}\right)^2\right)\left(\lambda^2 - \left(\frac{k}{4c_2}\right)^2\right)} \quad 4.59$$

Thus:

$$\beta = \sqrt{\lambda^2 + \left(\frac{k}{4c_2}\right)^2} = \sqrt{\lambda^2 + \left(\frac{k}{4\kappa GA}\right)^2} \quad 4.60$$

$$\eta = \sqrt{\lambda^2 - \left(\frac{k}{4c_2}\right)^2} = \sqrt{\lambda^2 - \left(\frac{k}{4\kappa GA}\right)^2} \quad 4.61$$

The previously made approach:

$$\alpha_{1234} = \pm(\beta + i\eta) \quad 4.62$$

Is combined with Eq. 4.48 to obtain:

$$\phi(x) = K_1 e^{(\beta+i\eta)x} + K_2 e^{(\beta-i\eta)x} + K_3 e^{(-\beta+i\eta)x} + K_4 e^{(-\beta-i\eta)x} \quad 4.63$$

The relationship:

$$e^{i\eta x} = \cos(\eta x) + i\sin(\eta x) \quad 4.64$$

$$e^{-i\eta x} = \cos(\eta x) - i\sin(\eta x) \quad 4.65$$

can be used to yield:

$$\begin{aligned} \phi(x) = e^{\beta x} [K_1 (\cos(\eta x) + i\sin(\eta x)) + K_2 (\cos(\eta x) - i\sin(\eta x))] \\ + e^{-\beta x} [K_3 (\cos(\eta x) + i\sin(\eta x)) + K_4 (\cos(\eta x) - i\sin(\eta x))] \end{aligned} \quad 4.66$$

Rearranging:

$$\begin{aligned} \phi(x) = e^{\beta x} [\cos(\eta x) (K_1 + K_2) + \sin(\eta x) (iK_1 - iK_2)] \\ + e^{-\beta x} [\cos(\eta x) (K_3 + K_4) + \sin(\eta x) (iK_3 - iK_4)] \end{aligned} \quad 4.67$$

Introducing new constants:

$$\phi(x) = (A_1 \cos(\eta x) + B_1 \sin(\eta x))e^{\beta x} + (A_2 \cos(\eta x) + B_2 \sin(\eta x))e^{-\beta x} \quad 4.68$$

By using the relationship:

$$c_1 \phi''' = -kw \quad 4.69$$

Thus:

$$w = -\frac{c_1}{k} \phi''' = -\frac{EI}{k} \frac{d\phi^3}{dx^3} \quad 4.70$$

The displacement function  $w(x)$  can be found:

$$w(x) = [(A_1 Z_1 + B_1 Z_1) \cos(\eta x) + (-A_1 Z_2 + B_1 Z_1) \sin(\eta x)]e^{\beta x} + [(-A_2 Z_1 + B_2 Z_2) \cos(\eta x) + (-A_2 Z_2 - B_2 Z_1) \sin(\eta x)]e^{-\beta x} \quad 4.71$$

With:

$$Z_1 = (\beta^3 - 3\beta\eta^2) \frac{EI}{k} \quad 4.72$$

$$Z_2 = (3\beta^2\eta - \eta^3) \frac{EI}{k} \quad 4.73$$

The constants  $A_i$  and  $B_i$  can be determined by using the following boundary conditions. It needs to be remarked that since the beam has to be divided into two parts (due to the discontinuity loaded fastener – hole), in the actual calculations eight constants –  $A_1, A_2, B_1, B_2, C_1, C_2, D_1, D_2$  – have to be taken into consideration and calculated.

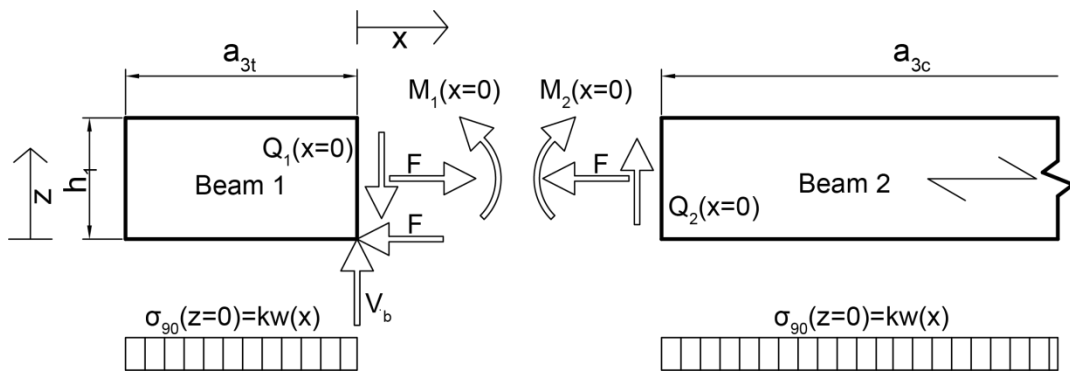


Figure 68: Situation of internal and external forces

For  $x = -a_{3t}$ :

$$M_1(x = -a_{3t}) = -EI \frac{d\phi_1(x = -a_{3t})}{dx} = 0 \quad 4.74$$

$$Q_1(x = -a_{3t}) = \kappa GA \left( -\phi_1(x = -a_{3t}) + \frac{dw_1(x = -a_{3t})}{dx} \right) = -EI \frac{d\phi_1^2(x = -a_{3t})}{dx^2} = 0 \quad 4.75$$

For  $x = 0$ :

$$w_1(x = 0) = w_2(x = 0) \quad 4.76$$

$$\phi_1(x = 0) = \phi_2(x = 0) \quad 4.77$$

$$Q_1(x = 0) - Q_2(x = 0) = V_b \hat{=} \frac{d\phi_1^2(x = 0)}{dx^2} - \frac{d\phi_2^2(x = 0)}{dx^2} = \frac{V_b}{EI} \quad 4.78$$

$$M_1(x = 0) - M_2(x = 0) = \frac{Fh_1}{2} \hat{=} \frac{d\phi_1(x = 0)}{dx} - \frac{d\phi_2(x = 0)}{dx} = \frac{Fh_1}{2EI} \quad 4.79$$

For  $x = a_{3c}$ :

$$w_2(x = a_{3c}) = 0 \quad 4.80$$

$$\phi_2(x = a_{3c}) = 0 \quad 4.81$$

With:

$$A = y_a h_1 \quad 4.82$$

$$I = \frac{y_a h_1^3}{12} \quad 4.83$$

$$\kappa = \frac{5}{6} \quad 4.84$$

- F half of the force acting parallel to the grain introduced by the fastener [N]
- $V_b$  part of the wedging force V that acts in the analytical stress distribution model [N]
- $\kappa$  shear coefficient for a rectangular cross section [-]

With the presented relationships the constants and therefore the displacement distribution along the connection length can be calculated.

#### 4.3.2.3 The Foundation Modulus

Next the determination of the foundation modulus k is shown. It represents the stiffness of the elastic foundation of the idealised beam.

As used in the derivation of the displacement distribution the distributed load acting on the idealised beam can be expressed as:

$$q = kw \quad 4.85$$

And thus:

$$k = \frac{q}{w} = \frac{\sigma_{90}(z=0)y_a}{w} = \frac{\sigma_{90,max}y_a}{w} \quad 4.86$$

The distribution of the stresses perpendicular to the grain in z-direction is derived by using the following boundary conditions:

- $z = 0$ :

$$\sigma_{90}(z=0) = \sigma_{90,max} \quad 4.87$$

$$\frac{d\sigma_{90}}{dz} = 0 \quad 4.88$$

- $z = h_1/2$ :

$$\sigma_{90}(z = \frac{h_1}{2}) = 0 \quad 4.89$$

A parabolic function satisfies the boundary conditions:

$$\sigma_{90}(z) = \sigma_{90,\max} - \sigma_{90,\max} \frac{z^2}{h_1^2} \quad 4.90$$

Notice that the function for  $\sigma_{90}(z)$  was rather arbitrarily chosen by Jorissen (1998) [1]. Other authors (Timoshenko and Goodier (1952) [12], Schmid et al. (2002) [10]) suggest a different function for the distribution of the stresses perpendicular to the grain that fulfils the boundary conditions, as well [8]. This has a quite considerable impact on the foundation modulus. However this matter is discussed later in this thesis. For now, it is continued with Eq. 4.90.

With Hooke's law:

$$\varepsilon_{90} = \frac{\sigma_{90}}{E_{90}} \quad 4.91$$

the displacement perpendicular to the grain at the neutral axis ( $z = h_1/2$ ) can be obtained with:

$$\begin{aligned} w\left(z = \frac{h_1}{2}\right) &= \int_0^{\frac{h_1}{2}} \varepsilon_{90}(z) dz = \int_0^{\frac{h_1}{2}} \frac{\sigma_{90}(z)}{E_{90}} dz \\ &= \frac{1}{E_{90}} \int_0^{\frac{h_1}{2}} \left(\sigma_{90,\max} - \sigma_{90,\max} \frac{z^2}{h_1^2}\right) dz = \frac{11}{24} \frac{\sigma_{90,\max}}{E_{90}} h_1 \\ &\approx 0.46 \frac{\sigma_{90,\max}}{E_{90}} h_1 \end{aligned} \quad 4.92$$

Eq. 4.92 and Eq. 4.86 can be combined and an Eq. 4.93 determining the foundation modulus  $k$  is obtained:

$$k = \frac{24 E_{90} Y_a}{11 h_1} = 2.18 \frac{E_{90} Y_a}{h_1} \quad 4.93$$

Based on Timoshenko and Goodier (1951), Schmid et al. (2002) assume another stress distribution of the stresses perpendicular to the grain in z-direction [10], [12]. Their function also satisfies (along with the already mentioned constraints):

- $z = h_1$ :

$$\frac{d\sigma_{90}}{dz} = 0 \quad 4.94$$

The function is:

$$\sigma_{90}(z) = \frac{\sigma_{90,\max}}{2} \left( \frac{3 \left(-\frac{h_1}{2} + z\right)}{2h_1} - \frac{2 \left(-\frac{h_1}{2} + z\right)^3}{h_1^3} \right) \sigma_{90,\max} \quad 4.95$$

Thus:

$$w \left( z = \frac{h_1}{2} \right) = \int_0^{\frac{h_1}{2}} \frac{\sigma_{90}(z)}{E_{90}} dz = \frac{13 \sigma_{90,\max}}{32 E_{90}} h_1 \approx 0.41 \frac{\sigma_{90,\max}}{E_{90}} h_1 \quad 4.96$$

And:

$$k = \frac{32 E_{90} Y_a}{13 h_1} \approx 2.46 \frac{E_{90} Y_a}{h_1} \quad 4.97$$

Figure 69 depicts the different stress distribution functions in z-direction across the timber member:

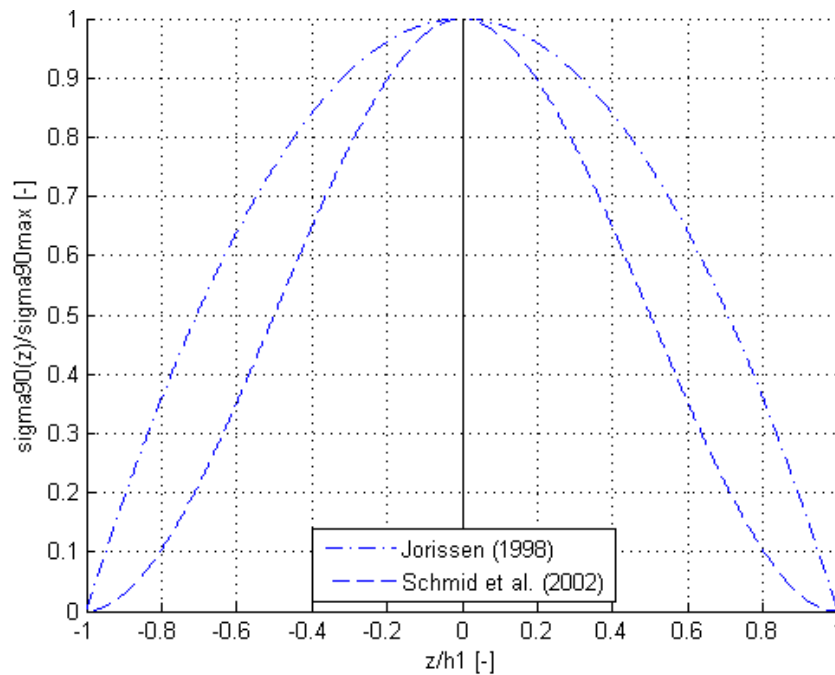


Figure 69: Comparison of different stress distribution functions

In further calculations the stress distribution function by Timoshenko and Goodier (1951) [12] is used to determine the foundation modulus because this function is an exact solution for a beam made of an isotropic material loaded with a uniformly distributed load [12]. Furthermore FEM-calculations conducted by Schmid et al. (2002) show that this function also depicts the stress distribution of the stresses perpendicular to the grain in the orthotropic material wood/timber quite well [10].

### Peak Stress Model

The peak stress at the fastener hole can be calculated with:

$$\sigma_{t,90,a}(x = 0) = \sigma_{t,90,a,max} = \frac{2V_a}{y_a L_{reg}} \quad 4.98$$

- $V_a$  part of wedging force  $V$  that is used for peak stresses [N]
- $L_{reg}$  length of the fracture process region at the tip of the crack [mm]

The factor 2 originates from the fact that a triangular stress distribution over the crack length  $L_{reg}$  is assumed. Thus the definition of the function is:

$$\sigma_{t,90,a}(x) = \begin{cases} -x_0 \leq x < -L_{\text{reg}} \rightarrow 0 \\ -L_{\text{reg}} \leq x \leq 0 \rightarrow \sigma_{t,90,a,\text{max}} + \sigma_{t,90,a,\text{max}} \frac{x}{L_{\text{reg}}} \\ 0 < x \leq x_3 \rightarrow 0 \end{cases} \quad 4.99$$

#### 4.3.2.4 The Length of the Fracture Process Region

This length represents the size of the fracture process region at the tip of the crack which is still able to transfer loads.

The equation for the length of the fracture process region for timber is based on FEM-calculations conducted by Gustafsson (1985) [22]:

$$L_{\text{reg}} = 0.25 \frac{G_c \sqrt{EG}}{f_t^2} \quad 4.100$$

For this model, which considers stresses perpendicular to the grain the expression changes to:

$$L_{\text{reg}} = 0.25 \frac{G_c \sqrt{E_{90}G}}{f_{t,90}^2} \quad 4.101$$

#### 4.3.2.5 Dividing the Wedging Force V

It is assumed that at failure a certain peak stress level  $\sigma_{zF}$  at the fastener hole is attained

$$\sigma_{t,90,a}(x=0) + \sigma_{t,90,b}(x=0) = \sigma_{zF} \quad 4.102$$

Furthermore the stresses comprise:

$$\sigma_{t,90,a}(x=0) = \frac{2V_a}{y_a L_{\text{reg}}} = C_a V_a \quad 4.103$$

With:

$$C_a = \frac{2}{y_a L_{reg}} \quad 4.104$$

And:

$$\begin{aligned} \sigma_{t,90,b}(x=0) &= \frac{w(x=0)k}{y_a} = C_b(V_b f_1(x=0) + F f_2(x=0)) \\ &= C_b \left( V_b f_1(x=0) + \frac{V}{2f_V(\varphi)} f_2(x=0) \right) \end{aligned} \quad 4.105$$

With:

$$C_b = \frac{k}{y_a} \quad 4.106$$

$$w(x=0)^{***} = V_b f_1(x=0) + F f_2(x=0) \quad 4.107$$

$$2F = \frac{V}{f(\varphi)} \quad 4.108$$

$$f_V(\varphi) = \frac{\frac{1 - \sin^2(\varphi)}{2} \cos(\varphi) - \left( \frac{\pi}{4} - \frac{\varphi}{2} - \frac{\sin(2\varphi)}{4} \right) \sin(\varphi)}{2 \cos(\varphi)} \quad 4.109$$

(\*\*\* The derivation of this relationship can be found in the appendix (chapter 10.2))

Combining Eq. 4.102, Eq. 4.103 and Eq. 4.105 results in:

$$C_a V_a + C_b \left( V_b f_1(x=0) + \frac{V}{2f_V(\varphi)} f_2(x=0) \right) = \sigma_{zF} \quad 4.110$$

With:

$$V = V_a + V_b \quad 4.111$$

Eq. 4.112 can be derived:

$$C_a V_a + C_b \left[ (V - V_a) f_1(x=0) + \frac{V}{2f_V(\varphi)} f_2(x=0) \right] - \sigma_{z,F} = 0 \quad 4.112$$

Thus, at failure  $V_a$  and  $V_b$ , dependent on a certain  $V$ , can be calculated that the stresses at the fastener hole are  $\sigma_{z,F}$ :

$$V_a = \frac{\sigma_{z,F} - VC_b \left( f_1(x=0) + \frac{f_2(x=0)}{2f_V(\varphi)} \right)}{C_a - C_b f_1(x=0)} \quad 4.113$$

Now an example for the determination of the forces ( $V$ ,  $V_a$ ,  $V_b$ ) is presented. The friction angle  $\varphi$  is varied between  $1^\circ$  and  $30^\circ$ :

The assumption is made that at failure due to stresses perpendicular to grain the embedment strength is reached and also failure according to Johansen-Theory arises. This is not necessarily the exact  $V$  at which failure due to stresses perpendicular to grain would occur, but it should be somewhere around this value (as long as only a single fastener connection is considered) if the model shall be accurate as the Johansen model can be seen as quite trustworthy (it has been successfully validated (see chapter 2.1.5.9)). Therefore  $V$  can be calculated with:

$$V = 2Ff_V(\varphi) = f_{h,y}df_V(\varphi) \quad 4.114$$

The following values for the parameters are used:

- $\sigma_{z,F} = f_{t,90} = 3 \text{ N/mm}^2$        $d = 12 \text{ mm}$        $y_a = y = t = 24 \text{ mm}$
- $h = 72 \text{ mm}$        $a_{3t} = 7d$        $E_0 = 12000 \text{ N/mm}^2$
- $E_{90} = 400 \text{ N/mm}^2$        $G = 640 \text{ N/mm}^2$        $\rho = 400 \text{ kg/m}^3$
- $G_c = 0.35 \text{ Nmm/mm}^2$

It is visible that the wedging force decreases with increasing friction angle, as already discussed and, as a consequence, the part of the wedging force that has to be substituted into the peak stress model increases to still attain  $f_{t,90}$  and therefore failure. The  $V_a$  to  $V$  ratio increases while the  $V_b$  to  $V$  ratio decreases.

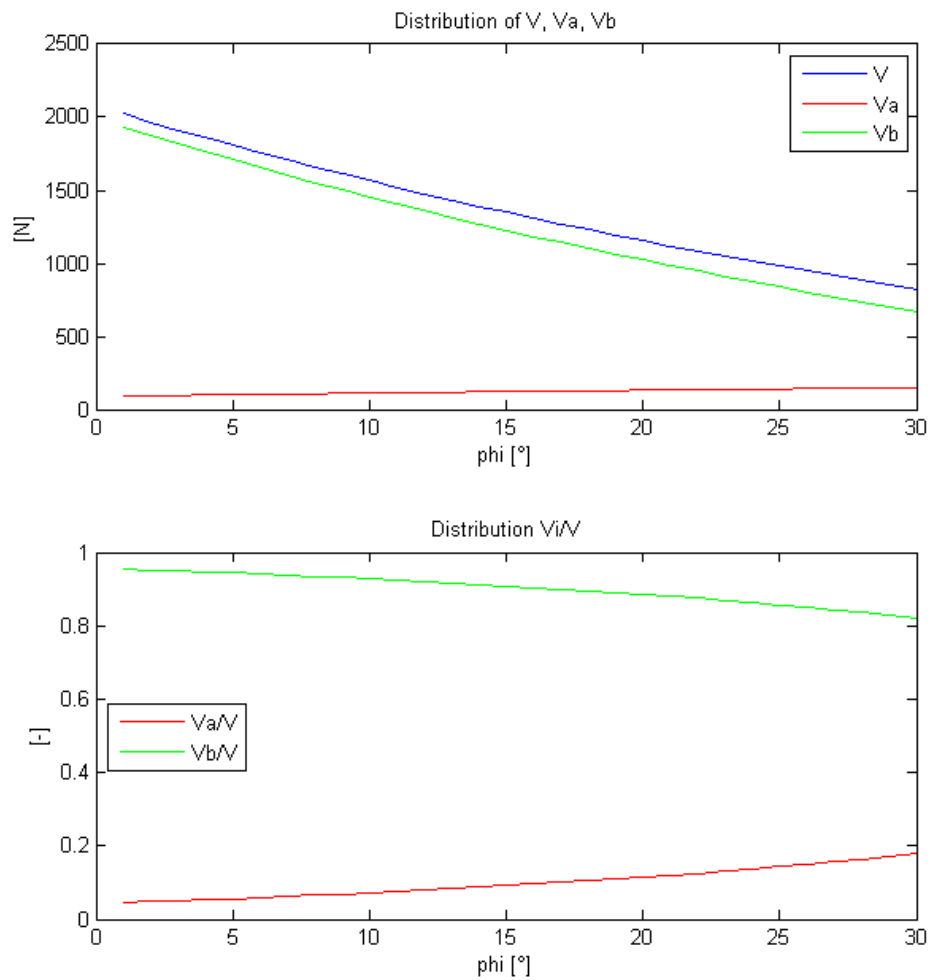


Figure 70: Wedging force substitution distribution over the friction angle

- $\varphi = 18^\circ$ :  $V = 1230 \text{ N}$   $V_a = 128 \text{ N} = 0.1 V$   $V_b = 1102 \text{ N} = 0.9 V$
- $\varphi = 30^\circ$ :  $V = 822 \text{ N}$   $V_a = 148 \text{ N} = 0.18 V$   $V_b = 674 \text{ N} = 0.82 V$

It has to be said that there is no difference in the partition of the wedging force with changing timber member thickness  $t$ . However, the splitting ratio changes with changing fastener diameter  $d$  and altering timber member width  $h$ , changing the foundation modulus  $k$  has an influence on the splitting ration as well.

The resulting distribution of tensile stresses perpendicular to the grain is shown in Figure 71 for the above described example with these parameters specified:

- $\varphi = 18^\circ$   $2F \sim 8300 \text{ N}$

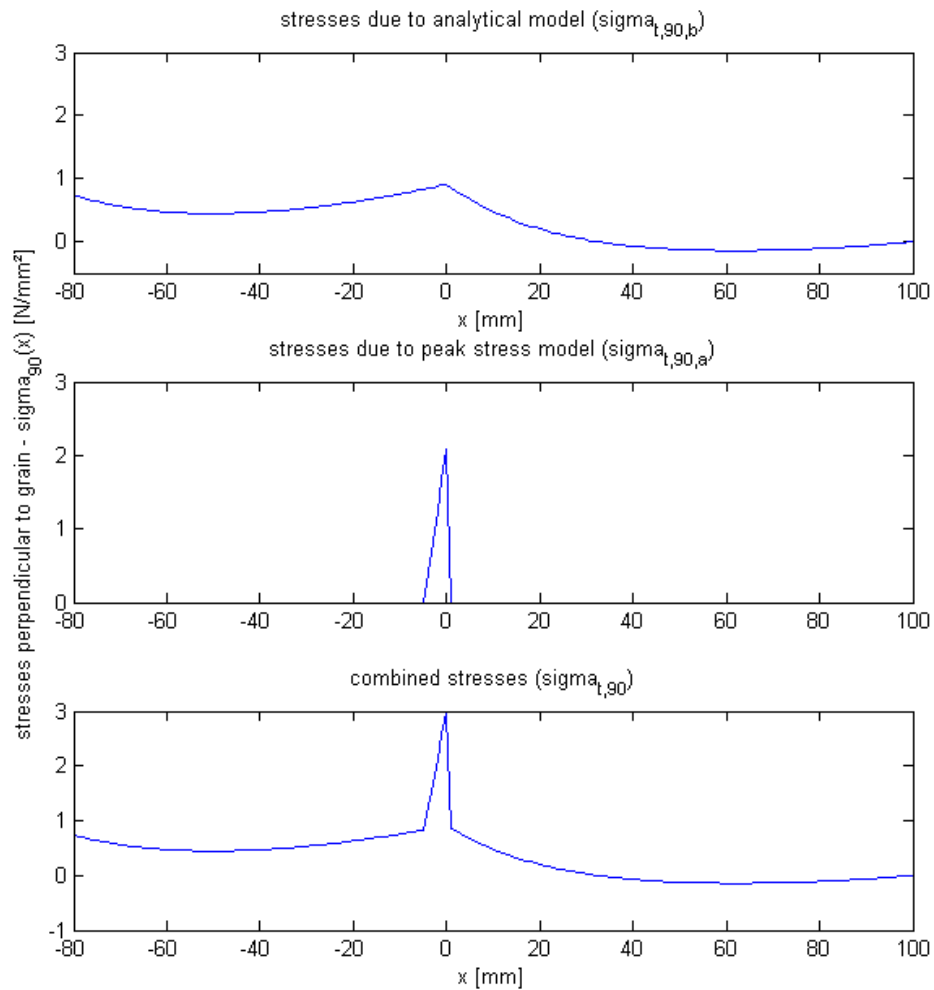


Figure 71: Distributions tensile stresses perpendicular to grain and their superposition

It needs to be stressed once more that the model depicting the stress situation of the tensile stresses perpendicular to the grain is linear elastic (with a slight consideration of plasticity, see chapter 4.1.2) with added fracture mechanics considerations which are superposed to obtain the final stress distribution. In reality at connection failure (which is the depicted state throughout this model) the whole situation exhibits plastic deformations. For this reason an accurate superposition of stresses becomes questionable. To not complicate matters too much this approach is chosen nonetheless with the results justifying the use to a certain extent (see chapter 4.3.2.6 and chapter 5.7.2).

#### 4.3.2.6 Extending the Model to Multiple Fastener Connections

The presented model can also depict the distribution of stresses perpendicular to the grain of multiple fasteners in a row. To achieve this, the stress distribution for every single fastener is determined treating it equally to a single fastener connection. Then the obtained stress distributions can be added to one overall stress distribution of the whole fastener row. The next example exhibits this matter and

shows how stress accumulation can arise. To generate Figure 72, the same parameters as in the last example were chosen and furthermore, these were added:

- $a_1 = 7d$                        $n = 2$

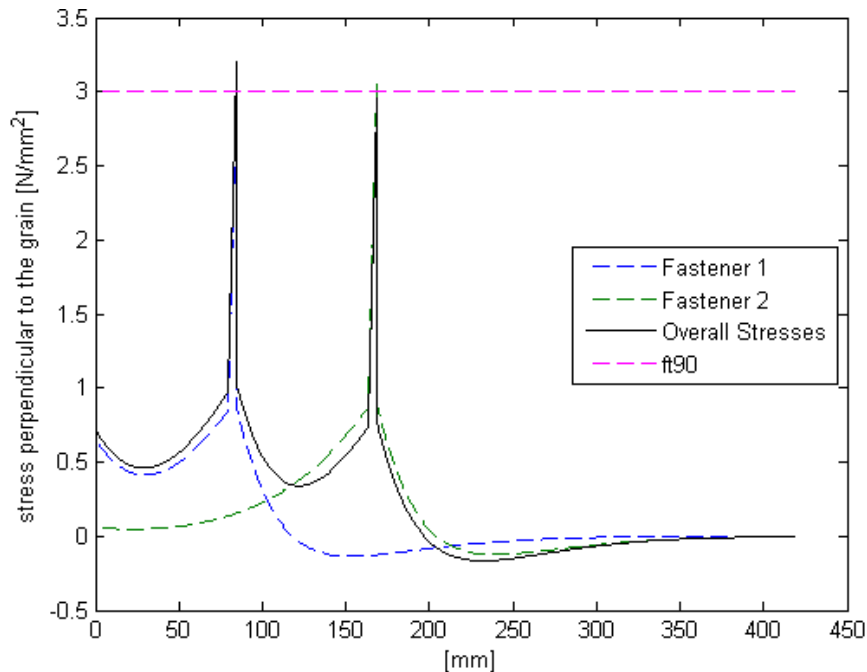


Figure 72: Stress distribution of two fasteners in a row

The stress at the fastener hole considering only every single fastener is  $f_{t,90}$ , but if the stresses are combined, the situation emerges that for the first fasteners the accumulated stresses attain a higher value than  $f_{t,90}$  while at the last fastener hole the stresses even decrease. This connection most likely would fail due to exceeding stresses perpendicular to the grain. This is the effect of stress accumulation in multiple fastener connections that is partly responsible for the reduction of the load carrying capacity in a multiple fastener connection compared to the strength of a single fastener connection according to Johansen's Yield Theory times the number of fasteners. In this example the assumption is made that all the fasteners are loaded with the same force at failure. This matter is discussed in more detail in chapter 5.

As a comparison Figure 73 is presented that shows the stress distribution according to FEM-calculations carried out by Werner (1993) [7]. There is a rather good agreement, considering that the FEM-calculations were carried out with similar parameters (same  $a_1$  and  $a_{3t}$ ) as the ones above.

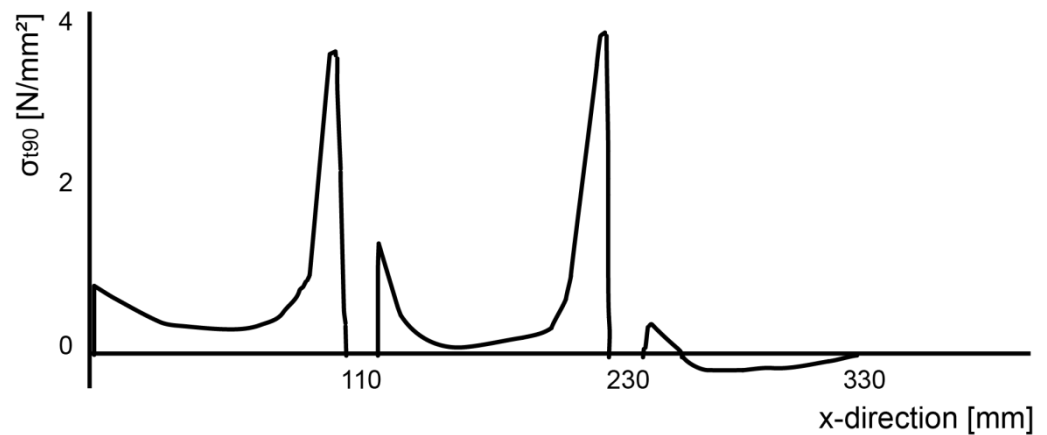


Figure 73: Distribution stresses perpendicular to the grain according to Werner (1993) [7]

#### 4.3.2.7 Elastic Beam Model – Fastener Loaded Perpendicular to the Grain

Hitherto only the load situation fastener loaded parallel to the grain was considered. However, it shall be mentioned that the model of the beam on elastic foundation is also capable of depicting the condition of stresses perpendicular to the grain in other load situations. From a certain load angle on, the beam-on-elastic-foundation-model alone is capable of depicting the stress distribution. This matter is further examined in chapter 5.2. For the above presented example the stress distribution is shown in Figure 74 for the loading situation fastener loaded perpendicular to the grain. The following parameters are changed:

- $a_{3t} = a_{3c} = 250 \text{ mm}$        $2F \sim 3500 \text{ N}$

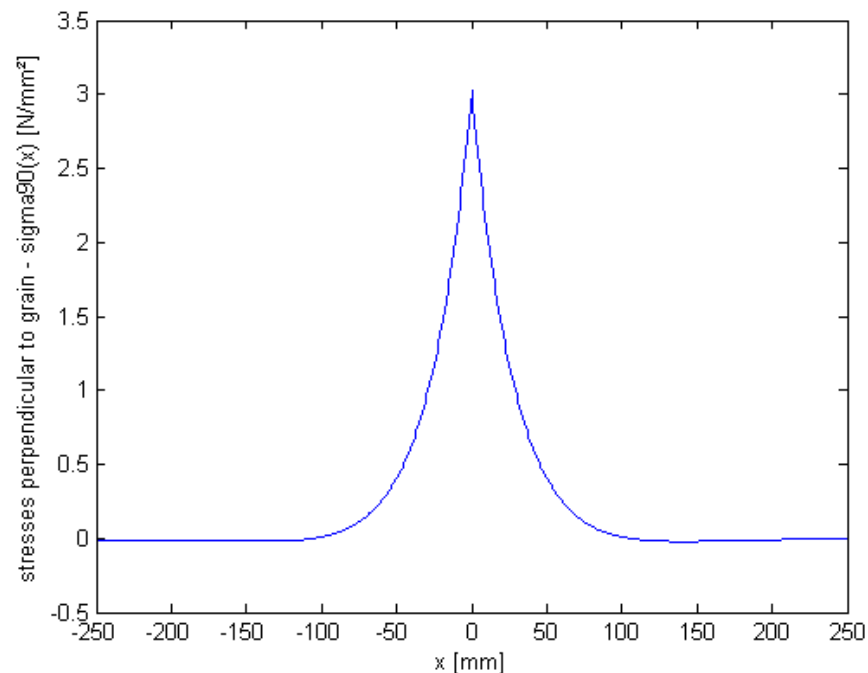


Figure 74: Stress distribution perpendicular to the grain – in case of a single fastener loaded perpendicular to the grain

This load situation can also be extended to multiple fastener connections as shown in Figure 75. One interesting matter that emerges is that stress accumulation also occurs in this case (according to linear elastic theory) while according to Eurocode [1] no reduction of the carrying capacity for the single fastener is taken into account for the loading situation perpendicular to the grain.

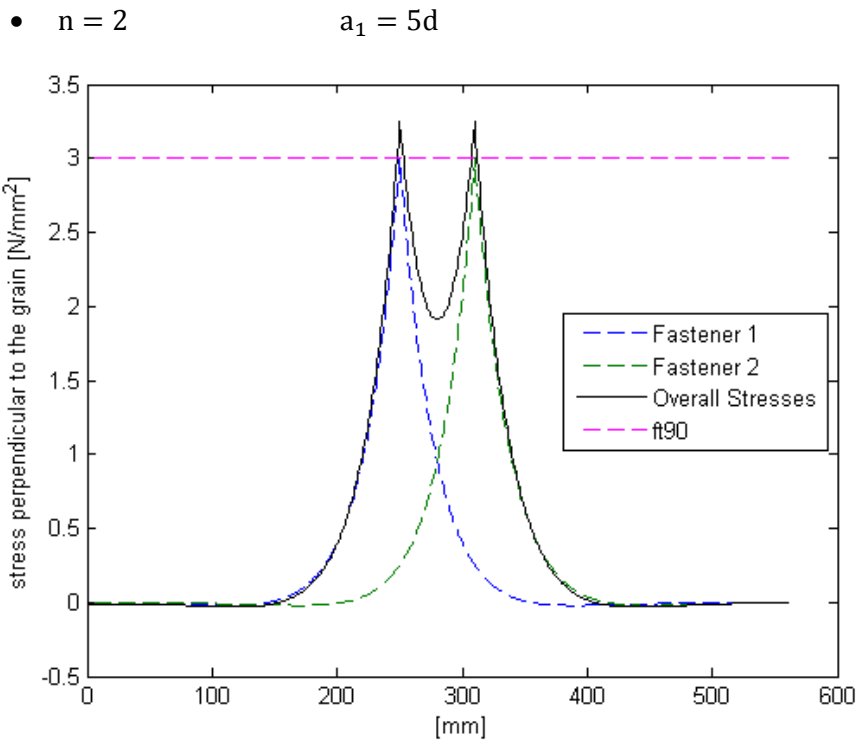


Figure 75: Stress distribution of two fasteners in a row fastener loaded perpendicular to the grain

### 4.3.3 Shear Stresses in a Connection

The approach to obtain the distribution of shear stresses along the connection is presented. It was derived by Jorissen (1998) [1] based on a theory devised by Volkersen (1938) [24] and extended by Gustaffson (1987) [23].

Again, it is assumed that the whole force  $2F$  is transferred by the area  $2h_2y$ , which is enclosed by the two shear planes where the cracks occur.

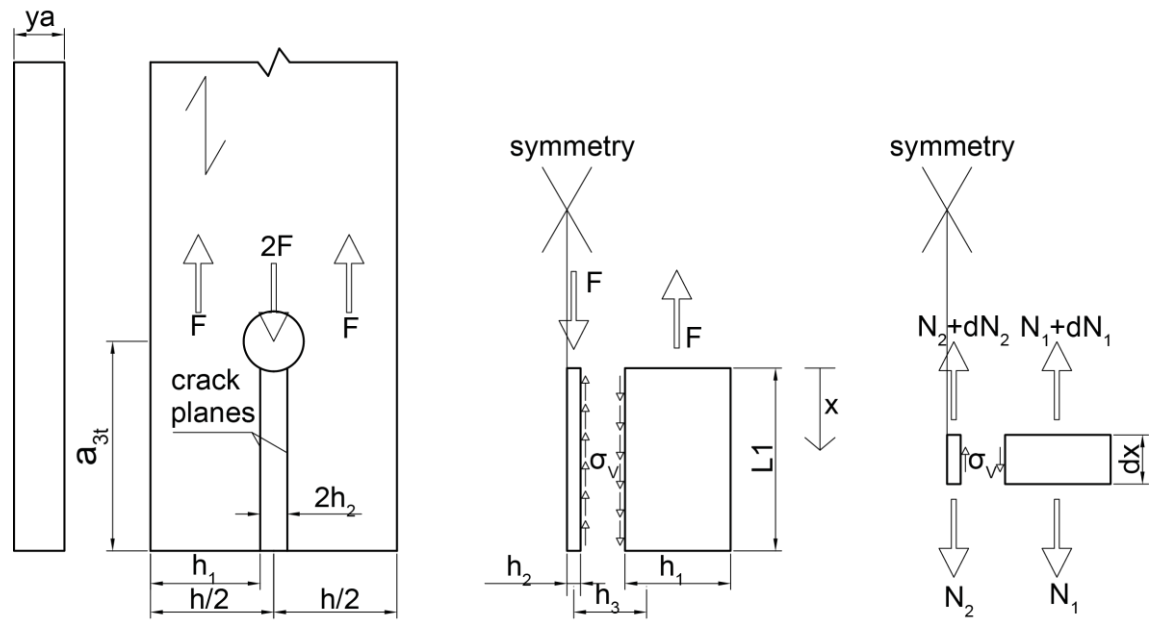


Figure 76: System to derive the shear model

Vertical Equilibrium:

$$dN_1 - \sigma_v y_a dx = 0 \quad 4.115$$

$$dN_2 + \sigma_v y_a dx = 0 \quad 4.116$$

Kinematic relations:

$$\varepsilon_1 = \frac{du_1}{dx} \quad 4.117$$

$$\varepsilon_2 = \frac{du_2}{dx} \quad 4.118$$

$$\gamma = \frac{u_1 - u_2}{h_3} \quad 4.119$$

Constitutive relations:

$$\sigma_1 = E_0 \varepsilon_1 \quad 4.120$$

$$\sigma_2 = E_0 \varepsilon_2 \quad 4.121$$

$$\sigma_v = G\gamma \quad 4.122$$

$$\sigma_i = \frac{N_i}{h_i y_a} + \frac{M_i}{W_i} \quad 4.123$$

It is assumed that the influence of bending moments can be neglected as they play a minor role in the emergence of the shear stresses and are mainly responsible for stresses perpendicular to the grain which have already been analysed. Therefore in this analysis

$$\sigma_i = \frac{N_i}{h_i y_a} \quad 4.124$$

Combining Eq. 4.117 – Eq. 4.124 leads to:

$$\sigma_1 = E_0 \frac{du_1}{dx} = \frac{N_1}{y_a h_1} \quad 4.125$$

$$\frac{du_1}{dx} = \frac{N_1}{E_0 y_a h_1} \quad 4.126$$

$$\sigma_2 = E_0 \frac{du_2}{dx} = \frac{N_2}{y_a h_2} \quad 4.127$$

$$\frac{du_2}{dx} = \frac{N_2}{E_0 y_a h_2} \quad 4.128$$

$$\frac{d\gamma}{dx} = \frac{1}{h_3} \left( \frac{du_1}{dx} - \frac{du_2}{dx} \right) = \frac{1}{E_0 y_a h_3} \left( \frac{N_1}{h_1} - \frac{N_2}{h_2} \right) \quad 4.129$$

Differentiating and inserting of Eq. 4.115 and Eq. 4.116 yields:

$$\frac{d^2\gamma}{dx^2} = \frac{1}{E_0 y_a h_3} \left( \frac{1}{h_1} \frac{N_1}{dx} - \frac{1}{h_2} \frac{N_2}{dx} \right) = \frac{1}{E_0 y_a h_3} \left( \frac{\sigma_v y_a}{h_1} + \frac{\sigma_v y_a}{h_2} \right) \quad 4.130$$

$$\frac{d^2\gamma}{dx} = \frac{h_1 + h_2}{h_1 h_2 h_3 y_a E_0} \sigma_v = \frac{h_1 + h_2}{h_1 h_2 h_3 y_a E_0} G\gamma \quad 4.131$$

$$\frac{d^2\gamma}{dx} - \frac{(h_1 + h_2)G}{h_1 h_2 h_3 y_a E_0} \gamma = 0 \quad 4.132$$

The factor

$$\omega^2 = \frac{(h_1 + h_2)G}{h_1 h_2 h_3 y_a E_0} \quad 4.133$$

is introduced which yields a homogeneous differential equation of second order:

$$\frac{d^2\gamma}{dx} - \omega^2 \gamma = 0 \quad 4.134$$

A solution can be given:

$$\gamma = A \cosh(\omega x) + B \sinh(\omega x) \quad 4.135$$

$$\frac{d\gamma}{dx} = A \omega \sinh(x) + B \omega \cosh(x) \quad 4.136$$

The constants A and B can be determined by considering the following boundary conditions:

For  $x = 0$ :

$$N_1 = F \quad 4.137$$

$$N_2 = -F \quad 4.138$$

$$\sigma_1 = \frac{F}{y_a h_1} \quad 4.139$$

$$\sigma_2 = -\frac{F}{y_a h_2} \quad 4.140$$

Therefore:

$$\frac{d\gamma}{dx} = \frac{1}{E_0 y_a h_3} \left( \frac{F}{h_1} + \frac{F}{h_2} \right) = \frac{(h_1 + h_2)F}{h_1 h_2 h_3 y_a E_0} \quad 4.141$$

For  $x = -L_1$ :

$$N_1 = \sigma_1 = 0 \quad 4.142$$

$$N_2 = \sigma_2 = 0 \quad 4.143$$

Thus:

$$\frac{d\gamma}{dx} = 0 \quad 4.144$$

Which yields:

$$B = \frac{(h_1 + h_2)F}{h_1 h_2 h_3 y_a E_0 \omega} \quad 4.145$$

$$A = B \frac{\cosh(\omega L_1)}{\sinh(\omega L_1)} = \frac{(h_1 + h_2)F}{h_1 h_2 h_3 y_a E_0 \omega} \frac{\cosh(\omega L_1)}{\sinh(\omega L_1)} \quad 4.146$$

Inserting the constants (Eq. 4.145 and Eq. 4.146) into Eq. 4.135 leads to:

$$\gamma = \frac{(h_1 + h_2)F}{h_1 h_2 h_3 y_a E_0 \omega} \left( \frac{\cosh(\omega L_1)}{\sinh(\omega L_1)} \cosh(\omega x) + \sinh(\omega x) \right) \quad 4.147$$

The fictitious shear strain layer  $h_3$  can be determined by considering the stress-strain curve for shear as shown in Figure 77.

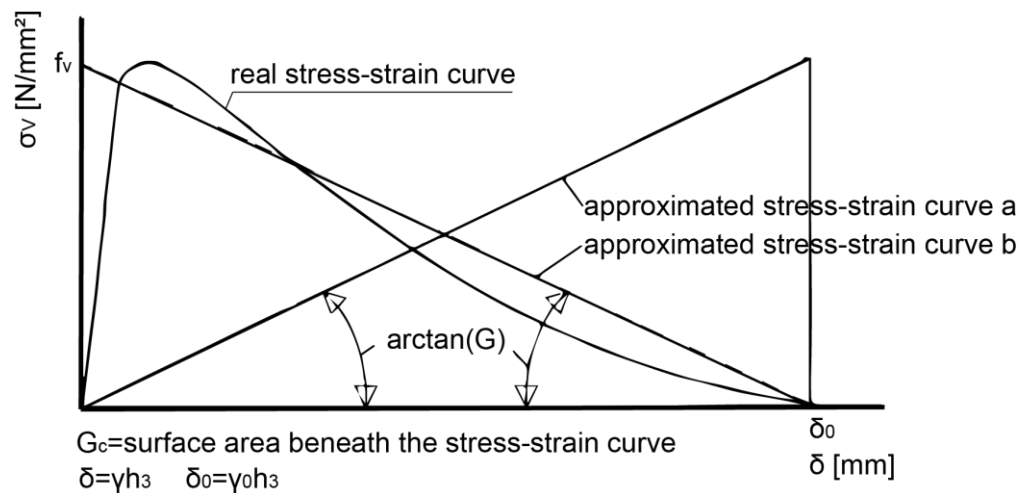


Figure 77: Stress-strain curve for shear with real curve and two approximated curves enclosing the same surface area as the real one [1]

$$G_c = \frac{1}{2} \delta_0 f_v = \frac{1}{2} \gamma_0 h_3 f_v \approx \frac{1}{2} \frac{f_v}{G} h_3 f_v = \frac{f_v^2 h_3}{2G} \quad 4.148$$

$$h_3 = \frac{2G_c G}{f_v^2} \quad 4.149$$

It should be mentioned that  $h_3$ , which describes the width of a fictitious layer deformed by shear strains, is dependent on the shear strength of the timber  $f_v$  because it is derived by considering the stress strain curve of the timber subjected to shear stresses.

This is somewhat contradictory as the size of the stresses in the shear plane is not only determined by the acting force but also by the shear strength. This means that for higher assumed shear strength the resulting stresses in the shear plane are higher as well although the force  $F$  could stay the same.

However, the shear stress distribution in a shear plane along the connection can be determined with:

$$\sigma_v(x) = \frac{F(h_1 + h_2)G}{h_1 h_2 h_3 y_a E_0 \omega} \left[ \frac{\cosh(\omega L_1)}{\sinh(\omega L_1)} \cosh(\omega x) + \sinh(\omega x) \right] \quad 4.150$$

With:

$$\omega = \sqrt{\frac{(h_1 + h_2)G}{2h_1h_2h_3E_0}} \quad 4.151$$

$$L_1 = a_{3t} \quad 4.152$$

$$h_2 = \frac{d}{2} \sin(\varphi) \quad 4.153$$

$$h_1 = \frac{h - 2h_2}{2} \quad 4.154$$

$$h_3 = \frac{2G_c G}{f_v^2} \quad 4.155$$

- $f_v$  shear strength of the timber [N/mm<sup>2</sup>]

An example of the obtained stress distribution for a single fastener connection is given in Figure 78 with the following parameters used:

- $\varphi = 18^\circ$                        $f_v = 4.5 \text{ N/mm}^2$                        $d = 12 \text{ mm}$
- $y_a = y = t = 24 \text{ mm}$                        $h = 72 \text{ mm}$                        $a_{3t} = 7d$
- $E_0 = 12000 \text{ N/mm}^2$                        $G_c = 0.35 \text{ Nmm/mm}^2$                        $2F \sim 5800 \text{ N}$

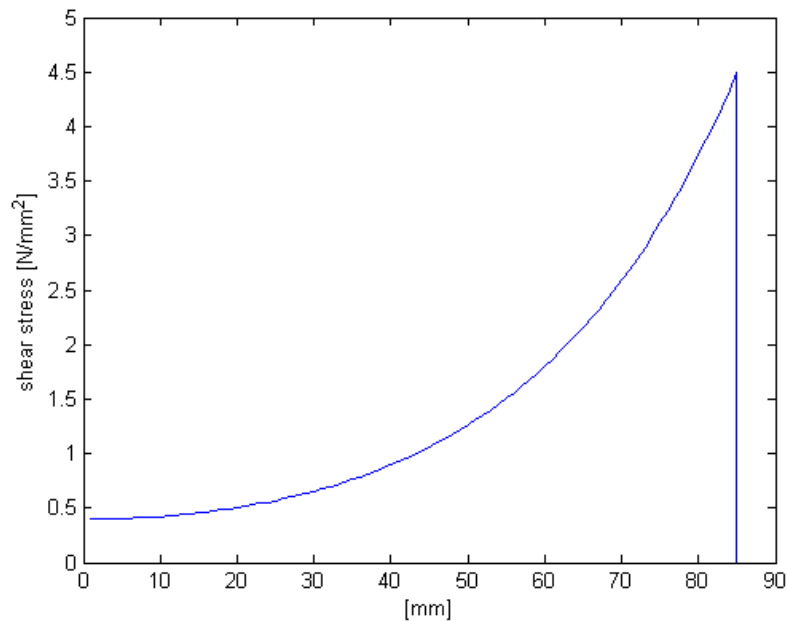


Figure 78: Shear stress distribution of a single fastener connection

This model can be extended to multiple fastener connections similarly to the one depicting stresses perpendicular to grain. The shear stress distribution for every single fastener is determined and then an overall distribution of the accumulated stresses can be calculated.

Figure 79 was generated with the same values as the one above adding these parameters:

- $n = 2$                        $a_1 = 7d$

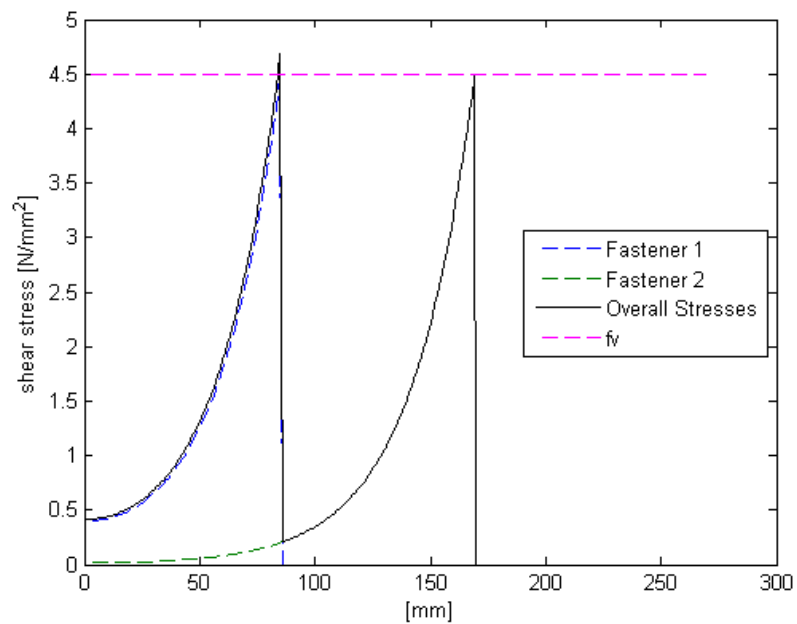


Figure 79: Stress distribution of two fasteners in a row

The shear strength is exceeded due to stress accumulation and therefore the overall bearing capacity regarding shear stresses decreases.

As a comparison the results of FEM-calculations by Werner [7] are shown in Figure 80.

Apparently Figure 80 also shows negative stress peaks “behind” the fastener hole (viewed in loading direction) that are not obtained by the analytical approximation. This is not seen as a major flaw, because they are remarkably smaller than the peaks in front of the fastener holes, which would consequently lead to failure.

However, this is just a linear elastic approximation. If the effect of plasticity were taken into consideration the shear stress distribution in front of a hole might look different in the sense that the peaks are more evened out with the rest of the distribution.

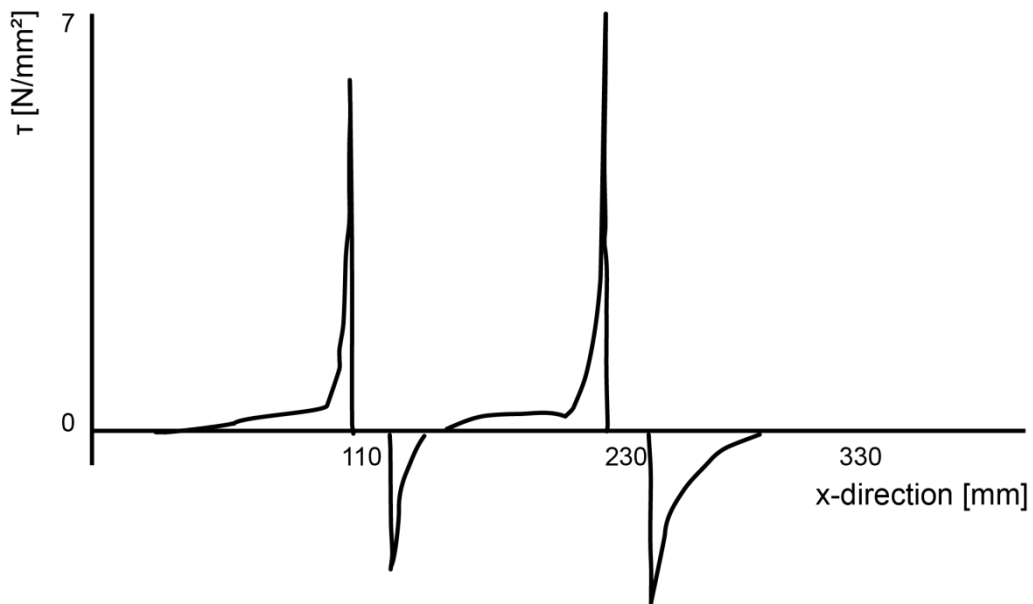


Figure 80: Shear stress distribution according to FEM calculations by Werner (1993) [7]

#### 4.3.4 Determination of the Critical Fracture Energy

As already discussed in chapter 4.2 the critical fracture energy depends strongly on the ratio between stresses perpendicular to the grain and shear stresses acting in the fracture process region.

$$G_c = f\left(\frac{\sigma_{t,90}}{\sigma_v}\right) \quad 4.156$$

To calculate this ratio the average stresses perpendicular to the grain are taken which can be determined by:

$$\sigma_{t,90} = \frac{\sigma_{t,90,a}(x=0)}{2} + \sigma_{t,90,b}(x=0) \quad 4.157$$

This is due to the triangular distribution of the assumed peak stresses and because the analytically determined stresses of the elastic beam model do not differ much along the fracture process region.

The average shear stresses can be approximately determined by assuming a linear distribution along the fracture process region with:

$$\sigma_v = \sigma_v(x=0) - \frac{(\sigma_v(x=0) - \sigma_v(x=L_{reg}))}{2} \quad 4.158$$

For the above shown examples the following values are obtained:

$$\sigma_{t,90} = \frac{2.7}{2} + 0.5 = 1.85 \quad 4.159$$

$$\sigma_v = 4.5 - \frac{(4.5 - 3.9)}{2} = 4.2 \quad 4.160$$

Therefore:

$$\frac{\sigma_{t,90}}{\sigma_v} = \frac{1.85}{4.2} = 0.44 \quad 4.161$$

Resulting in a critical energy release rate  $G_c$  (with a timber density of  $400 \text{ kg/m}^3$ ):

$$G_c = 0.35 \text{ Nmm/mm}^2$$

Generally it has to be said that the considered stress distributions might not be completely right because plasticity is not accounted for (especially in the case of the shear stress distribution). However this might have only a small impact on the resulting critical energy release rate  $G_c$  because from a  $\frac{\sigma_{t,90}}{\sigma_v}$  ratio of around 0.4 upwards it only changes very little (as shown in chapter 4.2.2)

## 5 ANALYTICAL FAILURE MODEL

With the shown approaches of approximating the stress situation along a multiple fastener shear connection a failure model can be devised to obtain the bearing capacity of a multiple fastener connection.

First of all it is shown how the presented ways of determining the stress distributions in a connection can be used to calculate a failure load of the connection loaded in grain direction. Additionally, this approach is extended to cases where the fasteners are stressed under a certain load angle to the grain. A relation between the shear strength and the tensile strength perpendicular to the grain and its incorporation in the model is presented. Finally modifications and simplifications introduced to receive a rather accurate and practicable model are presented.

Note that the model assumes linear elastic material behaviour and that at failure all fasteners are loaded with approximately the same load. This assumption is justified due to the fact that at failure rather large plastic deformations within the

connection emerge, which allow a rather uniform load distribution among the fasteners [1] [11]. Very stiff connections that fail rigidly due to premature timber splitting do not show these large plastic deformations. However, some plasticity in the timber is still activated. Manufacturing imperfections that might be mainly responsible for an uneven load distribution in the loading process are hard to assess analytically anyway.

## 5.1 Load Situation Parallel to the Grain

### 5.1.1 Stresses Perpendicular to the Grain

As already discussed in chapter 4.3.2 (see Figure 71), tensile stresses perpendicular to the grain in a single fastener connection at the fastener hole at time of failure can be calculated with:

$$\sigma_{t,90}(x=0) = \sigma_{t,90,a}(x=0) + \sigma_{t,90,b}(x=0) = f_{t,90} \quad 5.1$$

$$\frac{2V_a}{y_a L_{reg}} + \frac{k}{y_a} w(x=0) = f_{t,90} \quad 5.2$$

$$C_a V_a + C_b (V_b f_1(x=0) + F f_2(x=0)) = f_{t,90} \quad 5.3$$

$$C_a V_a + C_b V_b f(x=0) = f_{t,90} \quad 5.4$$

$$C_a r_a V + C_b r_b V f(x=0) = f_{t,90} \quad 5.5$$

With:

$$V_b f(x=0)^{***} = V_b f_1(x=0) + F f_2(x=0) \quad 5.6$$

$$r_a = \frac{V_a}{V} \quad 5.7$$

$$r_b = \frac{V_b}{V} \quad 5.8$$

(\*\*\* the derivation of this relation can be found in the appendix (chapter 10.2))

Thus the wedging force  $V$  at failure in a single fastener connection is given as:

$$V = \frac{f_{t,90}}{C_a r_a + C_b r_b f(x=0)} \quad 5.9$$

The force 2F on the fastener can be determined with:

$$2F = \frac{f_{t,90}}{f_V(\varphi)(C_a r_a + C_b r_b f(x=0))} \quad 5.10$$

With:

$$2F = \frac{V}{f(\varphi)} \quad 5.11$$

For a connection with n fasteners in a row in grain direction the calculation can be done by simply summing up the values of the stress distributions of every single fastener at one fastener hole. Assuming that at failure all fasteners are loaded with the same force 2F, leads to:

$$\sigma_{t,90}(x=0) = \sigma_{t,90,a}(x=0) + \sum_{i=1}^n \sigma_{t,90,b,i}(x_i) = f_{t,90} \quad 5.12$$

$$\frac{2V_a}{y_a L_{reg}} + \frac{k}{y_a} \sum_{i=1}^n w_i(x_i) = f_{t,90} \quad 5.13$$

$$C_a V_a + C_b V_b \sum_{i=1}^n f_i(x_i) = f_{t,90} \quad 5.14$$

It is apparent that the only part that distinguishes from a single fastener connection is a summation of function values instead of just one function value, therefore it can be written:

$$2F = \frac{f_{t,90}}{f_V(\varphi)(C_a r_a + C_b r_b \sum_{i=1}^n f_i(x_i))} \quad 5.15$$

### 5.1.2 Shear Stresses

Similar can be carried out for the shear stresses in a connection. First of all, for a single fastener connection at failure:

$$\sigma_v(x=0) = \frac{F(h_1 + h_2)G}{h_1 h_2 h_3 y_b E_0 \omega} \left[ \frac{\cosh(\omega L_1)}{\sinh(\omega L_1)} \cosh(0) + \sinh(0) \right] = f_v \quad 5.16$$

$$CF \frac{f(x=0)}{y_a} = f_v \quad 5.17$$

With:

$$C = \frac{(h_1 + h_2)G}{h_1 h_2 h_3 E_0 \omega} \quad 5.18$$

$$f(x=0) = \frac{\cosh(\omega L_1)}{\sinh(\omega L_1)} \cosh(0) + \sinh(0) \quad 5.19$$

Therefore:

$$2F = \frac{2f_v y_a}{C f(x=0)} \quad 5.20$$

In order to extend the equation to a multiple fastener connection, the summation of the shear stress distributions just has to be added:

$$2F = \frac{2y_a f_v}{C \sum_{i=1}^n f_i(x_i)} \quad 5.21$$

## 5.2 Load Situation under a Certain Load Angle $\alpha$

The loading situation fastener stressed in an angle to the grain is seen as a superposition of the loading situation parallel to the grain and perpendicular to the grain.

This means that a force  $2F_\alpha$  is divided into the part acting parallel ( $F_{II}$ ) and the one acting perpendicular to grain direction ( $F_L$ ). Thus:

$$F_{II} = F_{\alpha} \cos(\alpha) \quad 5.22$$

$$F_L = F_{\alpha} \sin(\alpha) \quad 5.23$$

The force component parallel to the grain is considered as in chapter 5.1.1 to calculate a wedging force and the force component perpendicular to the grain is simply added to or subtracted from the wedging force depending on the crack plane. Therefore:

$$V = 2F_{II}f_V(\varphi) \pm 2F_L = 2F_{\alpha}(\cos(\alpha) f_V(\varphi) \pm \sin(\alpha)) \quad 5.24$$

$$2F = 2F_{II} = 2F_{\alpha} \cos(\alpha) \quad 5.25$$

It is obvious that with increasing load angle  $\alpha$ , the wedging force ( $V$ ) for one crack plane increases while it decreases for the other one. In other words the conditions are not the same any more in both crack planes. Thus the likelihood for the appearance of two cracks decreases and it is more likely that only one crack emerges at failure on both sides of the fastener hole. At a load angle of  $\alpha = 90^\circ$  (loading entirely perpendicular to the grain) only one crack will arise, which agrees with reality [11]. To obtain the maximum bearing force Eq. 5.26 is applied to the wedging force:

$$V = 2F_{II}f_V(\varphi) + 2F_L = 2F_{\alpha}(\cos(\alpha) f_V(\varphi) + \sin(\alpha)) \quad 5.26$$

These terms can be added to the already devised Eq. 5.15 and Eq. 5.21 to obtain expressions for  $2F_{\alpha}$ .

For tensile stresses perpendicular to the grain:

$$2F_{\alpha,P} = \frac{f_{t,90}}{(\cos(\alpha) f_V(\varphi) + \sin(\alpha))(C_a r_a + C_b r_b \sum_{i=1}^n f_i(x_i))} \quad 5.27$$

For shear stresses:

$$2F_{\alpha,S} = \frac{2f_v y_a}{C \cos(\alpha) \sum_{i=1}^n f_i(x_i)} \quad 5.28$$

As apparent for a loading angle of  $\alpha = 90^\circ$  the shear forces in the assumed crack plane become 0 according to the model. This does not agree with reality where there are still shear stresses at this certain point. However, according to Schoenmakers (2010) [11], the shear stresses under a loading angle of  $90^\circ$  have a negligible influence on the failure behaviour which is mainly governed by tensile stresses perpendicular to the grain in this case. Thus, only a minor influence on the results is expected.

To obtain the overall load carrying capacity of the connection, the obtained force  $2F_\alpha$  per fastener is just multiplied with the number of fasteners in a row in grain direction.

$$F_{\text{Connection}} = 2F_\alpha n \quad 5.29$$

### 5.2.1 Splitting of the Wedging Force under a Load Angle $\alpha$

The division of the wedging force  $V$  into component  $V_a$  acting in the peak stress model and component  $V_b$  responsible for the elastic beam model has already been shown in chapter 4.3.2.5. It is necessary to reach a certain stress level at the fastener hole dependent on the friction angle at a load-fibre angle of  $\alpha = 0^\circ$  (load parallel to the grain). Thus:

$$V_a = r_a(\alpha = 0)V \quad 5.30$$

$$V_b = r_b(\alpha = 0)V \quad 5.31$$

With increasing load angle the stress situation at the fastener hole changes and the amount of peak stresses decreases while the wedging force  $V$  increases and therefore, the general stress level perpendicular to the grain increases too. Consequently, the share of stresses from the peak stress model decreases with increasing load-fibre angle. At a certain load-fibre angle  $\alpha$ , the elastic beam model alone is capable of depicting the situation of the stresses perpendicular to the grain. This “certain” load angle  $\alpha$  is assumed equal to the friction angle  $\varphi$ . Therefore:

$$r_a(\alpha) = \begin{cases} 0^\circ \leq \alpha \leq \varphi: r_a(\alpha = 0) \cos\left(\alpha \frac{90^\circ}{\varphi}\right) \\ \varphi < \alpha \leq 90^\circ: 0 \end{cases} \quad 5.32$$

$$r_b(\alpha) = \begin{cases} 0^\circ \leq \alpha \leq \varphi: r_b(\alpha = 0) + r_a(\alpha = 0) \sin\left(\alpha \frac{90^\circ}{\varphi}\right) \\ \varphi < \alpha \leq 90^\circ: 1 \end{cases} \quad 5.33$$

## 5.2.2 Calculation of the Critical Fracture Energy $G_c$ under a Load Angle $\alpha$

At a load angle of  $0^\circ$  (load parallel to the grain) the critical fracture energy has to depict a combined mixed mode energy consisting of and dependent on the energies for fracture mode I (tensile stresses perpendicular to the grain, opening mode) and mode II (shear stresses, sliding mode) because both stresses arise in the shear plane. It has been shown by [1] and in chapter 4.3.4 that for this case the ratio between stresses perpendicular and shear stresses is around 0.44.

At a load angle of  $90^\circ$ , however, the fracture mode responsible for the emergence of cracks is mode I and the influence of mode II is negligible [11]. According to Eq. 5.27 and Eq. 5.28 only stresses perpendicular to the grain arise and therefore, the  $\frac{\sigma_{t,90}}{\sigma_v}$  ratio approaches infinity resulting in mixed mode energy very close to mode I only.

To get hold of this development the ratio is altered according to the load angle  $\alpha$ :

$$\frac{\sigma_{t,90}}{\sigma_v}(\alpha) = \frac{\frac{\sigma_{t,90}}{\sigma_v}(\alpha = 0)}{10^{-3} + \cos(\alpha)} \approx \frac{0.44}{10^{-3} + \cos(\alpha)} \quad 5.34$$

The factor  $10^{-3}$  has been introduced rather deliberately to make the equation numerically stable. It does not falsify the results too much and keeps the ratio from reaching infinity at a load angle of  $\alpha = 90^\circ$ . Instead just a very high value is attained which satisfies the purpose.

## 5.3 Multiple Rows of Fasteners Perpendicular to the Grain

### 5.3.1 General

To obtain the failure load of a shear connection consisting of  $m$  rows of fasteners in grain direction, the connection can be divided into several virtual beams. It is assumed that failure in one row (at one beam) causes failure of the overall connection. It has to be distinguished between several loading situations:

### 5.3.2 Load Parallel to the Grain

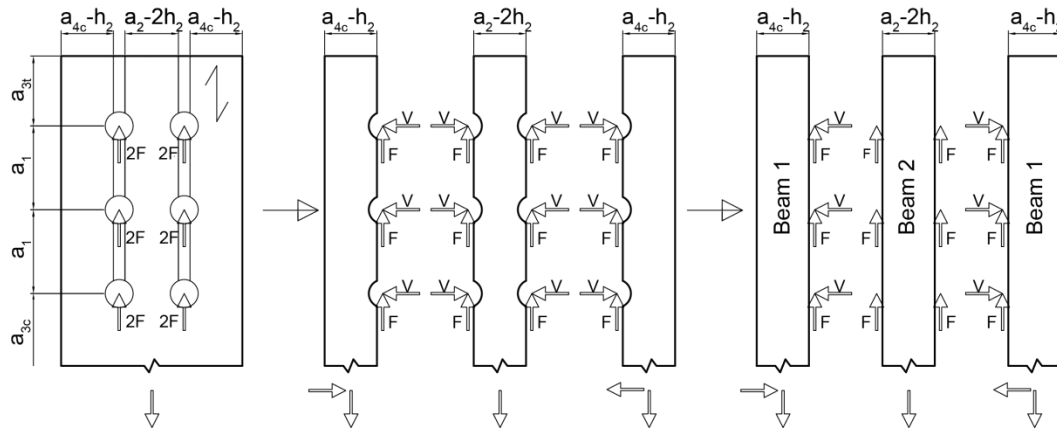


Figure 81: Division into elastically supported beams for the case load parallel to the grain for a shear connection with multiple rows of fasteners perpendicular to the grain

In this loading situation two different types of elastically supported beams have to be taken into account. Firstly, the maximum bearing capacity for the outer beam with the known loading setting has to be determined. Secondly, the inner beam has to be taken into consideration. As the wedging forces ( $V$ ) eliminate each other due to their opposing acting direction only the forces in loading direction are applied. Consequently, this beam only has to be examined via the shear stress model because no forces perpendicular to the grain exist that would introduce stresses perpendicular to the grain (only according to this model of course). However, for this beam only half of its height shall be taken because only this part of the beam is responsible for transferring the shear that is introduced by the forces  $F$  acting on one side of the beam.

For beam two, however, there still are tensile stresses perpendicular to the grain introduced locally at the fastener holes, but due to their opposing loading directions an accumulation of tensile stresses perpendicular to the grain with influence on adjacent fasteners in grain direction is unlikely to occur throughout the whole shear plane. To consider that, the calculation is conducted with a reduced shear strength of the timber (see chapter 5.4) since shear stresses and tensile stresses perpendicular to the grain still interact locally at the fastener hole Thus:

$$h_2 = \frac{d}{2} \sin(\varphi) \quad 5.35$$

*Beam 1:*

$$h_1 = a_{4c} - h_2 \quad 5.36$$

$$2F_P = \frac{f_{t,90}}{f_V(\varphi)(C_a r_a + C_b r_b \sum_{i=1}^n f_i(x_i))} \quad 5.37$$

$$2F_S = \frac{2f_{v,y} a}{C \sum_{i=1}^n f_i(x_i)} \quad 5.38$$

Beam 2:

$$h_1 = \frac{a_2 - 2h_2}{2} \quad 5.39$$

$$2F_S = \frac{2f_{v,y} a}{C \sum_{i=1}^n f_i(x_i)} \quad 5.40$$

### 5.3.3 Load Perpendicular to the Grain

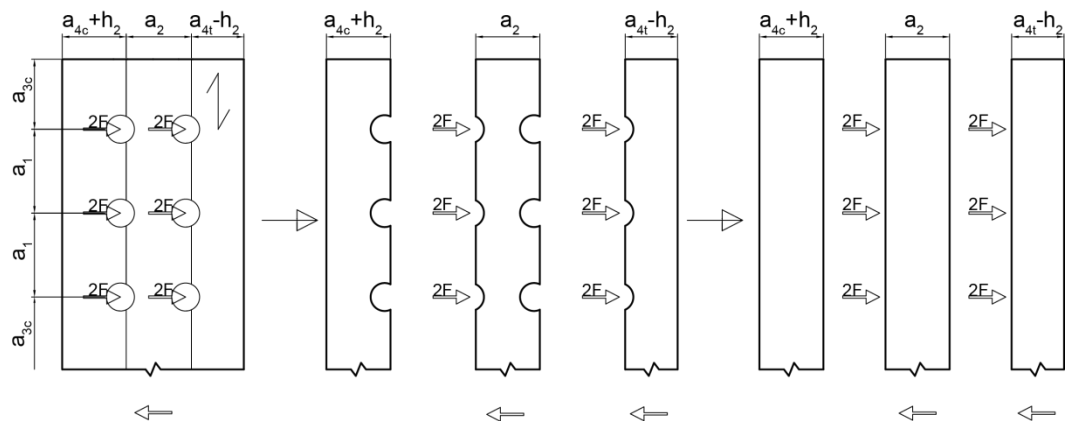


Figure 82: Division into elastically supported beams for the case load perpendicular to the grain for a shear connection with multiple rows of fasteners perpendicular to the grain

Here, only the beam with the smallest height has to be accounted for being loaded with the forces acting perpendicular to the grain (2F). Furthermore, only the model responsible for the stresses perpendicular to the grain (elastic beam model) is employed. Therefore:

$$h_2 = \frac{d}{2} \sin\left(\frac{\pi}{4} - \varphi\right) \quad 5.41$$

$$h_1 = \min[a_2, a_{4c} - h_2] \quad 5.42$$

$$2F_P = \frac{f_{t,90}}{(C_a r_a + C_b r_b \sum_{i=1}^n f_i(x_i))} \quad 5.43$$

It is important to mention that the height  $h_2$  is calculated differently than previously for the case of  $\alpha = 0^\circ$  because, in the current case, the fastener hole is loaded perpendicular to the grain and thus, only one crack plane emerges.

### 5.3.4 Load between $0^\circ < \alpha < \zeta$

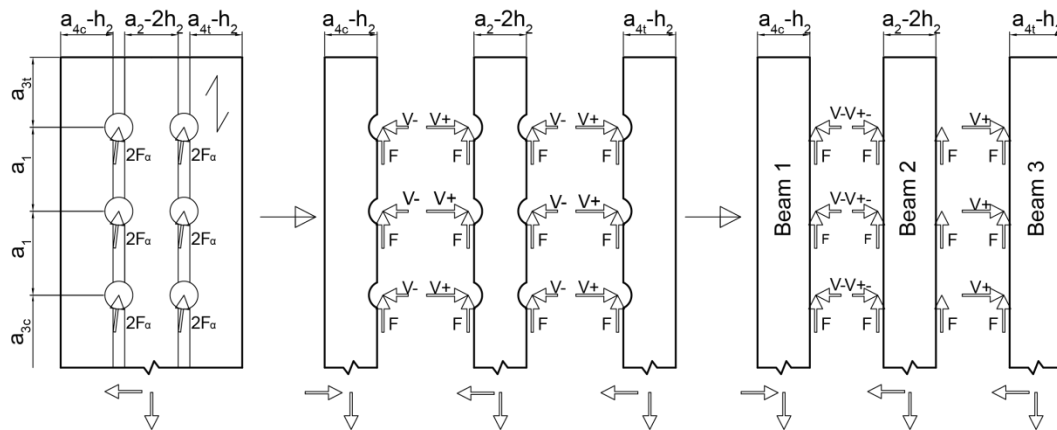


Figure 83: Division into elastically supported beams for the case load between the stress-fibre angles  $0^\circ < \alpha < \zeta$  for a shear connection with multiple rows of fasteners perpendicular to the grain

In this case, the situation is more complex. All the different beams are loaded with different wedging forces ( $V$ ) due to the load angle  $\alpha$ .

$$h_2 = \frac{d}{2} \sin(\varphi) \quad 5.44$$

Beam1:

$$V_- = 2F_\alpha (\cos(\alpha) f_V(\varphi) - \sin(\alpha)) \quad 5.45$$

$$h_1 = a_{4c} - h_2 \quad 5.46$$

$$2F_{\alpha,P} = \frac{f_{t,90}}{(\cos(\alpha) f_V(\varphi) - \sin(\alpha))(C_a r_a + C_b r_b \sum_{i=1}^n f_i(x_i))} \quad 5.47$$

$$2F_{\alpha,S} = \frac{2f_v y_a}{C \cos(\alpha) \sum_{i=1}^n f_i(x_i)} \quad 5.48$$

*Beam 2:*

$$\begin{aligned} V_{\pm} &= 2F_{\alpha}[(\cos(\alpha) f_v(\varphi) + \sin(\alpha)) - (\cos(\alpha) f_v(\varphi) - \sin(\alpha))] \\ &= 2F_{\alpha}(2 \sin(\alpha)) \end{aligned} \quad 5.49$$

$$h_{1,P} = a_2 - 2h_2 \quad 5.50$$

$$2F_{\alpha,P} = \frac{f_{t,90}}{(2 \sin(\alpha))(C_a r_a + C_b r_b \sum_{i=1}^n f_i(x_i))} \quad 5.51$$

$$h_{1,S} = \frac{a_2 - 2h_2}{2} \quad 5.52$$

$$2F_{\alpha,S} = \frac{2f_v y_a}{C \cos(\alpha) \sum_{i=1}^n f_i(x_i)} \quad 5.53$$

*Beam 3:*

$$V_+ = 2F_{\alpha}(\cos(\alpha) f_v(\varphi) + \sin(\varphi)) \quad 5.54$$

$$h_1 = a_{4t} - h_2 \quad 5.55$$

$$2F_{\alpha,P} = \frac{f_{t,90}}{(\cos(\alpha) f_v(\varphi) + \sin(\alpha))(C_a r_a + C_b r_b \sum_{i=1}^n f_i(x_i))} \quad 5.56$$

$$2F_{\alpha,S} = \frac{2f_v y_a}{C \cos(\alpha) \sum_{i=1}^n f_i(x_i)} \quad 5.57$$

This model is used until a certain angle  $\alpha = \zeta$ , which represents the load angle at which  $V_-$  is zero and therefore, the emergence of two crack planes gets unlikely due to a theoretical absence of stresses perpendicular to the grain in the second virtual crack plane.

$$V- = 2F_{\alpha}(\cos(\zeta) f_V(\varphi) - \sin(\zeta)) = 0 \quad 5.58$$

Thus:

$$\zeta = \arctan(f_V(\varphi)) \quad 5.59$$

### 5.3.5 Load between $\zeta < \alpha < 90^\circ$

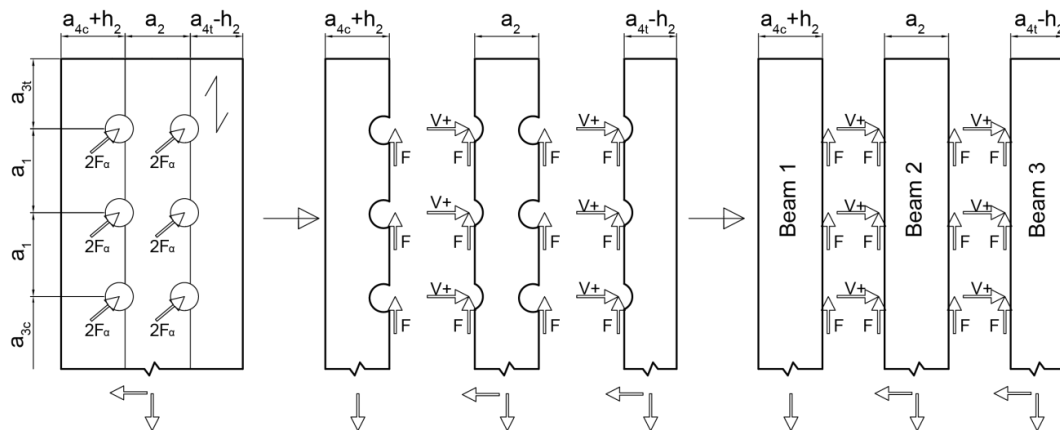


Figure 84: Splitting into beams that have to be considered

If the load angle surpasses  $\alpha = \zeta$ , the situation exhibits a different picture. It is assumed that only one crack plane arises and just one wedging force ( $V +$ ) is left to be taken into account.

$$h_2 = \frac{d}{2} \sin\left(\frac{\pi}{4} - \varphi\right) \quad 5.60$$

Beam 1:

$$h_1 = a_{4c} + h_2 \quad 5.61$$

$$2F_{\alpha,S} = \frac{2f_V y_a}{C \cos(\alpha) \sum_{i=1}^n f_i(x_i)} \quad 5.62$$

Beam 2:

$$h_{1,P} = a_2 \quad 5.63$$

$$2F_{\alpha,P} = \frac{f_{t,90}}{(\cos(\alpha) f_v(\varphi) + \sin(\alpha))(C_a r_a + C_b r_b \sum_{i=1}^n f_i(x_i))} \quad 5.64$$

$$h_{1,S} = \frac{a_2}{2} \quad 5.65$$

$$2F_{\alpha,S} = \frac{2f_v y_a}{C \cos(\alpha) \sum_{i=1}^n f_i(x_i)} \quad 5.66$$

*Beam 3:*

$$h_1 = a_{4c} - h_2 \quad 5.67$$

$$2F_{\alpha,P} = \frac{f_{t,90}}{(\cos(\alpha) f_v(\varphi) + \sin(\alpha))(C_a r_a + C_b r_b \sum_{i=1}^n f_i(x_i))} \quad 5.68$$

$$2F_{\alpha,S} = \frac{2f_v y_a}{C \cos(\alpha) \sum_{i=1}^n f_i(x_i)} \quad 5.69$$

Finally the overall bearing capacity of the connection can be obtained with:

$$F_{\text{Connection}} = \min[2F_{\alpha,P,i}, 2F_{\alpha,S,i}] n m \quad 5.70$$

## 5.4 Relation between $f_v$ and $f_{t,90}$

$f_v$  and  $f_{t,90}$  are in fact independent material properties. However, combined shear stresses and tensile stresses perpendicular to the grain lead to a different resistance of the timber than observed in pure stress conditions which can be depicted by an interaction dependency [1], [9].

In the calculation process of the model a dynamically adapted resistance is used. This means that the interaction between both stresses (situated on the interaction curve) is determined based on the stress situation exhibited by a single fastener loaded with the maximum force according to Johansen's Yield Theory. These resistances are then used to calculate the bearing strength of the whole connection using the models presented in this chapter. This should depict the real interactive behaviour of these strength properties better and might lead to more accurate load carrying capacities. The used interaction curve is shown in Figure 85.

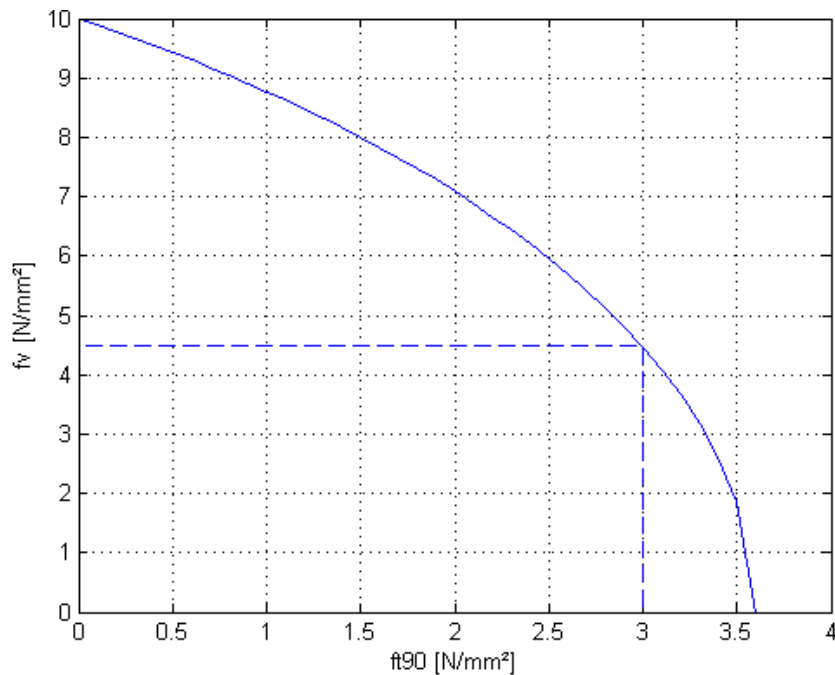


Figure 85: Interaction curve between shear and tensile perpendicular to the grain resistances according to [1], [9], [11]

Based on SIA 265: 2003 [9] the relation can be expressed mathematically with:

$$f_v(\sigma_{t,90}) = f_v(\sigma_{t,90} = 0) \frac{\sqrt{1 - \left(\frac{5.9 + f_{t,90}}{5.9 + f_{t,90}(\sigma_v = 0)}\right)^2}}{\sqrt{1 - \left(\frac{5.9}{5.9 + f_{t,90}(\sigma_v = 0)}\right)^2}} \quad 5.71$$

With [1], [11]:

- $f_{t,90,mean}(\sigma_v = 0) = 3.6 \text{ N/mm}^2$
- $f_{v,mean}(\sigma_{t,90} = 0) = 10 \text{ N/mm}^2$

## 5.5 Simplifications

### 5.5.1 Determination of the Fictitious Shear Strain Layer $h_3$

According to the derivation of the shear stress distribution in the crack plane by Jorissen (1998) [1] based on Gustaffsson (1987) [23] and Volkersen (1938) [24]  $h_3$  depends on  $f_v$  and so does the amount of the shear stresses. In the derivation of the failure model however the factor  $h_3$  has been treated as a constant independent from the shear strength  $f_v$ . This is important because during the calculation process the strength values are altered according to their interaction de-

pendency based on the stress situation. If  $h_3$  and therefore  $\sigma_v(x)$  were dependent on the shear strength, the failure model would not be practicable.

Thus  $h_3$  is explicitly introduced as a constant by calculating it once with the  $f_v$  given in Jorissen (1998) [1] ( $f_{v,mean} = 4.5 \text{ N/mm}^2$ ) without further altering even if the strength levels change.

$$h_3 = \frac{2G_c G}{f_v^2} \approx \frac{2G_c G}{4.5^2} \quad 5.72$$

The error made with this simplification is considered as rather small. Firstly, because for a load angle of  $0^\circ$  there is only minor influence on  $f_v$  and secondly, with increasing load angle the influence of the shear stresses decreases overall.

### 5.5.2 Determination of the Fictitious Length of the Crack Process Region $L_{reg}$

The fictitious length  $L_{reg}$  is dependent on the tensile strength perpendicular to the grain of the timber ( $f_{t,90}$ ). To keep  $L_{reg}$  a constant even if the strength values are altered during the calculation process, the mean value of the resistance given in [1] will be used to determine the length disregarding any variation of the strength values. Thus:

$$L_{reg} = 0.25 \frac{G_c \sqrt{E_{90} G}}{f_{t,90}^2} \approx 0.25 \frac{G_c \sqrt{E_{90} G}}{3^2} \quad 5.73$$

The error this simplification might bring along is supposed to be minor because the length is only used in the peak stress model which is just employed until a limited load angle and until this load angle the variation of strength values is not expected to be too big.

## 5.6 Calculation Process

A routine to calculate the maximum bearing capacity of a multiple fastener shear connection is implemented in “Matlab 2011a” using the presented theories and relations.

The routine uses the models presented in chapter 4.3 and chapter 5 to obtain the failure load of a multiple fastener connection. It is neither capable of calculating the slip at failure nor of telling the actual failure behaviour, although one could be able to extract some information on this by considering the actual beam that fails and the Johansen failure mode of the connection but it is not enough to make a

definite prediction. The model just approximates the mechanism of stress accumulation along the connection analytically to obtain the failure force.

The whole failure theory is (as already mentioned) based on one rough assumption stating that at failure every fastener per row parallel to the grain is loaded with the same force due to plastic deformations within the connection. Manufacturing imprecisions as well as imperfections of the material are not accounted for. The material is treated as perfectly orthotropic. Furthermore friction between the timber members is not considered as well as possible end fixities of the fastener.

However manufacturing imprecisions are hard to predict beforehand and so is the location and presence of material imperfections, which are also not taken into consideration in Eurocode [3] either. As the actual effect of end fixities during loading and unloading can only be predicted very vaguely because it depends on too many uncertainties (e.g. imprecisions in the application during the manufacturing, timber humidity, loading-unloading cycles) it is not accounted for in the calculation process.

## 5.7 Validation

### 5.7.1 General

The accuracy of the devised model is assessed by comparing the mean values of test results conducted by Jorissen (1998) [1] and Schoenmakers (2010) [11] to the maximum load carrying capacities of multiple fastener connections according to this model, calculated with mean values of the material parameters as well.

Jorissen (1998) carried out a huge number of multiple fastener connection tests loaded parallel to the grain while Schoenmakers (2010) did so for connections loaded perpendicular to the grain.

The comparison of the model with these test results allow to judge the accuracy and the influence of the assumptions and simplifications made.

### 5.7.2 Loading Parallel to the Grain

The data taken from Jorissen (1998) [1] to examine the model's accuracy for a loading situation parallel to the grain are the results of tests on symmetrical timber double shear connections conducted at TU Delft. The empirical approach to determine  $n_{ef}$  according to Eurocode [3] is based on these test results.

The following parameters are used according to [1] in the calculations apart from the ones given in Table 6 in chapter 10.4.

- $\rho_k = 450 \text{ kg/m}^3$
- $E_{0,mean} = 12500 \text{ N/mm}^2$
- $f_{u,k} = 500 \text{ N/mm}^2$
- $E_{90,mean} = 400 \text{ N/mm}^2$

- $G_{0,mean} = 640 \text{ N/mm}^2$        $\varphi = 18^\circ$

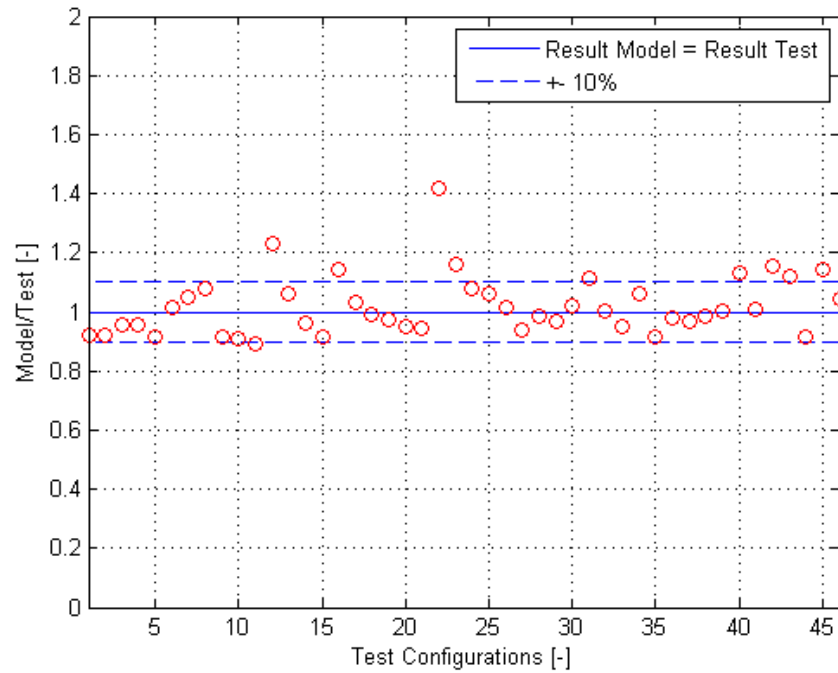


Figure 86: Ratio of model-test results for connections loaded in grain direction with  $m=1$

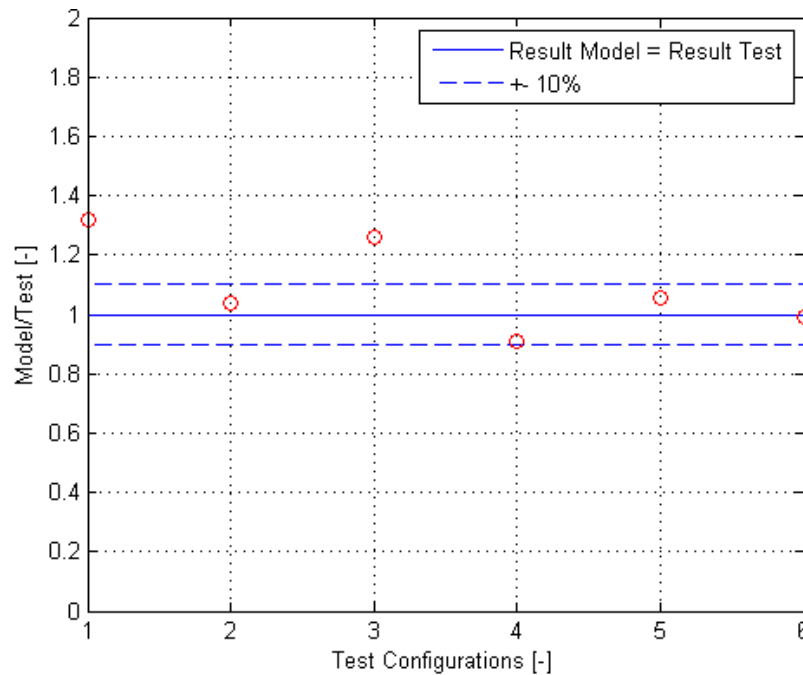


Figure 87: Ratio of model-test results for connections loaded in grain direction with  $m=2$

There is a quite good agreement between the test results and the model results. The average error is around 8%, which is a relatively good value especially considering that wood is an inhomogeneous material with imperfections that can influence the load carrying capacity remarkably and that has been treated as a per-

fectly orthotropic material by neglecting those imperfections in the calculation model.

Furthermore, it seems that the simplifications and assumptions made in the derivation of the failure model seem to be rather sound and lead to accurate results.

### 5.7.3 Loading Perpendicular to the Grain

Schoenmakers (2010) conducted structural size tests where wooden beams were loaded perpendicular to the grain with steel dowels by applying two (thick) steel plates at the sides of the wooden beam in the midpoint. This approach can be seen as Johansen type double shear with inner timber member and outer steel plates stressed perpendicular to the grain.

The following parameters were used in the calculations apart from the ones given in the tables.

- $\rho_k = 450 \text{ kg/m}^3$
- $E_{0,\text{mean}} = 12500 \text{ N/mm}^2$
- $G_{0,\text{mean}} = 640 \text{ N/mm}^2$
- $f_{t,90,\text{mean}} = 3 \text{ N/mm}^2$
- $f_{u,k} = 360 \text{ N/mm}^2$
- $E_{90,\text{mean}} = 500 \text{ N/mm}^2$
- $\varphi = 18^\circ$

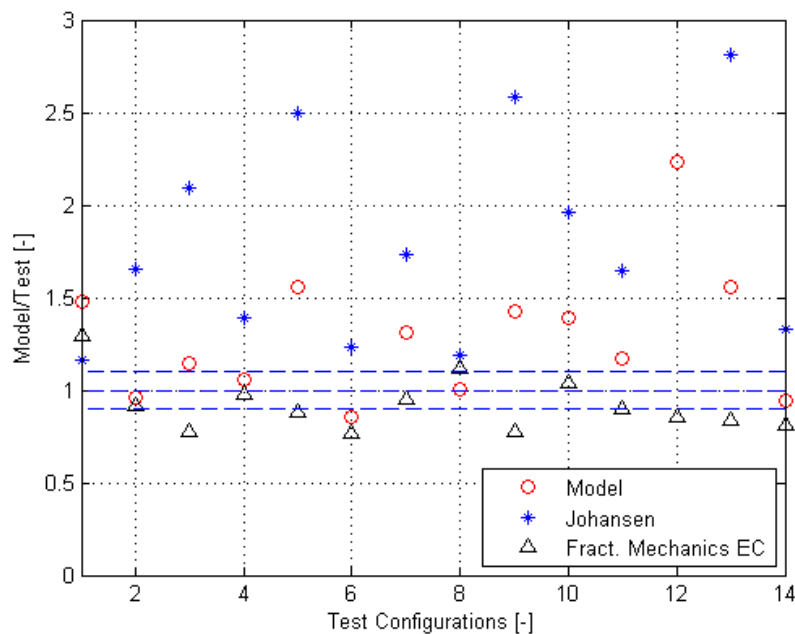


Figure 88: Ratio of model-test results for connections loaded perpendicular to the grain

Apparently, the agreement between model and test results is not that good. However, it is remarkably better than with the approach based on Johansen's Yield Theory used in Eurocode [3] now.

The calculated values are on average 29% higher than the carrying capacities in the test. This might be due to the fact that the assumption of same forces in every fastener cannot be applied to this loading situation the way it worked for fasteners loaded perpendicular to the grain. Furthermore, the tested specimens structural sized beams were loaded by a “single point force” (the connection) in the midpoint. This loading situation leads to a remarkable amount of shear, while the model didn’t take shear into consideration for this loading situation and calculated as if the stress situation were pure tension perpendicular to the grain. This might explain the shift in the model data.

The load carrying capacities obtained with the approach suggested in Eurocode [3] to design dowel type connections (as presented in chapter 2) are on average around 106% higher than the test results. It has to be said though that according to Eurocode most of the connections tested by Schoenmakers do not fulfil the minimum spacing requirements and are therefore not eligible to be calculated that way. There is another approach provided in Eurocode [3] (Eq. 5.74), however, to account for beams that are loaded perpendicular to the grain based on fracture mechanics which leads to results that are quite accurate (average error less than 20%).

$$F_{\text{Connection,t,90}} = 14bw \sqrt{\frac{h_e}{1 - \frac{h_e}{h}}} \quad 5.74$$

With:

- $w$  modification factor [-]  
(=1 for dowel type connections)
- $b$  thickness of the timber member [mm]
- $h_e$  loaded edge distance to the centre of the most distant fastener [mm]
- $h$  height of the beam [mm]

For further and more detailed examination of this loading situation the reader is referred to Schoenmakers (2010) [11] who derived several approaches based on fracture mechanics considerations accounting for this issue.

## 6 SUMMARY

In this first part of the thesis timber shear connections with multiple dowel type fasteners have been considered and dealt with. First of all, the design practice according to Eurocode [3], with Johansen's Yield Model [19], [20], has been presented and analysed critically. Then different approaches to account for the group effect, the reduction of the theoretically accountable load carrying capacity per fastener with increasing number of fasteners in a row parallel to the grain have been examined and compared. Furthermore, the path the load takes in a connection has been exhibited and the sensitive parts of the connection have been highlighted. In addition the influence of end fixities have been discussed and assessed. In the following a more into detail stress analysis at the fastener hole has been conducted. Based on the work of Jorissen (1998) [1] a model has been devised to calculate the ultimate load carrying capacity of a multiple fasteners with arbitrary load angle, arbitrary number of fasteners in grain direction and arbitrary number of fasteners perpendicular to the grain. This model has been validated for different arrangements of fasteners loaded parallel and perpendicular to the grain with results of tests carried out by Jorissen (1998) and Schoenmakers (2010) [11]. Load situation parallel to the grain shows good agreement with the test results while for connections loaded perpendicular to the grain the calculated results are around 29% too high.

However, for the load situation fastener loaded parallel to the grain the determination of the carrying capacity of a single fastener according to Johansen is quite accurate although it neglects some influences (humidity, friction between the timber members) and considers others only rather questionably (influence of end fixities) while for load perpendicular to the grain the theory according to Johansen does not generate very reasonable results. However there is another approach based on fracture mechanics provided in Eurocode [3] for this loading situation that leads to much more accurate results.

The group effect, if only stress accumulation is considered to be responsible for it and material imperfections as well as manufacturing imprecisions are unaccounted for, seems to reduce the carrying capacity per fastener as soon as more than one fastener is considered but the reduction remains constant with increasing number of fasteners as shown in Figure 89.

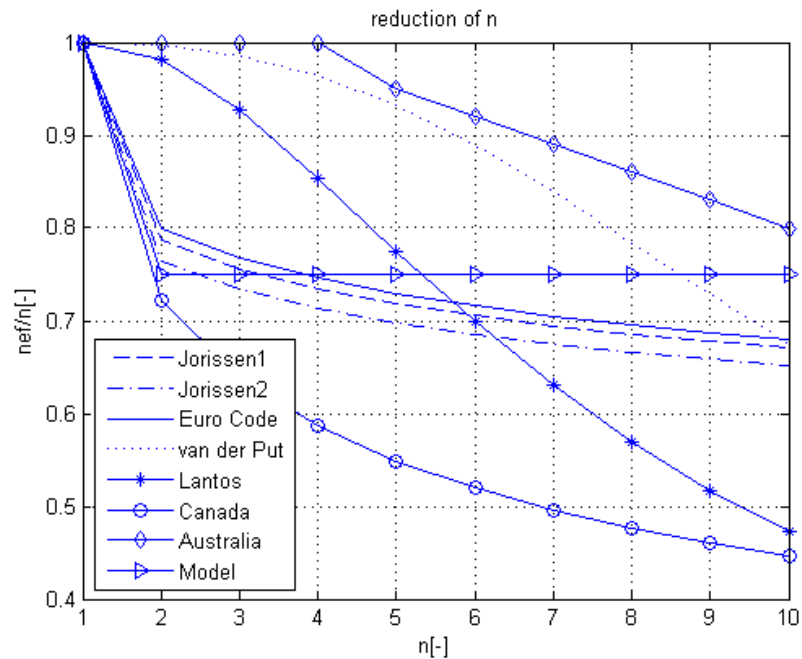


Figure 89: Comparison of different approaches accounting for  $n_{ef}$  including the model devised in this thesis (brittle connection)

Thus rather than using an approach like:

$$n_{ef} = C_1 n^{C_2} \quad 6.1$$

It might be reasonable to introduce the following relation:

$$n_{ef} = Cn \quad 6.2$$

Another apparent issue is that according to Eurocode [3] all types of connections (with brittle, intermediate and ductile failure) are treated the same although already Jorissen (1998) [1] has shown that there is a dependency on the slenderness ratio regarding the group effect. Therefore the influence of this effect is assumed to be way too strong in intermediate and especially slender connections than it actually is. In other words the bearing capacity of these types of connections is too conservatively calculated according to Eurocode [3]. It is thus suggested to distinguish between rigid, intermediate and slender connections when reducing the load carrying capacity with a certain  $n_{ef}$ .

Obviously the assumption that at failure all fasteners have to bear roughly the same load, no matter which slenderness ratio, seems to be sound for a loading parallel to the grain while for load applied perpendicular to the grain this approach might not be that valid.

## 7 CONNECTIONS WITH AXIALLY LOADED FASTENERS

In this chapter connections with axially loaded fasteners, focusing on self-tapping screws, are presented. The strength influencing parameters governing the resistance of a single fastener connection are outlined as well as the approach to determine the overall bearing capacity of a multiple fastener connection is discussed. Furthermore, the failure mode “block shear” is examined in more detail and an analytical approach to calculate the failure load due to this type is derived and validated.

In pull-out connections the connectors are loaded axially and the main fastener type used is self-tapping screws. The strength is mainly governed by the withdrawal resistance of the fastener, the tensile strength of the steel used for the connector and the resistance against pull-through of the screw head. All these factors are accounted for in the design process according to Eurocode [4].



Figure 90: Sketch of a pull-out connection

### 7.1 Stress-Strain Behaviour

A pull-out connection exhibits a rather stiff behaviour with relatively low deformations at failure compared to slender shear connections with dowel-type fasteners. It shows a linear elastic behaviour until quite close to failure as presented in Figure 91.

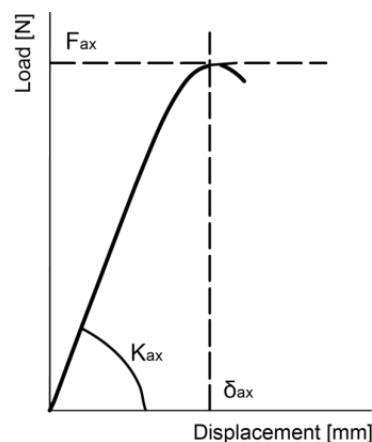


Figure 91: Typical load-displacement behaviour of a self-tapping timber screw loaded axially according to [3]

## 7.2 Strength Influencing Parameters

### 7.2.1 Withdrawal Strength

The withdrawal strength is not a material property but rather a feature describing the resistance of the timber against the pull-out of a steel fastener [2]. According to Eurocode [4] it can be determined by using Eq. 7.1.

$$f_{ax,k} = 0.52d^{-0.5}l_{ef}^{-0.1}\rho_k^{0.8} \quad 7.1$$

As apparent this is an empirical relation obtained from test results. It increases with increasing timber density and decreases with increasing diameter and fastener length.

The resistance of the connection for a deliberate stress-fibre angle  $90^\circ > \alpha > 30^\circ$  is determined as follows:

$$F_{ax,\alpha,k} = \frac{f_{ax,k}d l_{ef} k_d n_{ef}}{1.2 \cos^2(\alpha) + \sin^2(\alpha)} \quad 7.2$$

With:

$$k_d = \min \left\{ \frac{d}{8}, 1 \right\} \quad 7.3$$

### 7.2.2 Resistance of the Fastener Head against Pull-through

If rather thin outer timber members are used, the head of the screw can be “pulled through” the wood and therefore lead to failure. To minimise the risk for this failure mode to occur, it is accounted for in the design process by minimum timber thicknesses that have to be complied with. If the outer connection members are steel plates, this failure mode is, of course, not possible [5].

### 7.2.3 Tensile Strength of the Fastener

This failure type might be governing if the fastener is anchored long enough so that the resistance against withdrawal of the connector exceeds the axial tensile strength of the steel connector itself.

### 7.3 Minimum distances

Minimum distances have been introduced to avoid splitting of the timber when drilling the screws into the timber and block shear, which occurs due to a combination of shear failure and failure because of tensile stresses perpendicular to the grain if the distances between the screws are too small.

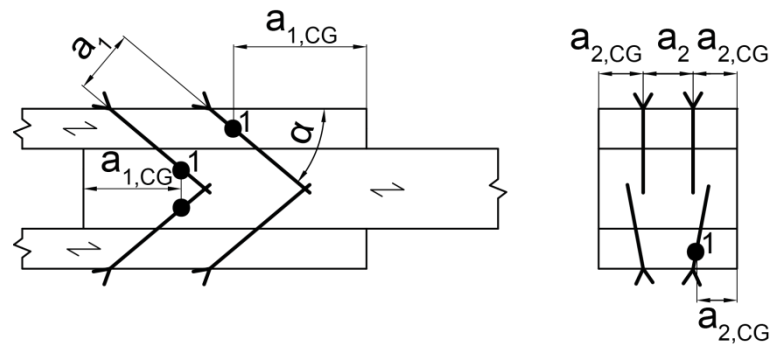


Figure 92: Minimum distances acc. to Eurocode [4] (1: Centre of gravity of the screw in this timber member)

- $a_1$  spacing between the fasteners parallel to the grain [mm]
- $a_{1,CG}$  loaded end distance [mm]
- $a_2$  spacing between fasteners perp. to grain [mm]
- $a_{2,CG}$  unloaded edge distance [mm]

Table 4: Minimum distances for screws loaded axially [4]

spacing and distance	screws
$a_1$	7d
$a_2$	5d
$a_{1,CG}$	10d
$a_{2,CG}$	4d

### 7.4 N-effective

The  $n_{ef}$  according to Eurocode [4] is calculated as follows:

$$n_{ef} = n^{0.9} \quad 7.4$$

However, tests have shown that under ideal laboratory conditions  $n = n_{ef}$  can be attained, at least for a stress-fibre angle of  $90^\circ$  [1]. As the conditions at the con-

struction site (accuracy of the conducted work, timber used) cannot be completely foreseen it seems legitimate to still employ Eq. 7.4, even though it has to be questioned if not a relation like  $n_{ef} = C n$  would be more accurate to account for these uncertainties.

## 7.5 Block Shear

### 7.5.1 General

Block shear is a phenomenon that is a combination of failure due to tensile stresses perpendicular to the grain in the plane beneath the screws with rolling shear failure in the planes in grain direction along the outermost rows of fasteners and shear in the transverse planes. It is caused if fasteners are arranged in great proximity.

Pull-out tests of screws perpendicular to the grain in timber have shown that block shear also can occur if all minimum distances are obeyed [1]. As block shear might arise at a load level smaller than predicted by the failure types accounted for in Eurocode [4], it is of interest to find an approach to calculate the failure load at which it emerges and include it into the design rules. Thus, a suggestion is made in the next chapter.

### 7.5.2 Failure Model

First of all, it is assumed that the governing factor for the emergence of block shear is an accumulation of tensile stresses perpendicular to the grain in the plane beneath the fasteners which leads to cracks in this plane and thus the block can be “pulled out”. Hence it is assumed that a failure of the plane beneath the fasteners automatically results in failure due to block shear as the plane loaded in rolling shear is considered as not being able to contribute to the resistance as soon as failure perpendicular to the grain arises

The tensile stresses perpendicular to grain caused by one single fastener can be calculated assuming two load dispersion angles ( $\beta, \gamma$ ) for the different axes to the grain. Consequently the area loaded beneath the fasteners is an ellipse for different angles and a circle if both angles are chosen the same.

$$\sigma_{t,90} = \frac{F}{l_{ef}^2 \tan(\beta) \tan(\gamma) \pi} \quad 7.5$$

- $\beta$  load dispersion angle in x-y-plane [°]
- $\gamma$  load dispersion angle in x-z plane [°]

Considering more than one fastener in grain direction, an accumulation of stresses can be the consequence if

$$l_{ef} \tan(\beta) > \frac{a_1}{2} \quad 7.6$$

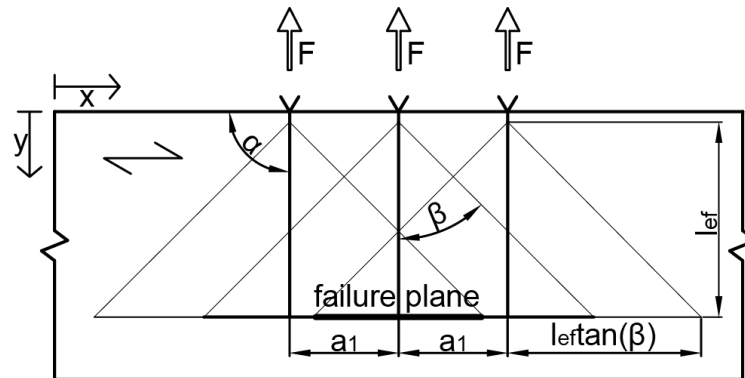


Figure 93: Stress accumulation in a row of screws in grain direction

In the area where accumulation of stresses occurs the stresses caused by different fasteners are added. Furthermore, the assumption is made that the exceeding stresses between the fasteners “even” out due to plastic deformations and load dispersion in the timber and thus, a uniform stress level between two fasteners is attained. Therefore, the following approach (Eq. 7.7) is suggested to calculate the accumulated level of tensile stresses perpendicular to the grain for a row of screws in grain direction.

$$\sigma_{t,90} = \left( \frac{l_{ef} \tan(\beta)}{a_1} + 1 \right) \frac{F}{l_{ef}^2 \tan(\beta) \tan(\gamma) \pi} \quad 7.7$$

Similar can be said about the accumulation of stresses in a row of fasteners perpendicular to the grain.

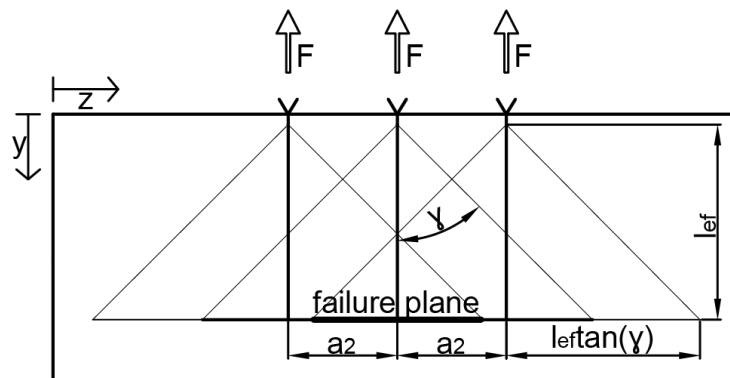


Figure 94: Stress accumulation in a row of screws perpendicular to grain

To obtain the resulting accumulation of both rows in and perpendicular to grain direction the influences have to be added. The maximum stress level that can be attained is  $f_{t,90}$ , exceeding leads to failure due to block shear according to this model. Thus:

$$\sigma_{t,90} = \left[ l_{ef} \left( \frac{\tan(\beta)}{a_1} + \frac{\tan(\gamma)}{a_2} \right) + 2 \right] \frac{F}{l_{ef}^2 \tan(\beta) \tan(\gamma) \pi} = f_{t,90} \quad 7.8$$

Rearranging leads to an expression for the maximum force per fastener accounting for block shear.

$$F = \frac{f_{t,90} l_{ef}^2 \tan(\beta) \tan(\gamma) \pi}{l_{ef} \left( \frac{\tan(\beta)}{a_1} + \frac{\tan(\gamma)}{a_2} \right) + 2} \quad 7.9$$

It has to be mentioned that Eq. 7.9 has been derived only for a stress-fibre angle of  $\alpha = 90^\circ$ .

The resistance of the overall connection is then obtained with:

$$F_{\text{Connection}} = F n m \quad 7.10$$

### 7.5.3 Validation

Mahlknecht et al. (2014) [1] conducted pull-out tests of self-drilling screws with a fastener-to-grain angle of  $90^\circ$ , where many of the specimens with smaller spacings among the fasteners failed due to block shear. In the following the above derived approach is compared to the test results where block shear was the governing failure mode.

Additionally to the parameters given in Table 9, which can be found in chapter 10.6 these parameters were chosen:

- $\beta = \gamma = 45^\circ$        $d = 6 \text{ mm}$        $f_{t,90} = 3 \text{ N/mm}^2$

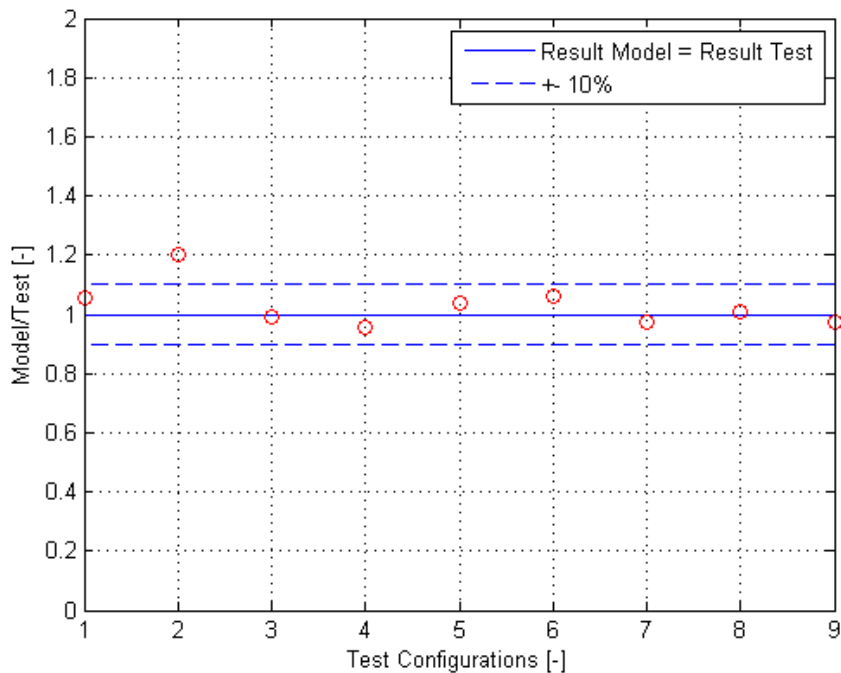


Figure 95: Graphical presentation of the comparison model/test results for connections with fasteners loaded axially and failing due to block shear

Apparently there is a very good agreement between calculated and tests results, so the model can be seen as quite accurate for a stress-fibre angle of  $90^\circ$  and the connection configurations tested in [1]. It has to be said that the load dispersion angle perpendicular to the grain ( $\gamma$ ), which was assumed to be  $45^\circ$ , is much smaller according to other authors (e.g. Schoenmakers (2010) [11]  $\gamma \sim 34^\circ$ ). This inconsistency remains but, at least, an approach has been shown that leads to accurate load carrying capacity predictions of this failure mode.

## 7.6 Summary

In chapter 7 connections with axially-loaded fasteners have been briefly discussed. Firstly, the design practice according to Eurocode [4] has been introduced and secondly block shear, which has not yet been taken explicitly into account in the design rules (just through introducing minimum distances), has been examined further. An analytical model to consider this failure mode in the design process has been derived and verified with results of tests conducted by Mahlkecht et al. (2014). Good agreement, supporting the model's accuracy, has been observed.

## 8 BIOMIMICRY IN CONNECTIONS

In this chapter, the performance of connections with regards to the load paths throughout them are examined and discussed. Areas where peak stresses normally occur are highlighted and the reasons for the appearance of these peak stresses are presented. Furthermore approaches to conduct shape optimisations on load supporting elements in order to reduce peak stresses through improvement of the load paths are presented. Based on this, some potential for optimisation is shown in connections with fasteners loaded in shear. To conclude, the example of the application of a connection employing biomimicry in an existing building is shown.

### 8.1 Load Transfer and Peak Stresses

Load tends to take the shortest and most direct way through the building's components towards the supports. This behaviour leads, on the one hand, to areas in these structures where peak stresses occur and, on the other hand, parts might not be used at all to support the load and are, thus, just a waste of material if the components are not designed optimally.

Figure 96 shows the strain distribution across the timber member of different kinds of connections. Those connections that allow the most direct load flow and, as a consequence, show the least peak strains (and peak stresses), have the most uniform loading of the cross section area and exhibit the highest effectiveness in load support.

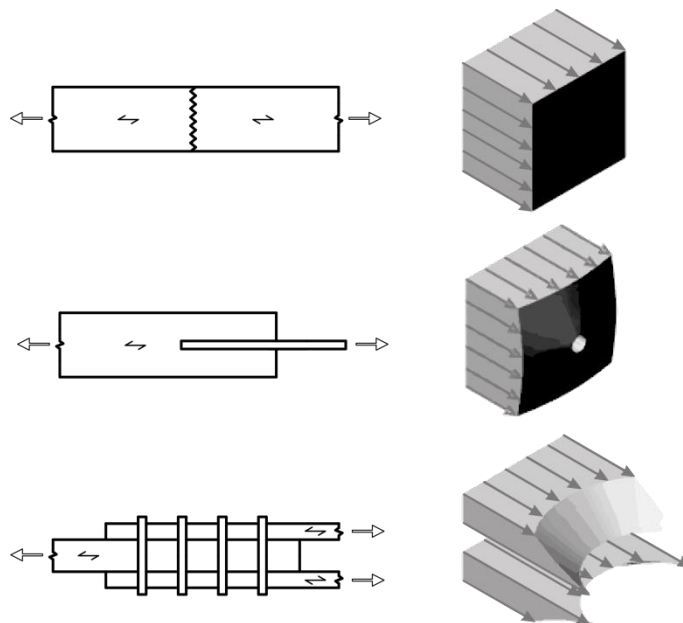


Figure 96: Different connections subjected to tensile forces with the strain distribution across the timber member(s) (distributions taken from [3])

First is a glued connection subjected to tensile loading which has the highest effectiveness as the load does not have to take any “detours” but is transferred in the most direct way. Secondly, a glued steel bar in a timber member loaded in tension is exhibited. The load is still transferred rather straight forwardly and the cross section of the timber member can nearly be used to its full extend to transfer the load. The third example is a (already quite comprehensively discussed) shear connection with dowel type fasteners. Here, the load has to make many direction changes until it is transferred. The strain distribution is the least uniform and the cross section that can be employed is the smallest. So in terms of load flow, this kind of connection shows the worst properties. However, it is the type that can exhibit the most ductile failure behaviour. Furthermore, it can be assembled and dismantled easiest.

How to avert peak stresses as much as possible can be seen in nature. Trees (or bones), for example, have a load oriented growth behaviour, meaning that they grow these parts most which are stressed most to achieve a uniform stress distribution across the surface. Based on this finding, Mattheck (1990, 1997) [6] [7] formulated the “axiom of constant stresses”, which is one of the foundations of the in chapter 8.2 presented optimisation methods. The part of the tree where a branch grows out of a trunk can be regarded as a naturally optimised connection. The edges are optimally smoothed out to reduce peak stresses to a minimum and thereby the durability and load carrying capacity of the connection are increased [1].



Figure 97: Trunk-branch-connection with optimally smoothed out shape to minimise peak stresses (left); root subjected to bending in one plane and therefore optimized cross section for this purpose (right) (taken from [1])

Characteristic areas in load supporting elements where peak stresses occur are notches and holes. In the following a component with an edge loaded in tension is shown in Figure 98.

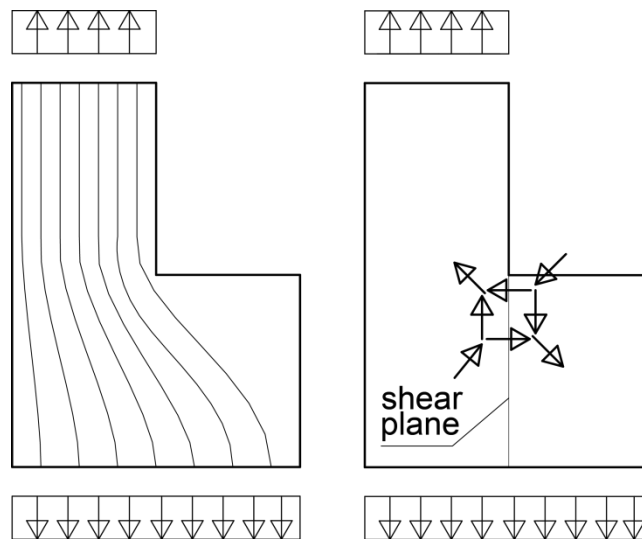


Figure 98: Notched element with peak stresses

The left part of Figure 98 shows the qualitative stress paths through the element. It is obvious that the stresses tend to accumulate at the edge to spread over the whole new cross section while there is a part that is not loaded at all and quite useless (in this particular loading situation). The stresses cannot utilise it because the maximum angle they can change their direction is  $45^\circ$ . This matter is explained in the right part, where a shear plane through the element is presented. To remain in an equilibrium the shear stresses need to have their equivalent in orthogonal direction and therefore a so called “shear quadrangle” (Mattheck) has to emerge. This condition of “pure shear” is equivalent to a situation of main stresses of pure tension in a rotated direction of  $45^\circ$  (and compressional main stresses in perpendicular direction, of course) [1] [2].

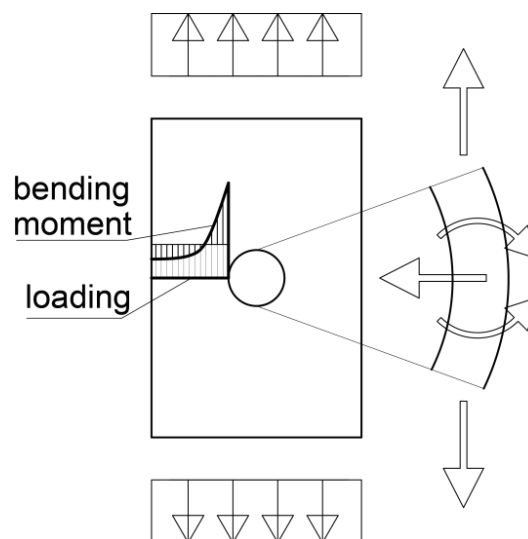


Figure 99: Hole with peak stresses

In Figure 99 peak stresses in the case of an element with a hole loaded in tension are shown. They can be seen as a superposition of tensile stresses due to

the external loading and stresses due to an internal bending moment introduced by deformations of the hole. This is because the parts beside the hole can be regarded as crooked beams subjected to tensile loading and, therefore, a bending moment develops creating the peak stresses as visible in Figure 99. Also stresses perpendicular to loading direction are caused by the deformation of the “crooked beam” [1] [2].

## 8.2 Shape Optimisation

### 8.2.1 Computer Aided Optimisation

Computer Aided Optimisation (CAO) developed by Mattheck (1990) is a method utilizing FEM to imitate load oriented growth in nature. First of all, the stresses are calculated for the original geometry of a certain element with the given loading. To achieve a “growth” equivalently to the stresses, a fictitious heat loading is then applied on a so called “expansion layer” with small E-modulus (1/400 of the original one to avoid coercive pressures due to the growing process):

$$T_i = A(\sigma_i - \sigma_{ref}) \quad 8.1$$

- |                  |  |                       |
|------------------|--|-----------------------|
| • A              | scaling factor, governs the amount of expansion                              | [Kmm <sup>2</sup> /N] |
| • $\sigma_{ref}$ | reference stress, depicts stress level that should be attained by the growth | [N/mm <sup>2</sup> ]  |
| • $\sigma_i$     | stress level at a certain point  | [N/mm <sup>2</sup> ]  |
| • $T_i$          | temperature loading that has to be applied on a certain point                | [K]                   |

A thermal expansion coefficient  $\alpha_T > 0$  is only assigned to the expansion layer, while the rest of the structure receives  $\alpha_T = 0$ . Having done so, the deformation (growth) of the material (expansion layer) due to only the temperature loading is calculated and with this new geometry of the element the process is repeated iteratively until the demanded stress level has been achieved and the reduction of peak stresses is sufficient. This method shows good results and is already widely used in industry. It is, however, rather computationally intense [1].

### 8.2.2 Analytical Method of Multilinearisation

The analytical method is characterised by smoothening the notch using multilinearisation and then putting a cubic spline through those points describing the linear segments. It can be applied without FEM and it is, therefore, much faster to use and provides results that are similar to those of the CAO-method. It has been devised by Mattheck by linearising curves generated with the CAO method and examining angles and appearing forces [1].

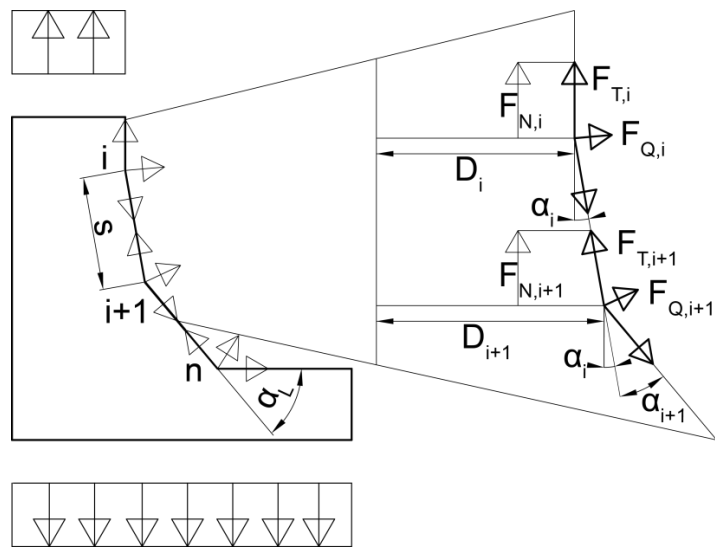


Figure 100: Analytical Method of Multilinearisation to minimize peak stresses in edges

If the surface direction changes under a certain angle  $\alpha_i$ , the forces acting in direction of the surface ( $F_T$ ) change and so do the forces perpendicular to it ( $F_Q$ ).

The whole method is based on the finding that the optimal linearisation has been found if the difference of forces acting tangentially ( $\Delta F_T$ ) to the surface equals the difference of forces acting perpendicularly to it ( $\Delta F_Q$ ), which can be seen as the forces depicting the peak stresses. Thus:

$$\Delta F_T = -\Delta F_Q \quad 8.2$$

$$F_{T_i} - F_{T_{i+1}} = -(F_{Q_i} - F_{Q_{i+1}}) \quad 8.3$$

If both forces equally change, the optimal angle has been found. With this approach a row of angles can be determined causing minimum peak stresses.

However, the start- and end angle have to be chosen. A start angle of  $\alpha_i = 3^\circ$  is recommended in [1] for most applications. The end angle ( $\alpha_L$ ) depends on several factors. A small angle is best because it leads to less peak stresses. By contrast, to optimise material- and space use a big angle is requested. Thus, a compromise has to be found. In general, comparisons with the CAO method have shown that an end angle of  $\alpha_L = 45^\circ$  fulfils the conditions quite well [1], [2].

### 8.2.3 Tension Triangles

The method of tension triangles is a graphical method (again devised by Mattheck) to reduce peak stresses and smoothen notches as well as to reduce material in useless parts of a certain component. It has been devised by observing

how nature smoothens its edges (again: trees, bones, but also stones subjected to wind or current). The construction is shown in Figure 101:

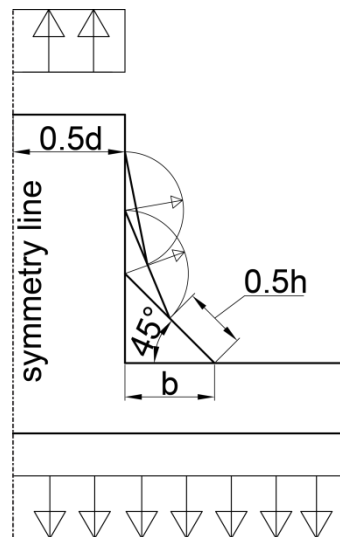


Figure 101: Construction of the tension triangles

In the midpoint of the rectangular triangle's hypotenuse ( $h$ ), the hypotenuse of the second triangle starts, reaching the original surface under an angle of  $22.5^\circ$ . The same procedure is executed for the third triangle which, thus, includes an angle of  $11.25^\circ$  with the former surface of the element.

Parameter studies [2] have shown that  $b$  should be around  $0.4d$  for an element loaded in tension and around  $0.2d$  for the component subjected to bending. The edges are then rounded off with the biggest circle radiuses possible.

This shape can be seen as the “universal notch shape in nature” since it appears as soon as something is rounded off by outer influences (stones) and in load oriented growth (trees, bones).

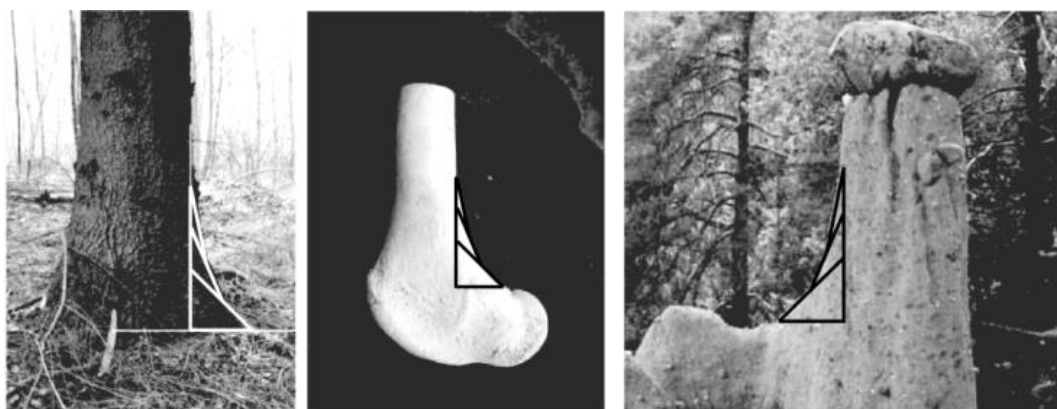


Figure 102: Examples in nature for the application of tension triangles (taken from [4])

Comparisons in [2] have shown that this shape shows good stress reducing capabilities similar to the CAO method and the analytical approach while it does not require any computing time and can be applied by hand drawing.

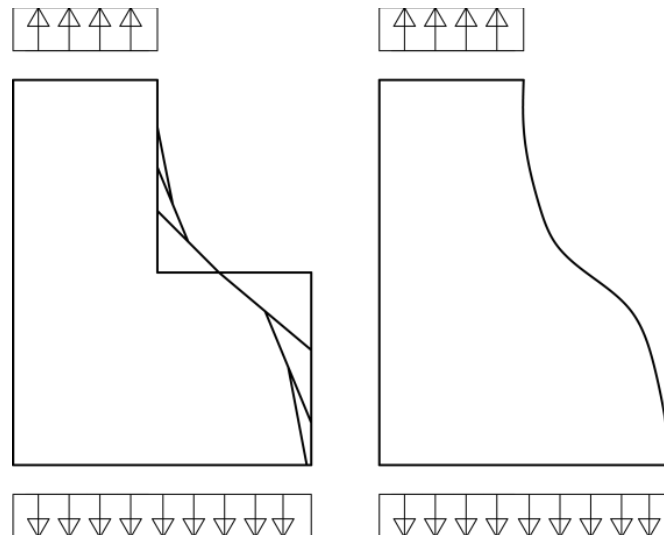


Figure 103: Rounding off the notch and reducing useless material with tension triangles

### 8.3 Application in Connections

In connections as well as any other part of the load transferring structure the load should go the most direct way possible. Detours should be avoided, as they might lead to peak stresses and uneven stressing of the components which has a smaller durability and effectiveness as a consequence.

Furthermore, sharp edges should always be smoothed to reduce peak stresses to a minimum. As presented above, there are quite a lot of tools to do so. Peak stresses caused by holes do not have to be seen that critically. Of course, the tensile stresses beside a hole reach values much higher than the reference stresses, but firstly, timber shows little plasticity to reduce peak stresses and divert them to less stressed parts and secondly, the sides of holes where the tensile peak stresses in grain direction appear are (under normal geometrical conditions) not the most sensible part of a connection. If minimum distances are obeyed a shear connection with dowel type fasteners loaded in grain direction, for example, will not fail due to tensile stresses in grain direction, but (as already shown in chapter 3) the crucial part is a combination of shear stresses and tensile stresses perpendicular to the grain in shear plane(s) in front of the hole. If such a connection is stressed perpendicular to the grain, however, the peak stresses acting now perpendicular to the grain are responsible for failure. Changing the shape of the hole (an ellipse instead of a circle for example) has to be seen critically, simply with regards to the fact that drilling holes other than circular at the construction site is more than inconvenient and if the load direction changes, there would be a hole clearance that might endanger safety and lead to great displacements in the structure. Reinforcing holes with timber of higher density, for

instance, might have a positive effect towards bearing capacity of peak stresses, although this measure has to be seen critically in light of higher construction effort. Upsides for the idea of changing the shape of fasteners could be that many parts of connections are industrially prefabricated which allows almost any shape at reasonable precision. Furthermore, many connections are only loaded in one way for the vast majority of their lifespan. Therefore, the idea of optimising the fastener for one load direction becomes quite practical.

Summing up, it can be stated that as far as possible a direct load flow should be attained when designing a connection. Sharp edges should always be rounded off and one thing that can be done about holes is to avoid them entirely (glued connections). However, if a certain ductility of a connection is required and, thus, connections with fasteners have to be used, peak stresses often occur and have to be coped with in the design process.

### 8.3.1 Shape Optimisation of a Connection with Dowel Type Fasteners

Based on the previously stated, the head of a tensile loaded bar connected with dowel type fasteners is shape optimised. It has to be said that the obtained shape is only an actual optimisation for the sole purpose of a tensile loading in grain direction. For other loading situations, it might turn out to be disadvantageous. This is also the way nature optimises its shapes. They are efficient and durable for the most frequent loading situation although this might go along with disadvantages in less occurring stress situations (e.g. the example of a bending root in Figure 97). Trees cannot change their position, so they have to make the best out of the given circumstances which means investing the limited present resources as efficiently and sustainably as possible to survive and thrive.

To enable a direct load flow with as little peak stresses as possible the fasteners are not arranged behind each other in grain direction anymore, but the spacing perpendicular to the grain ( $a_2$ ) is changed. This measure should avert stress accumulation of tensile stresses perpendicular to the grain and shear stresses among the different fasteners as no continuous (theoretical) crack plane could emerge anymore. Furthermore, with  $a_2$  the cross section is changed as well to allow the tensile main stresses to run without accumulation of peaks.

To construct the shape presented in Figure 104, initial values for  $a_1$ ,  $a_2$ ,  $a_{4c}$  and the angle  $\alpha$  ( $15^\circ$  in the figure) have to be chosen for the first row of fasteners perpendicular to the grain to determine the alteration  $\Delta$  in the following ones. If the spacing between the fasteners increases with  $\Delta$ , the sum of the additional edge distances, consequently, has to be the same to guarantee an unhindered load flow. Furthermore the method of tension triangles is employed to smoothen out the edges between the connection and the beam.

The shape, which is created by the above introduced construction (left in Figure 104) is finally rounded off by turning it into smooth sets of curves (a Bezier Spline that passes through all the endpoints of each line segment, to be precise) in AutoCAD 2011 by using the command “Pedit” – “Spline” as seen right in Figure 104.

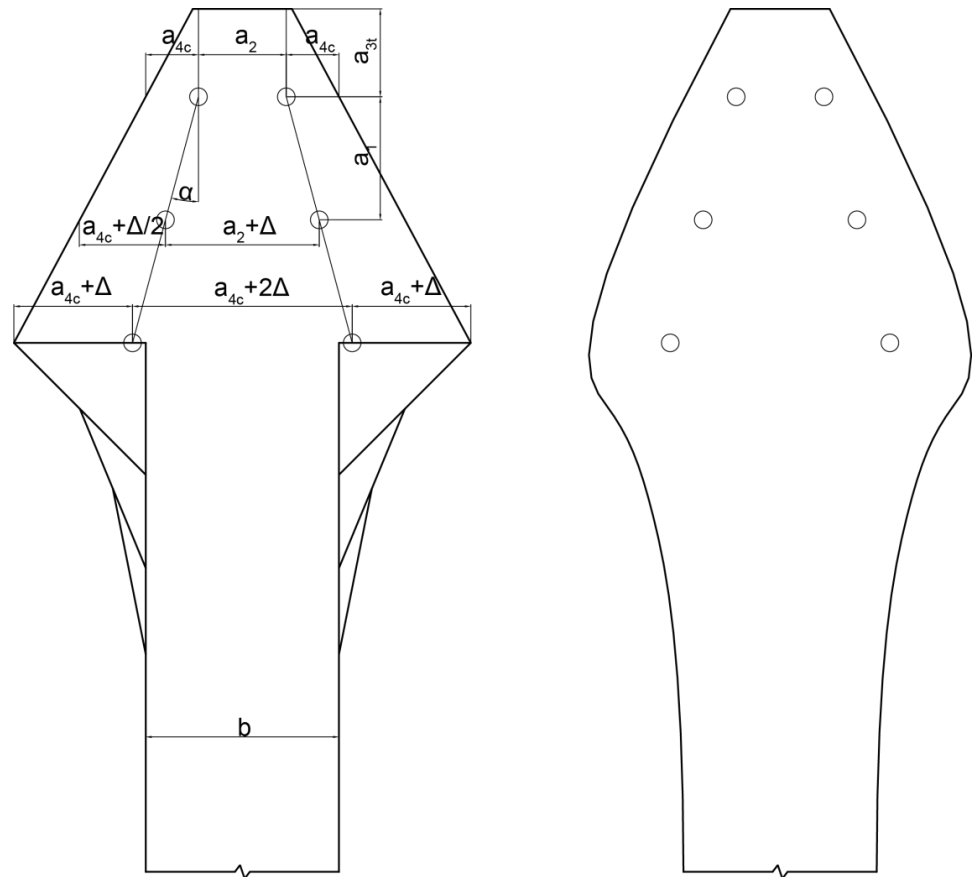


Figure 104: Construction of a shape optimised tension head (left); rounded off shape (right)

A second possibility of shape optimisation of a shear connection loaded in tension is shown in the following. The spacing between the connectors perpendicular to the grain ( $a_2$ ) are varied again, but this time in a reverse manner. In other words the spacing between the fasteners nearest to the loaded edge in grain direction is the highest and it decreases with each row of fasteners perpendicular to the grain. This leads to a situation that is especially favourable concerning the accumulation of shear and tensile stresses perpendicular to the grain. On the one hand it is unlikely that a straight shear plane can emerge due to alternating  $a_2$  (as with the shape above) and on the other hand a “wedge” between the fasteners further counteracts an occurrence of even a crooked shear plane.

Construction, as depicted in Figure 105, is similar to that of the above shown shape. Initial values for several parameters, like distances and spacings as well as an alternation angle have to be chosen, in order to determine the change in spacing and edge distance perpendicular to the grain,  $\Delta$ . The transition between

connection and undisrupted cross section of the bar can be rounded off by employing the method of tension triangles.

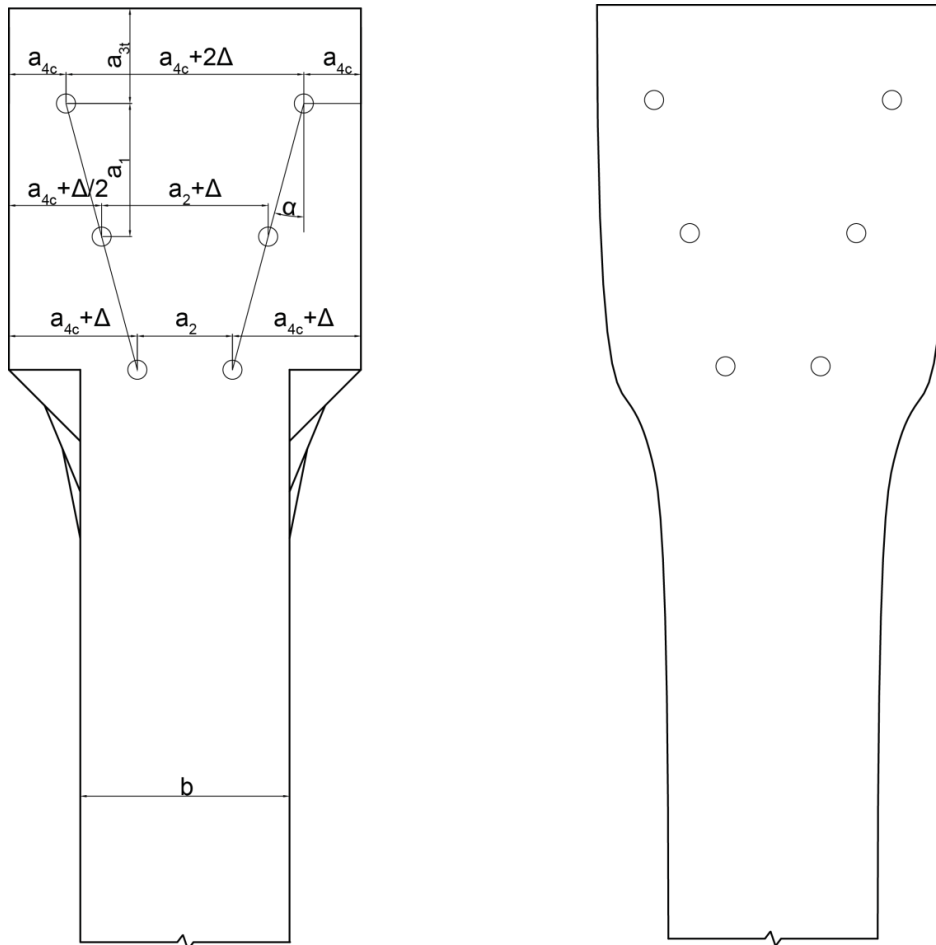


Figure 105: Construction of a shape optimised tension head (left); rounded off shape (right)

To verify the assumed improvement of the stress condition in the connection through shape optimisation, comparison calculations using the Finite-Element program RFEM 5.2 are conducted. The material is defined as two dimensional linear elastic orthotropic plane with constant thickness with the following material parameters:

- $E_0 = 12000 \text{ N/mm}^2$        $E_{90} = 400 \text{ N/mm}^2$        $G_0 = 640 \text{ N/mm}^2$
- $G_{90} = 75 \text{ N/mm}^2$        $\nu_{xy} = 0.5$

To achieve a loading situation as if the material were loaded by dowel-type fasteners, multiple simply supported coupling bars that are only capable of transferring normal forces originate from a loaded node in the midpoint of the fastener hole connecting it with the loaded half-circular edge of the hole. The effect attained by this measure can be regarded as loading of a fastener hole by a dowel-type fastener without hole clearance and without friction between the fastener

and the material timber (friction angle  $\varphi = 0^\circ$ ). Per fastener hole a force which corresponds to the failure load of a single fastener shear connection according to Eurocode EN 1995-1-1 [8] (Johansen failure mode I) is applied. With a material thickness of  $t = 24$  mm, a fastener diameter  $d = 12$  mm and a timber density  $\rho = 400$  kg/m<sup>3</sup> a force  $F = 8312.8$  N is the result (see chapter 4.1.2.2).

Apparently, as already discussed broadly, the usual shear connection loaded in tension shows an accumulation of shear and stresses perpendicular to the grain in the area of the fasteners, while the optimised shapes in fact only exhibit a smaller and partial one (Figure 107 and Figure 108). For the middle shape a crooked shear plane along the fasteners in grain direction could still emerge, but that should not be the case for the right one due to the arrangement of the fasteners. Both optimised types however show increased shear and stresses perpendicular to the plane in the narrowing transitional area leading to the undisrupted bar cross section. This increase however is small and could be further reduced through rounding off more generously.

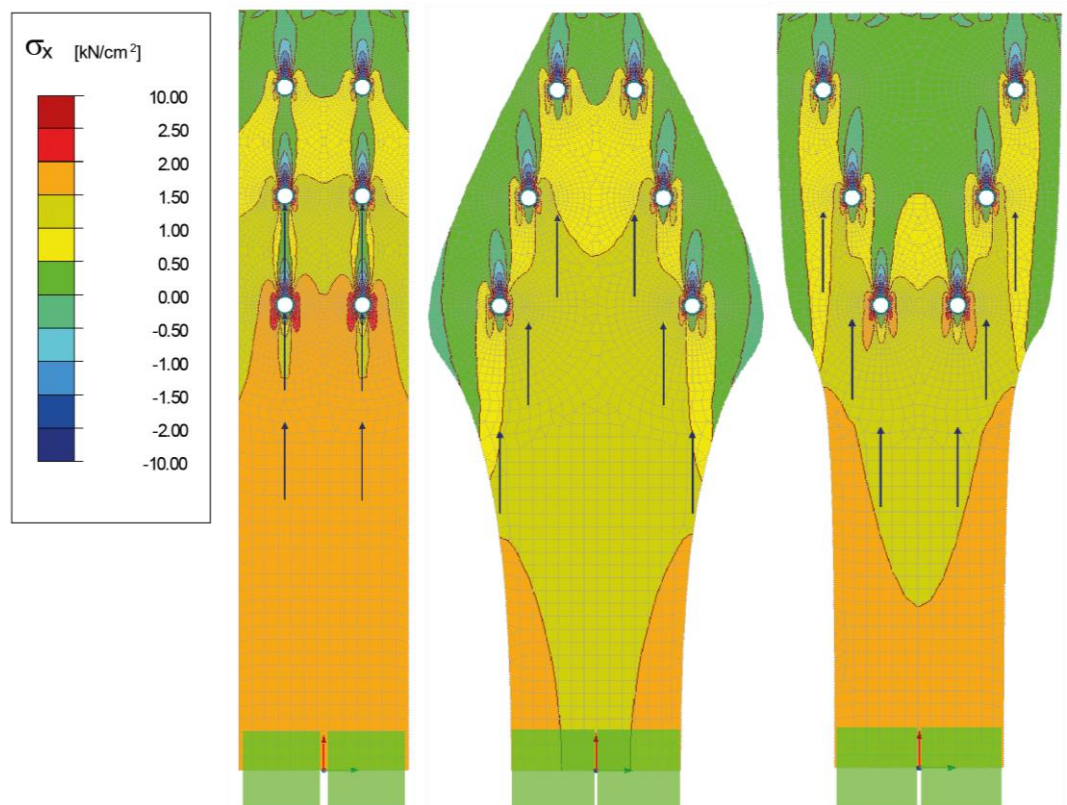


Figure 106: Comparisons of stresses in grain direction in RFEM 5.1

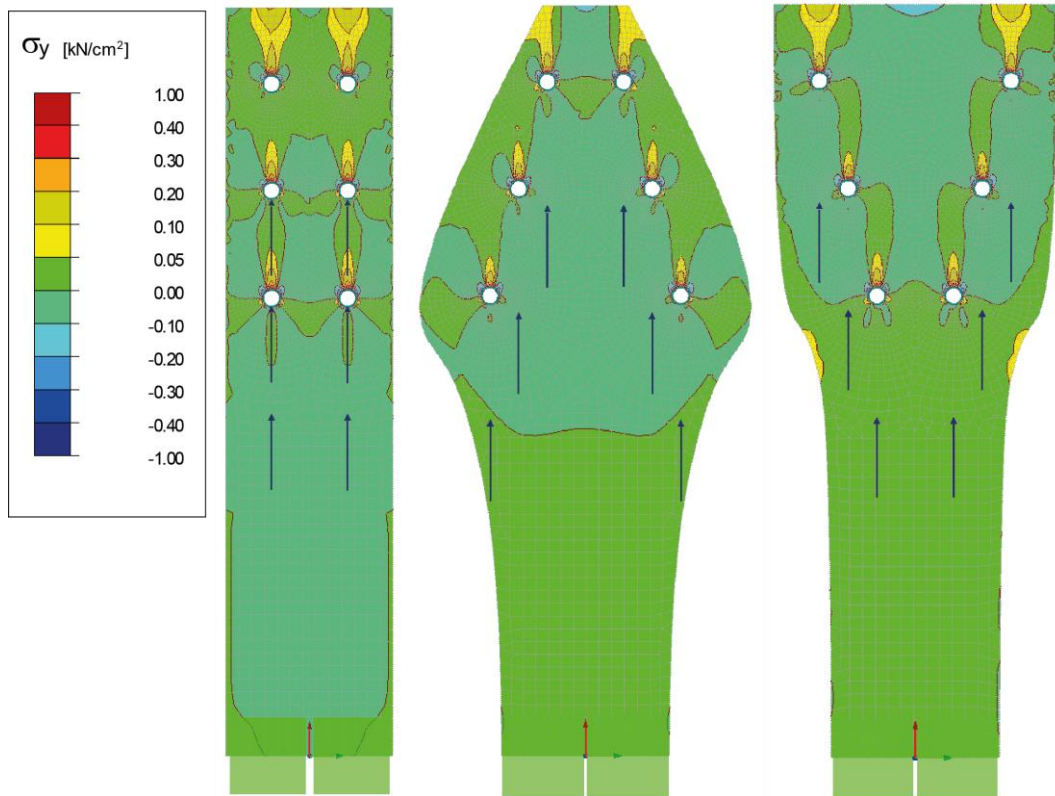


Figure 107: Comparison of stresses perpendicular to the grain in RFEM 5.1

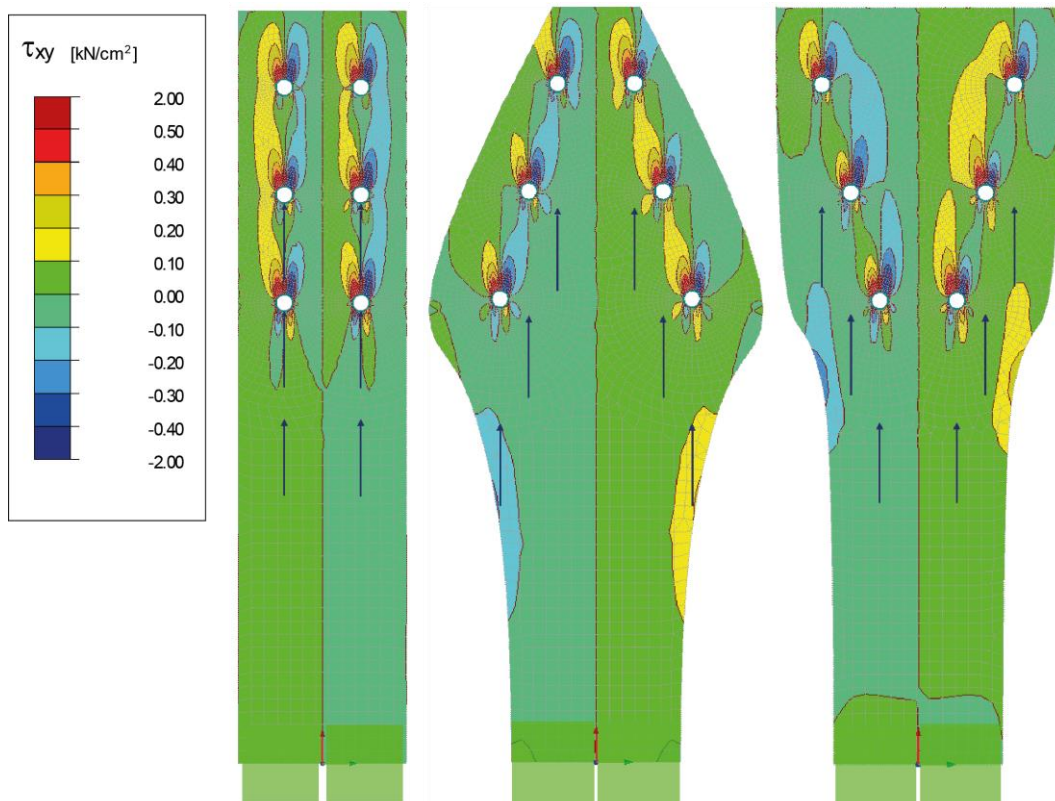


Figure 108: Comparison of shear stresses in RFEM 5.1

### 8.3.2 Shape Optimisation of the Fastener Cross Section

An analytical (linear elastic) approach to examine the influence of a change in the cross section of the fastener from a circle to an ellipse is presented. One of the main differences between an ellipse and a circle is that for an ellipse the location angle ( $\beta$ ) and the slope angle ( $\gamma$ ) are not the same but have to be transformed into each other by geometrical relations.

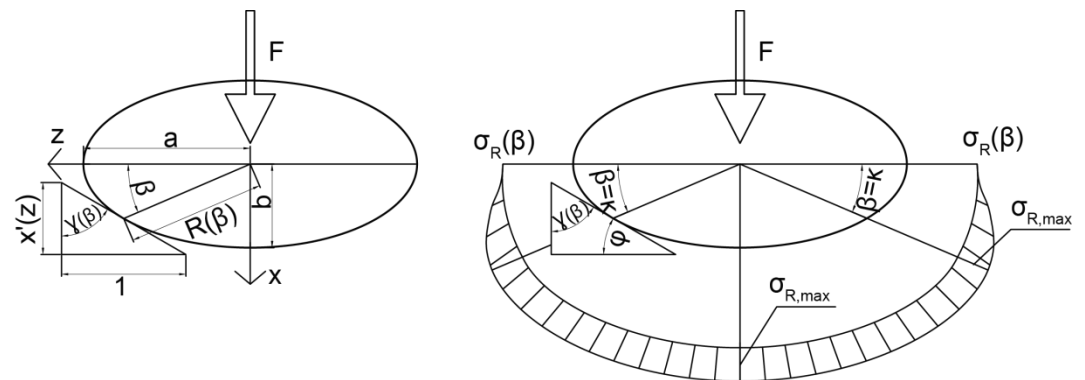


Figure 109: Geometrical and assumed stress conditions around an ellipse

With Eq. 8.4 – Eq. 8.8 a relation between the slope angle and the location angle can be established.

$$\text{atan}\left(\frac{1}{x'(z)}\right) = \gamma \quad 8.4$$

$$x(z) = \sqrt{1 - \frac{z^2}{a^2}} b \quad 8.5$$

$$\frac{dx}{dz} = x'(z) = -\frac{b^2 z}{a^2 \sqrt{b^2 \left(1 - \frac{z^2}{a^2}\right)}} \quad 8.6$$

$$x(\beta) = R(\beta) \sin(\beta) \quad 8.7$$

$$R(\beta) = \frac{ab}{\sqrt{(a \sin(\beta))^2 + (b \cos(\beta))^2}} \quad 8.8$$

The relation between the angles  $\beta$  and  $\gamma(\beta)$  is visible in Figure 110.

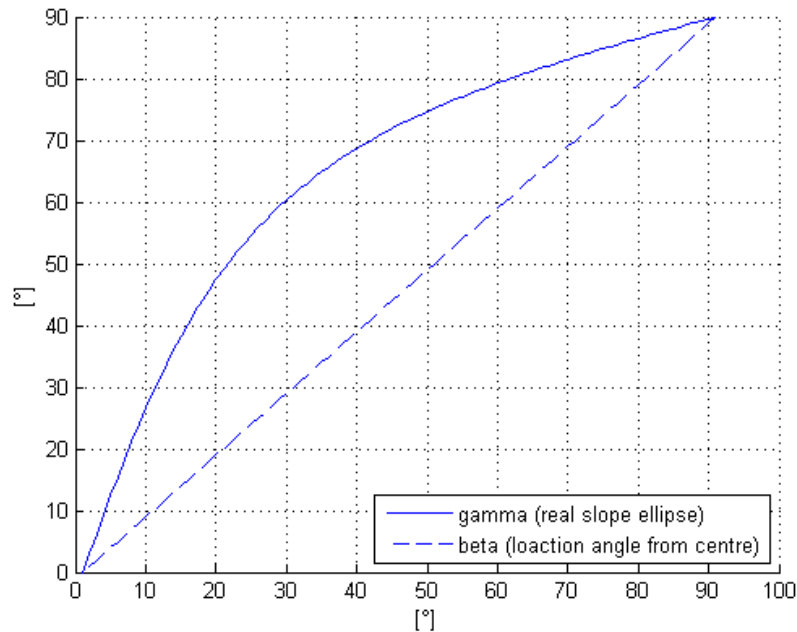


Figure 110: The difference between the location angle  $\beta$  and the slope angle  $\gamma$  at an ellipse,  $a/b=1.78$

To create a distribution of the radial (embedment stresses) it is assumed that the theoretical end of the compression section and thus the theoretical crack plane is situated where the slope of the ellipse is the same as in the case of a circle:

Thus, Eq. 8.9 can be used to depict the distribution:

$$\sigma_R(\beta) = \begin{cases} \text{for } \beta \leq \kappa: \sigma_{R,\max} \sin^2 \left( \frac{\beta\pi}{2\kappa} \right) \\ \text{for } \beta > \kappa: \sigma_{R,\max} \end{cases} \quad 8.9$$

The process to obtain the other stress distributions ( $\sigma_x, \sigma_z$ ) is the same as already shown in chapter 4.1.2.

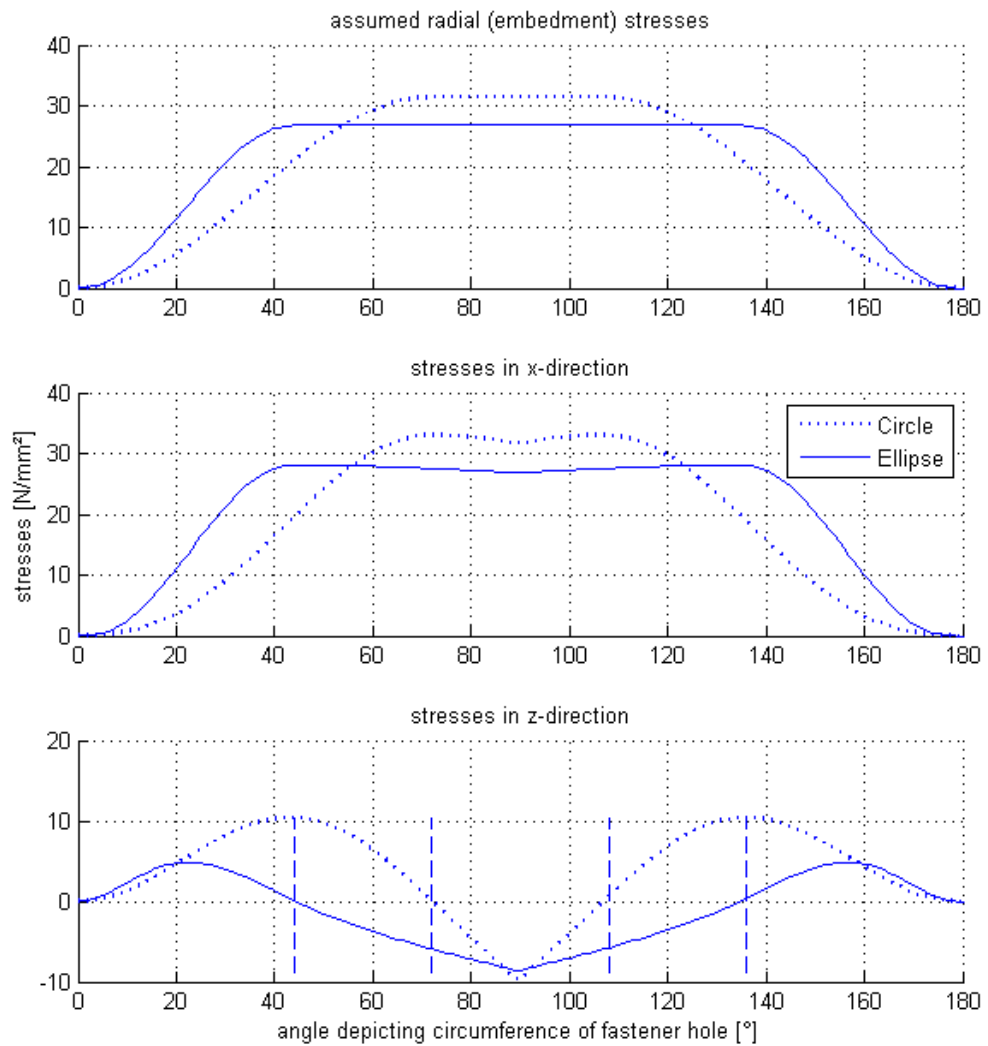


Figure 111: Comparison stresses around a fastener with an ellipsoid and a circular cross section ( $\varphi = 18^\circ$ )

Figure 111 depicts the comparison of the resulting stress distributions if the fastener is loaded with the same force ( $F = 8312.8 \text{ N}$ ) and has the same cross sectional area (achieved with e.g.  $a = 8 \text{ mm}$ ,  $b = 4.5 \text{ mm}$ ) as used in chapter 4.1.2 for the circular fastener.

The stresses perpendicular to the grain responsible for the emergence of the (theoretical) crack plane are smaller and at a different angle. The negative stresses perpendicular to the grain in the compression region can be neglected as they (again) act in opposing directions and thus eliminate each other. The stresses in grain direction are a little smaller than for the circular cross section. It can be said that an ellipsoid shape is considerably advantageous in this loading situation because remarkably less stresses perpendicular to the grain are introduced into the timber. The values between circular and elliptic cross section are compared in Table 5.

Table 5: Comparison between circle and ellipse

	<b>Circle</b> (r = 6 mm; A = 113 mm <sup>2</sup> )	<b>Ellipse</b> (a = 8, b = 4.5 mm; A = 113 mm <sup>2</sup> )	
$\sigma_{x,\max}(\varphi = 7^\circ)$	38.36	35.78	N/mm <sup>2</sup>
$\sigma_{z,\max}(\varphi = 7^\circ)$	13.75	5.45	N/mm <sup>2</sup>
V( $\varphi = 7^\circ$ )	1570.99	560.51	N
$\sigma_{x,\max}(\varphi = 18^\circ)$	33.04	28.16	N/mm <sup>2</sup>
$\sigma_{z,\max}(\varphi = 18^\circ)$	10.42	4.84	N/mm <sup>2</sup>
V( $\varphi = 18^\circ$ )	1038.84	350.15	N
$\sigma_{\sigma_{x,\max}}(\varphi = 30^\circ)$	29.34	25.25	N/mm <sup>2</sup>
$\sigma_{z,\max}(\varphi = 30^\circ)$	7.81	4.49	N/mm <sup>2</sup>
V( $\varphi = 30^\circ$ )	651.53	225.6	N

## 8.4 Example of a Bionic Connection

A connection employing biomimicry is used in the Tamedia building in Zurich, Switzerland, which opened in 2013. One of the most interesting features of this building is a joint used to connect the load supporting structures. The timber connection works entirely without steel fasteners, all the edges are rounded off to guarantee an as direct load transfer as possible and where high stresses occur inevitably, timber with high density is used.

In the area of the connection, the cross section of the 21 m long continuous column increases and to support the occurring stresses perpendicular to the grain, plates with a thickness of 4 cm made of beech are glued into both sides of the column as well as the connecting beams. This rounded off enlargement results in an elliptic shape of the connection and consequently the wooden dowel (again made of beech wood) that sticks out to attach the beams is shaped like an ellipse as well. This elliptic shape was chosen to achieve a higher bending stiffness of the connection and hence keep the beams from rotating [8].

In front of the wooden dowel sticking out of the connection is a hook to attach the bar leading perpendicular to the beams. This bar, however, will be only able to transfer small tensile forces due to the fact that only one wooden hook is used and will be mainly used in compression.



Figure 112: Tamedia building in Zurich, Switzerland (taken from [5])

## 8.5 Summary

In this chapter the reason for the emergence of peak stresses has been shown qualitatively and how nature avoids them. Additionally, three approaches to obtain shapes that reduce peak stresses to a minimum have been presented. Furthermore, the application of these bionic ideas in connections in timber construction has been discussed and finally an example for a building where a bionic connection had been used has been presented.

It can be stated that a connection that follows bionic premises should have the following feature: a direct load flow without “detours” made possible by a shape resembling the load oriented growth behaviour of trees leading to a more or less uniform distribution of stresses across the surface. This leads to high durability and effectiveness of the connection.

## 9 REFERENCES

### 9.1 Part I – Connections with Fasteners Loaded in Shear

- [1] Jorissen, A. (1998). *Double Shear Timber Connections with Dowel Type Fasteners*. Delft University Press. Delft, Netherlands
- [2] Schickhofer, G. (2009). *Holzbau Nachweisführung für Konstruktionen aus Holz*. Graz University of Technology. Graz, Austria
- [3] ÖNORM EN 1995-1-1. (2009). *Eurocode 5: Bemessung und Konstruktion von Holzbauten Teil1-1: Allgemeines – Allgemeine Regeln und Regeln für den Hochbau*. Austrian Standards Institute. Vienna, Austria
- [4] Köhler, Leijten, Jorissen (2006). *Uncertainties Related to the Strength Modelling of Dowel Type Fasteners*.
- [5] Heine, C.P. (2001) *Simulated Response of Degrading Hysteretic Joints With Slack Behaviour*. Virginia Polytechnic Institute and State University. Blacksburg, USA.
- [6] AS 1720.1-1997. (2002) *Australian Standard Timber Structures Part 1: Design methods*. ISBN 0 7337 1493 5. Standards Australia. Sydney, Australia
- [7] Werner H. (1993) *Tragfähigkeit von Holz-Verbindungen mit stiftförmigen Verbindungsmitteln unter Berücksichtigung streuender Einflussgrößen*. Berichte der Versuchsanstalt für Stahl, Holz und Steine der Universität Fride-ricana in Karlsruhe. 4. Folge – Heft 28. Karlsruhe, Germany
- [8] Schmid, Blaß, Frasson. (2002). *Effect of Distances, Spacing and Number of Dowels in a Row on the Load Carrying Capacity of Connections with Dowel Type Fasteners*. CIB-W18/35-7-7. International Council for Research and Innovation in Building and Construction.
- [9] SIA 265:2003. (2003) *Holzbau (Timber Structures)*. Schweizerischer Ingenieur- und Architekturverein. SN 505 265. Zurich, Switzerland
- [10] Schmid M. (2002). *Anwendung der Bruchmechanik auf Verbindungen mit Holz*. Karlsruhe Institute of Technology. Karlsruhe, Germany
- [11] Schoenmakers D. (2010). *Fracture and failure mechanisms in timber load- ed perpendicular to the grain by mechanical connections*. ISBN: 978-90-386-2223-1. Technische Universiteit Eindhoven. Eindhoven, The Nether- lands
- [12] Timoshenko, Goodier (1951). *Theory of Elasticity*. McGraw-Hill Book Com- pany, Inc.. New York, United States. Toronto, Canada. London, Great Brit- ain.
- [13] Wyss, Th. (1923). *Beitrag zur Spannungsuntersuchung an Knotenblechen eiserner Fachwerke*. ETH Zürich. Zürich, Switzerland.

- [14] Van der Put, T.A.C.M. (1976). *Tests on timber connections with dowel type fasteners in glulam and sawn structural timber*. (in Dutch). Rapport 4-76-2, Stevin Laboratorium, TU Delft, Delft, Netherlands. Cited in and taken from [1].
- [15] Lantos, G. (1969). *Load Distribution in a Row of Fasteners Subjected to Lateral Load*. Wood Science, Vol.1, No. 3, P. 129-136. Cited in and taken from [1].
- [16] Petersson, H. (1995). *Fracture Design Analyses of Wooden Beams with Holes and Notches*. Paper 28-19-3, Proceedings CIB-W18 meeting. Copenhagen, Denmark. Cited in and taken from [1].
- [17] ÖNORM EN 409. (2009). *Holzbauwerke – Prüfverfahren – Bestimmung des Fließmoments von stiftförmigen Verbindungsmitteln (Timber structures – Test methods – Determination of the yield moment of dowel type fasteners)*. Austrian Standards Institute. Vienna, Austria.
- [18] ÖNORM EN 26891. (1991). *Holzbauwerke - Verbindungen mit mechanischen Verbindungsmitteln - Allgemeine Grundsätze für die Ermittlung der Tragfähigkeit und des Verformungsverhaltens. (Timber structures - Joints made with mechanical fasteners - General principles for the determination of strength and deformation characteristics)*. Austrian Standards Institute. Vienna, Austria. Cited in and taken from [1] and [2]
- [19] Johansen, K. W. (1949). *Theory of Timber Connections*. International Association of Bridge and Structural Engineering, Publication 9:249-262. Cited in and taken from [1]
- [20] Meyer, A. (1957). *Die Tragfähigkeit von Nagelverbindungen bei statischer Belastung*. Holz als Roh- und Werkstoff, 15 Jg. Heft 2, P.96-109. Cited in and taken from [1]
- [21] De Jong, T. (1982). *Stresses around pin loaded holes in composite materials*. Mechanics of Composite Materials Recent Advances. Pergamon Press, P.339-353. Cited in and taken from [5]
- [22] Gustafsson, P.J. (1985). *Fracture Mechanics Studies of non-yielding Materials like Concrete: Modelling of Tensile Fracture and Applied Strength Analyses*. Report TVBM-1007. Lund Institute of Technology, Sweden Cited in and taken from [1]
- [23] Gustafsson, P.J. (1987). *Analysis of generalized Volkersen-joints in terms of non-linear fracture mechanics*. Mechanical Behaviour of Adhesive Joints, P.323-338, Edition Pluralis. Paris, France. Cited in and taken from [1]
- [24] Volkersen, O. (1938). *Die Nietkraftverteilung in zugbeanspruchten Nietverbindungen mit konstanten Laschenquerschnitten*. Luftfahrtforschung, Vol. 35, P.4-47. Cited in and taken from [1]
- [25] Kuipers, J. (1960). *Research into split ring connections. Elements connected at an angle*. (in Dutch). Rapport 4-60-1-HV-18, Stevin Laboratorium, TU Delft, Netherlands. Cited in and taken from [1]

- [26] Hetenyi, M. (1974). *Beams on elastic foundation. Theory with application in the field of civil and mechanical engineering*. University of Michigan Press, Scientific Series, Volume XVI. Michigan, USA. Cited in and taken from [1]

## 9.2 Part II – Connections with Fasteners Loaded Axially

---

- [1] Mahlknecht et al. (2014). *Resistance and Failure Modes of Axially Loaded Groups of Screws. (From: Materials and Joints in Timber Structures Recent Developments of Technology)*. Rilem Bookseries Vol.9. Springer.
- [2] Ringhofer et al. (2014). *Investigations Concerning the Force Distribution along Axially Loaded Self-tapping Screws. (From: Materials and Joints in Timber Structures Recent Developments of Technology)*. Rilem Bookseries Vol.9. Springer.
- [3] Blaß et al. (2006). *Tragfähigkeit von Verbindungen mit selbstbohrenden Holzschrauben mit Vollgewinde*. Band 4 der Reihe Karlsruher Berichte zum Ingenieurholzbau. Universität Karlsruhe. Karlsruhe, Germany
- [4] ÖNORM EN 1995-1-1. (2009). *Eurocode 5: Bemessung und Konstruktion von Holzbauten Teil1-1: Allgemeines – Allgemeine Regeln und Regeln für den Hochbau*. Austrian Standards Institute. Vienna, Austria
- [5] Schickhofer, G. (2009). *Holzbau Nachweisführung für Konstruktionen aus Holz*. Graz University of Technology. Graz, Austria

## 9.3 Part III – Biomimicry in Connections

---

- [1] Scherrer M. (2004). *Kerbspannung und Kerbformoptimierung*. Wissenschaftliche Berichte FZKA 7021. Forschungszentrum Karlsruhe GmbH. Technische Universität Karlsruhe. Karlsruhe, Germany
- [2] Sörensen J. (2009). *Untersuchungen zur Vereinfachung der Kerbformoptimierungen*. Wissenschaftliche Berichte FZKA 7397. Forschungszentrum Karlsruhe GmbH. Technische Universität Karlsruhe. Karlsruhe, Germany
- [3] Schickhofer, G. (2009). *Holzbau Nachweisführung für Konstruktionen aus Holz*. Graz University of Technology. Graz, Austria
- [4] Mattheck C. (2010). *Denkwerkzeuge nach der Natur*. ISBN: 978-3-923704-73-6
- [5] Internet (retrieved 5/2014). <http://aasarchitecture.com/2013/10/tamedia-by-shigeru-ban-architects.html>
- [6] Mattheck, C. (1997). *Design in der Natur – Der Baum als Lehrmeister*. 3. Auflage, Rombach Verlag. Freiburg, Germany. Cited in and taken from [1]
- [7] Mattheck, C. (1990). *Why they grow, how they grow: The Mechanics of Trees*. Arboricultural Journal, 14, P.1-17. Cited in and taken from [1]

- [8] Pfäffinger J. (2013). „*Sicherer als Stahl und Beton*“. Mikado Magazin (Unternehmermagazin für Holzbau und Ausbau). 2:14-21. WEKA MEDIAEN-1995-1-1
- [9] ÖNORM EN 1995-1-1. (2009). *Eurocode 5: Bemessung und Konstruktion von Holzbauten Teil1-1: Allgemeines – Allgemeine Regeln und Regeln für den Hochbau*. Austrian Standards Institute. Vienna, Austria

## 10 APPENDIX

### 10.1 Determination of Constants – Beam on Elastic Foundation

In the following the determination of the constants for the displacement distribution of the beam on elastic foundation shall be presented. Generally the constants can be calculated by solving this system of equations:

$$C = S * K^{-1} \quad 10.1$$

With:

$$K = \begin{pmatrix} K_{11} & \cdots & K_{18} \\ \vdots & \ddots & \vdots \\ K_{81} & \cdots & K_{88} \end{pmatrix} \quad 10.2$$

$$S = \begin{pmatrix} S_1 \\ \vdots \\ S_8 \end{pmatrix} \quad 10.3$$

$$C = \begin{pmatrix} A_1 \\ B_1 \\ A_2 \\ B_2 \\ C_1 \\ D_1 \\ C_2 \\ D_2 \end{pmatrix} \quad 10.4$$

With these boundary conditions the matrices can be defined:

$$M_1(x = -a_{3t} = x_0) = EI \frac{d\phi_1(x = -a_{3t} = x_0)}{dx} = 0$$

$$K_{11} = (\beta \cos(\eta x_0) - \eta \sin(\eta x_0))e^{\beta x_0}$$

$$K_{12} = (\eta \cos(\eta x_0) + \beta \sin(\eta x_0))e^{\beta x_0}$$

$$K_{13} = (-\beta \cos(\eta x_0) - \eta \sin(\eta x_0))e^{-\beta x_0}$$

$$K_{14} = (\eta \cos(\eta x_0) - \beta \sin(\eta x_0))e^{-\beta x_0}$$

$$K_{15} = K_{16} = K_{17} = K_{18} = 0$$

$$S_1 = 0$$

$$Q_1(x = -a_{3t} = x_0) = EI \frac{d\phi_1^2(x = -a_{3t} = x_0)}{dx^2} = 0$$

$$K_{21} = [(\beta^2 - \eta^2) \cos(\eta x_0) - 2\beta\eta \sin(\eta x_0)]e^{\beta x_0}$$

$$K_{22} = [2\beta\eta \cos(\eta x_0) + (\beta^2 - \eta^2) \sin(\eta x_0)]e^{\beta x_0}$$

$$K_{23} = [(\beta^2 - \eta^2) \cos(\eta x_0) + 2\beta\eta \sin(\eta x_0)]e^{-\beta x_0}$$

$$K_{24} = [-2\beta\eta \cos(\eta x_0) + (\beta^2 - \eta^2) \sin(\eta x_0)]e^{-\beta x_0}$$

$$K_{25} = K_{26} = K_{27} = K_{28} = 0$$

$$S_2 = 0$$

$$w_1(x = 0) = w_2(x = 0)$$

$$K_{31} = Z_1$$

$$K_{32} = Z_2$$

$$K_{33} = -Z_1$$

$$K_{34} = Z_2$$

$$K_{35} = -Z_1$$

$$K_{36} = -Z_2$$

$$K_{37} = Z_1$$

$$K_{38} = -Z_2$$

$$S = 0$$

$$\phi_1(x = 0) = \phi_2(x = 0)$$

$$K_{41} = 1$$

$$K_{42} = 0$$

$$K_{43} = 1$$

$$K_{44} = 0$$

$$K_{45} = -1$$

$$K_{46} = 0$$

$$K_{47} = -1$$

$$K_{48} = 0$$

$$S = 0$$

$$Q_1(x=0) - Q_2(x=0) = V_b \hat{=} \frac{d\phi_1^2(x=0)}{dx^2} - \frac{d\phi_2^2(x=0)}{dx^2} = \frac{V_b}{EI}$$

$$K_{51} = (\beta^2 - \eta^2)$$

$$K_{52} = 2\beta\eta$$

$$K_{53} = (\beta^2 - \eta^2)$$

$$K_{54} = -2\beta\eta$$

$$K_{55} = -(\beta^2 - \eta^2)$$

$$K_{56} = -2\beta\eta$$

$$K_{57} = -(\beta^2 - \eta^2)$$

$$K_{58} = 2\beta\eta$$

$$S = \frac{V_b}{EI}$$

$$M_1(x=0) - M_2(x=0) = \frac{Fh_1}{2} \hat{=} \frac{d\phi_1(x=0)}{dx} - \frac{d\phi_2(x=0)}{dx} = \frac{Fh_1}{2EI}$$

$$K_{61} = \beta$$

$$K_{62} = \eta$$

$$K_{63} = -\beta$$

$$K_{64} = \eta$$

$$K_{65} = -\beta$$

$$K_{66} = -\eta$$

$$K_{67} = \beta$$

$$K_{68} = -\eta$$

$$S = \frac{Fh_1}{2EI}$$

$$w_2(x = a_{3c} = x_3) = 0$$

$$K_{71} = K_{72} = K_{73} = K_{74} = 0$$

$$K_{75} = (Z_1 \cos(\eta x_3) - Z_2 \sin(\eta x_3))e^{\beta x_3}$$

$$K_{76} = (Z_2 \cos(\eta x_3) + Z_1 \sin(\eta x_3))e^{\beta x_3}$$

$$K_{77} = (-Z_1 \cos(\eta x_3) - Z_2 \sin(\eta x_3))e^{-\beta x_3}$$

$$K_{78} = (Z_2 \cos(\eta x_3) - Z_1 \sin(\eta x_3))e^{-\beta x_3}$$

$$S = 0$$

$$\phi_2(x = a_{3c} = x_3) = 0$$

$$K_{81} = K_{82} = K_{83} = K_{84} = 0$$

$$K_{85} = \cos(\eta x_3) e^{\beta x_3}$$

$$K_{86} = \sin(\eta x_3) e^{\beta x_3}$$

$$K_{87} = \cos(\eta x_3) e^{-\beta x_3}$$

$$K_{88} = \sin(\eta x_3) e^{-\beta x_3}$$

$$S = 0$$

## 10.2 Derivation of the relation $w(x) = V_b f_1(x) + F f_2(x)$

The function for the displacement distribution is:

$$w(x) = [(A_1 Z_1 + B_1 Z_1) \cos(\eta x) + (-A_1 Z_2 + B_1 Z_1) \sin(\eta x)] e^{\beta x} + [(-A_2 Z_1 + B_2 Z_2) \cos(\eta x) + (-A_2 Z_2 - B_2 Z_1) \sin(\eta x)] e^{-\beta x} \quad 10.5$$

With:

$$A_i, B_i = K_{bj} V_b + K_{vj} F \quad 10.6$$

Thus:

$$w(x) = \left[ \left( \frac{(K_{b1} V_b + K_{v1} F) Z_1}{A_1} + \frac{(K_{b2} V_b + K_{v2} F) Z_1}{B_1} \right) \cos(\eta x) + \left( -\frac{(K_{b1} V_b + K_{v1} F) Z_2}{A_1} + \frac{(K_{b2} V_b + K_{v2} F) Z_1}{B_1} \right) \sin(\eta x) \right] e^{\beta x} + \left[ \left( -\frac{(K_{b3} V_b + K_{v3} F) Z_1}{A_2} + \frac{(K_{b4} V_b + K_{v4} F) Z_2}{B_2} \right) \cos(\eta x) + \left( -\frac{(K_{b3} V_b + K_{v3} F) Z_2}{A_2} - \frac{(K_{b4} V_b + K_{v4} F) Z_1}{B_2} \right) \sin(\eta x) \right] e^{-\beta x} \quad 10.7$$

This can be decomposed to:

$$\begin{aligned}
 w(x) = & \left[ \left( \left( \frac{K_{b1}Z_1 + K_{b2}Z_2}{C_I} \right) V_b + \left( \frac{K_{v1}Z_1 + K_{v2}Z_2}{C_{II}} \right) F \right) \cos(\eta x) \right. \\
 & + \left( \left( \frac{-K_{b1}Z_2 + K_{b2}Z_1}{C_{III}} \right) V_b \right. \\
 & \left. \left. + \left( \frac{-K_{v1}Z_2 + K_{v2}Z_1}{C_{IV}} \right) F \right) \sin(\eta x) \right] e^{\beta x} \\
 & + \left[ \left( \left( \frac{-K_{b3}Z_1 + K_{b4}Z_2}{C_V} \right) V_b + \left( \frac{-K_{v3}Z_1 + K_{v4}Z_2}{C_{VI}} \right) F \right) \cos(\eta x) \right. \\
 & + \left( \left( \frac{-K_{b3}Z_2 - K_{b4}Z_1}{C_{VII}} \right) V_b \right. \\
 & \left. \left. + \left( \frac{-K_{v3}Z_2 - K_{v4}Z_1}{C_{VIII}} \right) F \right) \sin(\eta x) \right] e^{-\beta x}
 \end{aligned} \tag{10.8}$$

$$\begin{aligned}
 w(x) = & [(C_I V_b + C_{II} F) \cos(\eta x) + (C_{III} V_b + C_{IV} F) \sin(\eta x)] e^{\beta x} \\
 & + [(C_V V_b + C_{VI} F) \cos(\eta x) + (C_{VII} V_b + C_{VIII} F) \sin(\eta x)] e^{-\beta x}
 \end{aligned} \tag{10.9}$$

$$\begin{aligned}
 w(x) = & [V_b (C_I \cos(\eta x) + C_{III} \sin(\eta x)) + F (C_{II} \cos(\eta x) + C_{IV} \sin(\eta x))] e^{\beta x} \\
 & + [V_b (C_V \cos(\eta x) + C_{VII} \sin(\eta x)) \\
 & + F (C_{VI} \cos(\eta x) + C_{VIII} \sin(\eta x))] e^{-\beta x}
 \end{aligned} \tag{10.10}$$

$$\begin{aligned}
 w(x) & \\
 = & V_b \underbrace{[e^{\beta x} (C_I \cos(\eta x) + C_{III} \sin(\eta x)) + e^{-\beta x} (C_V \cos(\eta x) + C_{VII} \sin(\eta x))]}_{f_1(x)} \\
 & + F \underbrace{[e^{\beta x} (C_{II} \cos(\eta x) + C_{IV} \sin(\eta x)) + e^{-\beta x} (C_{VI} \cos(\eta x) + C_{VIII} \sin(\eta x))]}_{f_2(x)}
 \end{aligned} \tag{10.11}$$

$$w(x) = V_b f_1(x) + F f_2(x) \tag{10.12}$$

For  $x = 0$ :

$$w(x = 0) = V_b(C_I + C_V) + F(C_{II} + C_{VI}) =$$

$$V_b(K_{b1}Z_1 + K_{b2}Z_2 - K_{b3}Z_1 + K_{b4}Z_2) + F(K_{v1}Z_1 + K_{v2}Z_2 - K_{v3}Z_1 + K_{v4}Z_2)$$
10.13

### 10.3 Derivation of the Relation $w(x) = V_b f_1(x) + F f_2(x) = V_b f(x)$

As shown in chapter 10.2 the displacement distribution for the elastic beam can be split into:

$$w(x) = V_b f_1(x) + F f_2(x)$$
10.14

$$w(x) = V_b f_1(x) + \frac{V}{2f_V(\varphi)} f_2(x)$$
10.15

$$w(x) = V_b f_1(x) + \frac{V_b}{2f_V(\varphi)r_b} f_2(x)$$
10.16

With:

$$F = \frac{V}{2f_V(\varphi)}$$
10.17

$$\frac{V_b}{r_b} = V$$
10.18

Thus:

$$w(x) = V_b \left( \frac{f_1(x) + \frac{f_2(x)}{2f_V(\varphi)r_b}}{f(x)} \right)$$
10.19

$$w(x) = V_b f(x)$$
10.20

## 10.4 Comparison Test Results – Parallel to the Grain to Model

Table 6: Comparison test results and calculations, m=1

n	a <sub>3t</sub>	a <sub>1</sub>	d	h	t <sub>1</sub>	t <sub>2</sub>	Jorissen	Model	M/J
[-]	[mm]	[mm]	[mm]	[mm]	[mm]	[mm]	[N]	[N]	[-]
3	84	60	12	72	12	24	18265	16818	0,921
3	84	84	12	72	12	24	19836	18265	0,921
3	84	132	12	72	12	24	20101	19250	0,958
3	60	60	12	72	24	48	31116	29727	0,955
3	84	60	12	72	24	48	33480	30610	0,914
3	84	84	12	72	24	48	32768	33243	1,014
3	84	132	12	72	24	48	33298	35036	1,052
3	60	60	11	72	59	72	36619	39600	1,081
3	84	60	11	72	59	72	41331	37707	0,912
3	84	84	11	72	59	72	44910	40754	0,907
3	84	132	11	72	59	72	47826	42734	0,894
5	84	36	12	72	12	24	18313	22574	1,233
5	84	60	12	72	12	24	26355	27954	1,061
5	84	84	12	72	12	24	31716	30434	0,960
5	84	132	12	72	12	24	35112	32083	0,914
5	84	36	12	72	24	48	35863	41087	1,146
5	84	60	12	72	24	48	49371	50878	1,031
5	84	84	12	72	24	48	55876	55391	0,991
5	84	132	12	72	24	48	59794	58393	0,977
5	60	60	12	72	24	48	52015	49412	0,950
5	60	84	12	72	24	48	56808	53732	0,946
5	84	36	12	72	59	72	42735	60596	1,418
5	84	60	12	72	59	72	64748	75036	1,159
5	84	84	12	72	59	72	75758	81693	1,078
5	60	60	12	72	59	72	68745	72874	1,060
5	60	84	12	72	59	72	77978	79246	1,016
5	84	36	11	72	36	48	41330	38869	0,940
5	84	84	11	72	36	48	52637	51723	0,983
5	84	132	11	72	36	48	56130	54246	0,966
5	84	36	12	72	48	48	45892	46799	1,020
5	84	84	12	72	48	48	56683	63093	1,113
5	84	132	12	72	48	48	66276	66512	1,004
5	112	112	16	72	48	64	104862	99817	0,952
5	140	140	20	72	60	80	145764	154690	1,061
9	84	60	12	120	12	24	55444	50659	0,914
9	84	84	12	120	12	24	56537	55233	0,977

9	84	60	12	120	24	48	95162	92201	0,969
9	84	84	12	120	24	48	100830	99471	0,987
9	84	132	12	120	24	48	103761	104139	1,004
9	60	60	12	120	24	48	78977	89448	1,133
9	60	84	12	120	24	48	96450	97406	1,010
9	84	60	12	120	59	72	117467	135981	1,158
9	84	84	12	120	59	72	131000	146703	1,120
9	84	132	12	120	59	72	168039	153588	0,914
9	60	60	12	120	59	72	115557	131921	1,142
9	60	84	12	120	59	72	130524	135981	1,042

Table 7: Comparison test results and calculations, n=5, m=2

n	a <sub>3t</sub>	a <sub>1</sub>	d	h	t <sub>1</sub>	t <sub>2</sub>	Jorissen	Model	M/J
[-]	[mm]	[mm]	[mm]	[mm]	[mm]	[mm]	[N]	[N]	[-]
84	36	48	12	120	12	24	34208	45149	1,320
84	84	48	12	120	12	24	58478	60868	1,041
84	36	48	12	120	24	48	65348	82173	1,257
84	84	48	11	120	24	48	102357	93156	0,910
84	36	48	11	120	36	48	73766	77738	1,054
84	84	48	11	120	36	48	104299	103446	0,992

## 10.5 Comparison Test Results – Perpendicular to the Grain to Model

Table 8: Test results and calculations

n	m	a <sub>3c</sub>	a <sub>1</sub>	a <sub>2</sub>	a <sub>4t</sub>	d	h	t	Schoenm.	Model	M/S	Eurocode	EC/S
[-]	[-]	[mm]	[mm]	[mm]	[mm]	[mm]	[mm]	[mm]	[N]	[N]	[-]	[N]	[-]
2	1	800	48	0	143	12	220	45	19674	29000	1,474	22921	1,165
2	2	800	48	48	95	12	220	45	27662	26462	0,957	45843	1,657
2	3	800	48	48	47	12	220	45	32810	37480	1,142	68764	2,096
1	3	1300	0	64	67	16	300	60	40386	42611	1,055	56144	1,390
2	3	800	64	64	67	16	300	60	45070	70070	1,555	112287	2,491
2	1	700	48	0	49	12	244	95	27159	23292	0,858	33553	1,235
2	1	500	48	0	55	12	145	70	19399	25389	1,309	33553	1,730
2	1	300	48	0	85	12	120	45	19354	19419	1,003	22921	1,184
2	2	1300	48	48	48	12	480	45	17764	25387	1,429	45842	2,581
2	2	700	48	48	51	12	219	95	34282	47807	1,395	67107	1,957
2	2	500	48	48	55	12	145	70	40910	47807	1,169	67107	1,640
2	3	1800	48	48	48	12	720	70	30787	68799	2,235	100660	3,270
2	3	900	48	48	48	12	320	45	24465	38081	1,557	68764	2,811
2	3	700	48	48	59	12	219	95	75789	71711	0,946	100660	1,328

## 10.6 Comparison Test Results – Block Shear Screws to Model

Table 9: Comparison test results to model block shear

n*m	l <sub>ef</sub>	a <sub>1</sub>	a <sub>2</sub>	Tests	Model	M/T
[-]	[mm]	[mm]	[mm]	[N]	[N]	[-]
12	28.3d	6d	2.5d	175625	180789	1,029
12	28.3d	8d	2.5d	167000	193435	1,158
12	17.8d	5d	3.5d	125000	121177	0,969
12	17.8d	7d	3.5d	140333	133978	0,955
12	17.8d	10d	3.5d	140500	145506	1,036
25	11.3d	5d	3.5d	135000	144634	1,071
25	11.3d	7.5d	3.5d	165000	160812	0,975
25	11.3d	10d	3.5d	170000	170338	1,002
25	11.3d	12.5d	3.5d	175000	176615	1,009





Dies ist eine Veröffentlichung des

### **FACHBEREICHS INGENIEURBAUKUNST (IBK) AN DER TU GRAZ**

Der Fachbereich Ingenieurbaukunst umfasst die dem konstruktiven Ingenieurbau nahe stehenden Institute für Baustatik, Betonbau, Stahlbau & Flächentragwerke, Holzbau & Holztechnologie, Materialprüfung & Baustofftechnologie, Baubetrieb & Bauwirtschaft, Hochbau & Industriebau, Bauinformatik und Allgemeine Mechanik der Fakultät für Bauingenieurwissenschaften an der Technischen Universität Graz.

Dem Fachbereich Ingenieurbaukunst ist das Bautechnikzentrum (BTZ) zugeordnet, welches als gemeinsame hochmoderne Laboreinrichtung zur Durchführung der experimentellen Forschung aller beteiligten Institute dient. Es umfasst die drei Laboreinheiten für konstruktiven Ingenieurbau, für Bauphysik und für Baustofftechnologie.

Der Fachbereich Ingenieurbaukunst kooperiert im gemeinsamen Forschungsschwerpunkt „Advanced Construction Technology“. Dieser Forschungsschwerpunkt umfasst sowohl Grundlagen- als auch praxisorientierte Forschungs- und Entwicklungsprogramme.

Weitere Forschungs- und Entwicklungskooperationen bestehen mit anderen Instituten der Fakultät, insbesondere mit der Gruppe Geotechnik, sowie nationalen und internationalen Partnern aus Wissenschaft und Wirtschaft.

Die Lehrinhalte des Fachbereichs Ingenieurbaukunst sind aufeinander abgestimmt. Aus gemeinsam betreuten Projektarbeiten und gemeinsamen Prüfungen innerhalb der Fachmodule können alle Beteiligten einen optimalen Nutzen ziehen.

Durch den gemeinsamen, einheitlichen Auftritt in der Öffentlichkeit präsentiert sich der Fachbereich Ingenieurbaukunst als moderne Lehr- und Forschungsgemeinschaft, welche die Ziele und Visionen der TU Graz umsetzt.

Nummerierungssystematik der Schriftenreihe:

D – Diplomarbeiten/Dissertationen | F – Forschungsberichte  
S – Skripten, Vorlesungsunterlagen | V – Vorträge, Tagungen

Institutskennzahl:

1 – Allgemeine Mechanik | 2 – Baustatik | 3 – Betonbau  
4 – Holzbau & Holztechnologie | 5 – Stahlbau & Flächentragwerke  
6 – Materialprüfung & Baustofftechnologie | 7 – Baubetrieb & Bauwirtschaft  
8 – Hochbau & Industriebau | 9 – Bauinformatik  
10 – Labor für Konstruktiven Ingenieurbau

Fortlaufende Nummer pro Reihe und Institut / Jahreszahl